Bowhead whale localization and environmental characterization in the Chukchi Sea using nonlinear Bayesian inversion

by

Graham Andrew Warner
B.Sc., University of Victoria, 2006

A Dissertation Submitted in Partial Fulfillment of the
Requirements for the Degree of

DOCTOR OF PHILOSOPHY

in the School of Earth and Ocean Sciences

Bowhead whale localization and environmental characterization in the Chukchi Sea using nonlinear Bayesian inversion

by

Graham Andrew Warner
B.Sc., University of Victoria, 2006

Supervisory Committee

Dr. S. E. Dosso, Supervisor
(School of Earth and Ocean Sciences, University of Victoria)

Dr. N. R. Chapman, Departmental Member
(School of Earth and Ocean Sciences, University of Victoria)

Dr. M. J. Wilmut, Departmental Member
(School of Earth and Ocean Sciences, University of Victoria)

Dr. D. J. Berg, Outside Member
(Department of Chemistry, University of Victoria)

Mr. D. E. Hannay, Additional Member
(JASCO Applied Sciences)

Supervisory Committee

Dr. S. E. Dosso, Supervisor
(School of Earth and Ocean Sciences, University of Victoria)

Dr. N. R. Chapman, Departmental Member
(School of Earth and Ocean Sciences, University of Victoria)

Dr. M. J. Wilmut, Departmental Member
(School of Earth and Ocean Sciences, University of Victoria)

Dr. D. J. Berg, Outside Member
(Department of Chemistry, University of Victoria)

Mr. D. E. Hannay, Additional Member
(JASCO Applied Sciences)

ABSTRACT

This thesis develops and applies nonlinear Bayesian inversion methods for localization of bowhead whales and environmental characterization, with quantitative uncertainty estimation, based on acoustic measurements from a set of asynchronous single-channel recorders in the Chukchi Sea. Warping analysis is applied to estimate modal-dispersion data from airgun sources and whale calls. Whale locations and the water-column sound-speed profile (SSP) and seabed geoacoustic properties are estimated using reversible-jump Markov-chain Monte Carlo sampling in trans-dimensional inversions that account for uncertainty in the number of SSP nodes and subbottom layers. The estimated SSP and seafloor sound speed are in excellent agreement with independent estimates, and whale localization uncertainties decrease

substantially when jointly-inverting data from multiple whale calls. Bowhead whales are also localized using a fixed-dimensional inversion of time-difference-of-arrival data derived using cross-correlation for the same recorders. The nonlinear localization uncertainty estimates are found to depend strongly on the source locations and receiver geometry.

Contents

List of Tables

List of Figures

ACKNOWLEDGEMENTS

I am indebted to many people for this work. In particular, I would like to thank:

My supervisor Stan Dosso, for mentoring me as a scientist, countless hours of insightful discussion, and support through academic and non-academic challenges. I am extremely fortunate and grateful for the opportunity and experience of learning under your supervision.

David Hannay and Roberto Racca, for your leadership, encouragement, and providing me work/school/life flexibility to pursue this degree.

Jan Dettmer, for providing an initial trans-dimensional FORTRAN inversion code, help troubleshooting inversions, and editing papers.

Julien Bonnel, for sharing your mode-warping code.

My colleagues at JASCO Applied Sciences, for companionship, advice, and covering for me while I was puking over the side of a ship.

Shell Offshore Inc., for allowing me to analyze and publish their data.

My parents, for the decades of my upbringing and continuing support, of which my appreciation grows daily.

My wife Shyla, for manning the fort while I was away doing fieldwork or attending conferences, and your encouragement, patience, and understanding. You make my world go around.

Funding for this work was provided through the NSERC Industrial Postgraduate Scholarship program and was generously supported by JASCO Applied Sciences.

DEDICATION

This thesis is dedicated to my deeply-missed grandparents:
Robert and Kathleen Look, and
Harry and Joan Warner.

Acronyms

2D two-dimensional

2SD two-standard deviation

AGC automatic gain control

AMAR Autonomous Multichannel Acoustic Recorder

AR auto-regressive

AR(1) first-order auto-regressive

BIC Bayesian information criterion

CTD conductivity-temperature-depth

DASAR Directional Autonomous Seafloor Acoustic Recorder

fixed-D fixed-dimensional

FM frequency-modulated

GPS global positioning system

IF instantaneous frequency

MAP maximum *a posteriori*

MC Monte Carlo

MCMC Markov-chain Monte Carlo

MH Metropolis-Hastings

NCF noise cross-correlation function

OBH ocean-bottom hydrophone

PDF probability density function

PPD posterior probability density

rjMCMC reversible jump Markov-chain Monte Carlo

RL received level

SSP sound-speed profile

STFT short-time Fourier transform

TDOA time-difference-of-arrival

TF time-frequency

TL transmission loss

trans-D trans-dimensional

TWTT two-way-travel-time

Chapter 1

Introduction

1.1 Overview

The overall objective of this thesis is to develop hydroacoustic inversion methods for localizing bowhead whales and characterizing the environment in the Chukchi Sea, including rigorous uncertainty estimation. The ability to localize these whales is important for understanding their spatial distributions relative to anthropogenic noise sources such as the airgun arrays used in marine seismic surveys for oil and gas exploration. In addition, localizing these animals and characterizing the environment is important for assessing their acoustic exposure levels and for observing changes to migration tracks or movement behaviours that might result from such exposures. Whale localization can be achieved by non-acoustic methods such as attaching satellite tags to the animals or visual (aerial or ship-based) surveys, but these methods can be invasive to the animals, limited to a relatively small fraction of a population, or inhibited by poor visibility. The passive acoustic localization methods developed in this thesis are useful because they are not subject to these limitations. Passive acoustic methods might identify movement patterns for a larger fraction of the population than can be tagged, and may also show evidence of whale response to other whale calls.

In the northeastern Chukchi Sea, bowhead whales migrate directly through areas recently experiencing substantial oil and gas exploration activity, heading east in the spring and west in the fall.[1] In the same region, decreasing Arctic ice coverage[2] provides potential for increased vessel traffic. The northeastern Chukchi Sea and Beaufort Sea are now experiencing higher noise levels due to these activities than just a

few years ago,[3,4] which can reduce the zone over which animals can communicate with each other.[5] There is concern that industrial noise may directly injure bowhead whales or disturb their behaviour,[6–8] with detrimental effects to the animals and potential interference with subsistence hunting by coastal native communities. A common mitigation strategy is to reduce the intensity of sound emission when bowheads are near anthropogenic activities, which requires the ability to localize the animals and predict sound levels. Although the methods developed here are applied specifically to bowhead whales in the Chukchi Sea, they represent general methods suitable for passive localization of marine mammals and environmental characterization in other settings.

This thesis focuses on acoustic data collected on single-channel, omni-directional autonomous acoustic recorders as they are relatively inexpensive and simple to deploy compared to cabled observatories, directional sensors, or multichannel arrays, allowing them to be used to monitor much larger spatial areas and longer recording durations for a given budget. One of the drawbacks to using autonomous recorders, however, is that their internal clocks tend to drift out of synchronization due to rapid temperature changes at deployment and recovery and over long deployment durations. Such clock drift precludes some well-established localization and environmental estimation methods (e.g., time-difference-of-arrival[9–11] and matched-field inversion[12–14]). The inversion methods developed in this thesis account for clock drift and can be used with varying levels of prior clock-drift information.

This thesis develops remote sensing methods to quantify whale locations and environmental parameters with rigorous uncertainties in a Bayesian (probabilistic) inversion framework. Uncertainty estimates are critical for interpreting inversion results when independent methods are not available for comparison (e.g., true whale locations are not known in this thesis).

To understand the inversion framework, consider first the forward problem: given a set of model parameters $\mathbf{m}$ (e.g., source location, water-column sound-speed profile, SSP, and seabed geoacoustic properties) for a mathematical operator f that simulates a physical system of interest (e.g., acoustic propagation in the ocean), predict the data $\mathbf{d}_{\text{pred}} = f(\mathbf{m})$ that would be observed in an experiment (e.g., acoustic normal-mode arrival times as a function of frequency). The forward function f maps model space to data space. The inverse problem is: given observed data $\mathbf{d}_{\text{obs}}$ arising from a physical system, estimate the corresponding model parameters $\hat{\mathbf{m}} = f^{-1}(\mathbf{d}_{\text{obs}})$. The inverse function f^{-1} maps data space to model space. Generally an analytic form of f^{-1}

does not exist for nonlinear problems, so $\hat{\mathbf{m}}$ is estimated numerically by searching for models for which $\mathbf{d}_{\text{pred}}$ is statistically consistent with $\mathbf{d}_{\text{obs}}$ given the noise on the data (here noise represents all error processes causing differences between observed and predicted data). While the forward problem is typically stable and a unique solution exists, the inverse problem (given that measured data have noise) may or may not have a solution, is generally non-unique, and is often unstable, all of which necessitate rigorous uncertainty estimation.[15,16]

Acoustic data from two measurement programs are considered in this thesis. The first involves short-duration (one day) measurements of airgun sounds recorded on a single autonomous recorder in the Chukchi Sea (71°17.4'N, 163°38.1'W) on 16 August, 2009.[17] This data set is used to characterize the water-column SSP and subbottom geoacoustic properties using normal-mode dispersion data (described below). The second data set involves recordings of bowhead whale calls recorded on a Y-shaped cluster of seven autonomous recorders in the Chukchi Sea (71°18.5'N, 163°12.7'W) from 1 August to 16 October, 2013.[18] This data set is used for localizing bowhead whales (and simultaneously characterizing the environment) using two different methods involving either modal-dispersion or time-difference-of-arrival (TDOA) data. Neither of the two acoustic measurement programs were designed primarily for environmental characterization or precise bowhead whale localization so in this sense the methods developed in this thesis are applied somewhat opportunistically.

As mentioned previously, one type of data used for whale localization and environmental characterization is normal-mode dispersion. Long-range sound propagation in range-independent shallow-water environments is well modelled with normal-mode theory.[19] The normal-mode solution to the acoustic wave equation is found by assuming that the acoustic field is a product of separable range and depth functions. The resulting solution is a discrete sum of modes which are mathematically equivalent to the interference pattern between up-going and down-going plane waves at specific angles for constructive interference. The interference pattern represents a resonance of the waveguide, determined by the environment (SSP and subbottom), and dominates the total acoustic field at long ranges. In shallow water, only a few modes are often required to accurately model the acoustic field. The mode propagation angles (defining horizontal wavenumbers) have a nonlinear dependence on frequency so the mode group speeds are also frequency dependent. Modes are therefore dispersive, and, in addition, modes of different orders propagate with different group speeds for a given frequency. Modal dispersion contains substantial information about the environment

and source-receiver range.

Modal-dispersion data can be extracted from recordings on single-hydrophone recorders using time-frequency (TF) analysis. Resolving mode arrivals in the TF plane requires sufficient signal bandwidth and is dependent on the difference in mode group speeds, source-receiver range, and the signal-processing techniques applied. For highly-dispersed signals with well-separated modes, arrival times can be determined from spectrograms; however, for weakly-dispersed signals, TF resolution limitations degrade arrival-time estimates. This thesis uses recent nonlinear resampling techniques, called warping,[20,21] to improve mode arrival-time estimates for weakly-dispersed data. Warping transforms modes into (nearly) constant-frequency tones, allowing them to be separated with conventional filtering techniques. Warping is an invertible transform so the filtered signals can be transformed back into the original TF domain for extracting mode arrival times. This thesis applies mode warping to impulsive airgun signals and to up-swept or down-swept bowhead whale calls; the latter requires an additional deconvolution step to precondition the signal.[22] Mode arrival times are quantified as a function of frequency and mode number at multiple receivers for multiple whale calls, providing a highly-informative data set.

The second type of data inverted in this thesis for bowhead whale localization is whale-call TDOA data. TDOA data are less informative than modal-dispersion data; however, extracting TDOA data from acoustic recordings and modelling TDOAs in an inversion algorithm is much simpler and less computationally expensive, allowing applications to large whale-call data sets. TDOA-based localization methods have been developed extensively for synchonized recorders (e.g., Refs. [9–11]). Whale-call TDOA data depend on the source (whale) and receiver locations, sound speed, and, for data extracted from asynchronous recorders, relative recorder clock offsets. This thesis develops a nonlinear TDOA inversion to estimate whale locations and uncertainties using data from asynchronous recorders and also accounts for recorder-location uncertainties. Here the acoustic propagation is approximated as the time-of-flight along straight acoustic paths in the horizontal plane with an unknown effective sound speed. Since the low-frequency bowhead whale calls propagate as normal modes and disperse, the effective sound speed is a frequency- and mode-weighted average of the modal group speeds. For a call recorded on multiple recorders, the TDOA can be determined by cross-correlating the acoustic data from recorder pairs and calculating the time of the maximum of the cross-correlation envelope. Solving the TDOA inverse problem for one whale call with unsynchronized recorders is an underdeter-

mined problem; however, if many calls occur within a short-enough time period that the relative recorder clock offsets can be assumed constant (e.g., half an hour), the problem becomes overdetermined and whale locations can be estimated.

1.2 Bayesian inversion methods

A Bayesian[23,24] approach is applied to the inverse problems in this thesis. In a Bayesian framework, the data $\mathbf{d}$ and unknown model parameters $\mathbf{m}$ are considered as random variables with underlying probability densities. Bayes' rule defines the conditional probability of the model given the data. If the parameterization of the model is known, Bayes' rule is

$$P(\mathbf{m}|\mathbf{d}) = \frac{P(\mathbf{d}|\mathbf{m})P(\mathbf{m})}{P(\mathbf{d})}. \tag{1.1}$$

For fixed (measured) data, $P(\mathbf{d})$ is the propability of the data (a normalizing constant) and $P(\mathbf{d}|\mathbf{m})$ is interpreted as the likelihood of the model. $P(\mathbf{m})$ is probabilistic prior information about the model that is independent of the data. This thesis uses relatively uninformative bounded uniform priors to minimize subjectivity (a joint prior between sediment sound speed and density is also used to restrict models to physically-realistic combinations[25,26]). Finally, $P(\mathbf{m}|\mathbf{d})$ is the posterior probability density (PPD), the general solution to the inverse problem. Equation (1.1) quantitatively updates the prior with data information to estimate the posterior. The PPD represents the combined information of the prior and data with probabilities that represent a degree of belief.

In nonlinear inverse problems an analytic solution rarely exists, so the PPD is sampled numerically. The Monte Carlo (MC) method[27] can be used to draw independent samples from the PPD, but the fractional volume of good models relative to the entire multi-dimensional model space is usually very small, making MC inefficient. In this thesis, Metropolis-Hastings (MH) sampling,[28] a Markov-chain Monte Carlo (MCMC) method,[29] is applied to sample the PPD. For nonlinear problems, it is often difficult to conceptualize the multi-dimensional PPD; however, properties of the PPD such as the maximum *a posteriori* (MAP) model or marginal probability densities are straightforward to calculate and interpret, given sufficient PPD samples.

In some inverse problems the most appropriate form of the model (parameterization) is not well known *a priori*. For example, the number of seabed layers required

to predict the observed data is often unknown. Even when "ground truth" information is available, such as from sediment cores or independent geophysical surveys, the resolution and accuracy of the information may not correspond to the information content of the acoustic data. Overparameterizing the problem generally leads to over-fitting the data (fitting noise) and over-estimating parameter uncertainties as models are overly flexible and parameters compensate for each other. Conversely, underparameterizing the problem can lead to poorly-fit data, unresolved structure, and underestimated uncertainties. Hence, determining an appropriate parameterization (or set of parameterizations) is an important issue in quantitative inversions.

If the model parameterization is uncertain, the probabilities in Bayes' theorem [Eq. (1.1)] can be conditioned on the parameterization $\mathcal{K}$ as

$$P(\mathbf{m}|\mathbf{d},\mathcal{K}) = \frac{P(\mathbf{m}|\mathcal{K})P(\mathbf{d}|\mathbf{m},\mathcal{K})}{P(\mathbf{d}|\mathcal{K})}. \tag{1.2}$$

$P(\mathbf{m}|\mathcal{K})$ is the prior information given the parameterization. $P(\mathbf{d}|\mathbf{m},\mathcal{K})$ is the data probability density (uncertainty) but is interpreted as the likelihood of the model for fixed (measured) data. Through a similar interpretation, $P(\mathbf{d}|\mathcal{K})$ is the likelihood of the parameterization, referred to as Bayesian evidence. The evidence favours parameterizations that allow for models that fit the observed data, but since the evidence is a normalized probability density function, overly-general parameterizations that can predict unnecessarily-large regions of data space have lower probability density.[30] In this way, Bayesian evidence simultaneously accounts for data fit and prefers simpler models. Because the PPD is a normalized probability function, the evidence is equivalent to

$$P(\mathbf{d}|\mathcal{K}) = \int_{\mathcal{K}} P(\mathbf{m}'|\mathcal{K})P(\mathbf{d}|\mathbf{m}',\mathcal{K})d\mathbf{m}'. \tag{1.3}$$

This integral is often difficult to evaluate.[30] An alternative approach is trans-dimensional (trans-D) sampling,[31–34] which avoids directly evaluating the evidence but samples models from the PPD in proportion to their evidence support using a variant of MH sampling. Specifically, a reversible jump Markov-chain Monte Carlo (rjMCMC) method is used to perform a random walk through the model and parameter space. At each step, the model parameters or parameterization may be changed so that the Markov chain samples models from the trans-D PPD. The uncertainty in parameterization is therefore accounted for in the model parameter uncertainty estimates. The trans-D PPD shows structure that can be resolved by the data and prior information.

The trans-D formulation is desirable because it allows the information content of the data to determine the appropriate parameterization, reducing subjectivity. Trans-D inversion is applied in this thesis to modal arrival-time data to consider unknown parameterizations for the water-column SSP and subbottom layers, as well as for an auto-regressive data error model.

1.3 Thesis outline

The main body of this thesis consists of three chapters which correspond to three journal papers (with minor modifications) on inversion of modal dispersion or TDOA data. Data acquisition and processing, inversion methods, and results are described in each chapter. Since the chapters were originally written as stand-alone papers which in some cases use similar data sets, there is some repetition in the introduction, methods, and data acquisition sections of these chapters. The papers involve work that I carried out in collaboration with co-authors, so in the overview that follows I explain my specific contributions.

Chapter 2 (Published as Ref. [35] with authors Warner, Dosso, Dettmer, and Hannay.) This chapter develops a trans-D inversion method that is applied to simulated and measured airgun modal-dispersion data to estimate environmental properties. The original intent was to characterize the subbottom for subsequent use in whale localization. A mode-warping technique was used to extract mode arrival times from airgun pulses recorded on single-hydrophone recorders. Data are inverted primarily for the water-column SSP and subbottom geoacoustic properties. The inversion is trans-D over the number of SSP nodes, subbottom layers, and first-order auto-regressive error parameters. The results show that the SSP and upper sediment layer are well constrained by inverting mode arrival times from few pulses. The estimated SSP is in excellent agreement with a measured profile, and an independent analysis of headwaves[36] agrees well with the upper sediment-layer sound speed estimated in the inversion. The trans-D methods are briefly described in this chapter but are fully developed in Appendix A. I lead the field study and collected the acoustic data for this work while working for JASCO Applied Sciences in 2009. Jan Dettmer provided a trans-D code for matched-field inversion where the number of subbottom layers and first-order auto-regressive error parameters were unknown. I modified

this code to invert modal-dispersion data and added the (trans-D) SSP to the inversion. I wrote my own warping-based data processing algorithm based on a routine by Julien Bonnel. I analyzed the data, ran the inversions, analyzed the results, and wrote the paper with editing assistance from Stan Dosso, Jan Dettmer, and David Hannay.

Chapter 3 (Published as Ref. [37] with authors Warner, Dosso, Hannay, and Dettmer.) This chapter develops an inversion method that is applied to bowhead whale-call modal-dispersion data (both simulated and measured) for localizing whales and estimating environmental properties. Originally the intent was to use subbottom properties estimated in Chapter 2 as prior information for localization, but treating the environment as unknown proved successful and more general/useful. A modified mode-warping technique is used to extract mode arrival times from (non-impulsive) bowhead whale calls recorded on asynchronous recorders. The inversion uses the trans-D methods developed in Chapter 2 to account for uncertain SSP complexity and subbottom layering structure. Results show whale location uncertainties are significantly reduced in joint inversions of multiple calls. Estimates of the environmental properties are less certain than in Chapter 2 as whale calls are not as loud or impulsive as airguns, but are nevertheless useful for predicted sound-exposure levels. Acoustic data were collected by JASCO Applied Sciences. I manually detected and associated the bowhead whale calls and processed the data using the mode warping code from Chapter 2 that I adapted to account for non-impulsive sources. I modified the inversion code used in Chapter 2 and added principal-component parameter rotations[38] to the fixed-dimensional (fixed-D) parameters to account for strong parameter correlations. I ran the inversions, analyzed the results, and wrote the paper with editing assistance from Stan Dosso, David Hannay, and Jan Dettmer.

Chapter 4 (Submitted as Ref. [39] with authors Warner, Dosso, and Hannay.) This chapter develops a fixed-D inversion method that is applied to simulated and measured bowhead-whale call TDOA data for whale localization. The motivation for this work was to develop a faster and simpler whale localization method (compared to that in Chapter 3) that could be applied to a large number of whale calls (at the expense of some accuracy). Waveform cross-correlations are used to determine TDOA data from bowhead whale calls recorded on asynchronous recorders (the same recorders as in Chapter 3). The inversion treats

whale locations, effective waveguide sound speed, relative recorder clock offsets, and recorder locations as unknowns with varying levels of prior information. Nonlinear whale location uncertainty estimates are found to be highly dependent on the source-receiver geometry. Whale location uncertainties are small enough to track migrating whales that call repeatedly over several minutes. Relative recorder clock drift rates are obtained by inverting batches of whale call TDOA data during 30-minute periods spanning two weeks. Acoustic data were collected by JASCO Applied Sciences. I manually annotated the bowhead whale calls and processed the data. I initially wrote a linearized inversion code in Interactive Data Language (IDL) and when linearization was found to be an inappropriate approximation, I wrote a nonlinear inversion which proved successful but slow. To speed up the convergence time I converted the inversion code to FORTRAN by adapting a modal-dispersion inversion code from Stan Dosso. I added parallel tempering[40–43] to the code, ran the inversions, analyzed the results, and wrote the paper (to be submitted) with editing assistance from Stan Dosso.

Appendix A This appendix fully develops the trans-D inversion methodology first used in Chapter 2 for the SSP, subbottom layering, and first-order autoregressive error model. The trans-D SSP and subbottom layering formulation is also used in Chapter 3.

Chapter 2

Bayesian environmental inversion of airgun modal dispersion using a single hydrophone in the Chukchi Sea

This chapter presents estimated water-column and seabed parameters and uncertainties for a shallow-water site in the Chukchi Sea, Alaska, from trans-dimensional Bayesian inversion of the dispersion of water-column acoustic modes. Pulse waveforms were recorded at a single ocean-bottom hydrophone from a small, ship-towed airgun array during a seismic survey. A warping dispersion time-frequency analysis is used to extract relative mode arrival times as a function of frequency for source-receiver ranges of 3 and 4 km which are inverted for the water sound-speed profile (SSP) and subbottom geoacoustic properties. The SSP is modelled using an unknown number of sound-speed/depth nodes. The subbottom is modelled using an unknown number of homogeneous layers with unknown thickness, sound speed, and density, overlying a halfspace. A reversible-jump Markov-chain Monte Carlo algorithm samples the model parameterization in terms of the number of water-column nodes and subbottom interfaces that can be resolved by the data. The estimated SSP agrees well with a measured profile, and seafloor sound speed is consistent with an independent headwave arrival-time analysis. Environmental properties are required to model sound propagation in the Chukchi Sea for estimating sound-exposure levels and environmental research associated with marine-mammal localization.

2.1 Introduction

Knowledge of ocean sound-speed profiles (SSP) and seabed geoacoustic properties is required for the accurate prediction of underwater sound propagation, such as used for marine mammal noise impact assessments and for sonar-performance studies. For long-range propagation in shallow water, the geoacoustic properties are particularly important because of numerous interactions with the bottom. Low frequencies are more sensitive to deep subbottom structure and large-scale SSP features. High frequencies do not penetrate the subbottom as deeply but are more sensitive to finer-scale SSP features. These environmental dependencies mean measurements of broadband sound contain substantial information about the environment.

In range-independent shallow-water environments, long-range sound propagation is well modelled with normal-mode theory.[19] The environment acts as a dispersive waveguide which supports a limited number of propagating modes, with the modal group speeds directly dependent on the environment. The frequency-dependence of mode arrival times (i.e., modal dispersion) can be used as data in an environmental inversion if the source-receiver range is known. Dispersion measurements can be made using a single hydrophone; however, resolving mode arrival times in the time-frequency (TF) plane is dependent on the difference in modal group speeds, source-receiver range, and the signal-processing techniques applied. At long ranges, modes are well separated in time and arrival times can be determined from a spectrogram; however, there is likely more impact from variability in the environment along the propagation path to affect arrival times. Also, higher attenuation for higher-order modes degrades environmental information contained in long-range data. Short-range measurements are less susceptible to range-dependent effects and have higher bandwidth but TF resolution limitations can degrade estimates of mode arrival times. Recent studies have used mode-warping techniques to improve the TF resolution of modal arrival times for close-range dispersion measurements[21,44–47] and this approach is used here. Fourier series or variations thereof[48] are then used for the TF representations but the inherent side lobes (leakage) from Fourier transforms means that correlated errors can exist between arrival times for adjacent frequencies. These correlations should be taken into account in an inversion algorithm.

Environmental inversion of modal-dispersion data has been carried out for several types of impulsive sources.[44,45,47–51] These studies have either used prior knowledge or the Bayesian information criterion[52] (BIC) to determine the subbottom layering

parameterization (i.e., the number of layers). Parameterization is important because having too few layers under-parameterizes the model and under-fits the data, potentially leaving structure unresolved and under-estimating uncertainties. Conversely, too many layers over-parameterizes the model and overfits data, allowing spurious unconstrained structure and over-estimating uncertainties. Prior knowledge of the layering structure (e.g., from a core or high-resolution seismic survey), even if accurate, may not be appropriate if the resolution of the dispersion data is not consistent with that of the prior information. Often data do not uniquely define the parameterization (e.g., the number of seabed layers is uncertain). The BIC estimates the most appropriate parameterization (given strong assumptions), but because it is a point estimate, parameter uncertainties may be underestimated. This chapter uses a trans-dimensional[31–34] (trans-D) Bayesian inversion approach for subbottom layering that allows the information content of the data to determine how much subbottom structure can be resolved. The trans-D algorithm samples probabalistically over possible parameterizations, and model parameter uncertainties include the uncertainty in parameterization. The geoacoustic model consists of an unknown number of homogeneous layers, defined by interface depths, sound speeds, and densities, overlying a halfspace.

The same concerns for parameterization apply to the SSP. Several studies have inverted for the SSP using empirical orthogonal functions calculated from existing SSP measurements for the location.[49,50] This method simplifies the inversion in that only a small number (e.g., 2 or 3) coefficients of SSP eigenfunctions are inverted for instead of the sound speed at a series of depths; however, the eigenfunctions must be calculated from a comprehensive SSP database which may not be available for all environments. Another approach is to assume a fixed number of nodes defining the SSP but this requires *a priori* knowledge of an appropriate number of nodes which may not be available. Given the above limitations, an alternative and more general approach to estimating the SSP is developed here. The SSP is modelled in terms of a set of depth/sound-speed nodes, with the profile interpolated from these nodes as $1/c_w^2$ linear gradients (c_w is water sound speed). The number of nodes is sampled probabilistically with a trans-D algorithm so the data estimate how much SSP structure can be resolved. The node at the base of the SSP determines the water depth and sound speed at the seafloor, coupling the two trans-D stacks (SSP and subbottom). To my knowledge, trans-D inversion has not been previously applied to modal dispersion inversion.

Previous Bayesian modal-dispersion work[47] has taken error correlations into account using a fixed (point) estimate of the data covariance matrix from residual analysis. However, for trans-D models this assumes that the parameterization used for the point estimate is representative for the trans-D posterior which is difficult to assess and may not be sufficient for measured data. In this chapter, I use a trans-D first-order auto-regressive [AR(1)] error model to account for potential residual error correlations.[53]

The Bayesian approach applied here quantifies model parameter uncertainties and the trans-D formulation for the SSP and geoacoustic profile accounts for the uncertainty in the environmental parameterization. The trans-D auto-regressive error model accounts for residual error correlations without overparameterizing the error model when correlations are weak or absent. This approach reduces subjective choices in determining appropriate model parameterizations.

The trans-D Bayesian inversion is applied to acoustic data collected using autonomous ocean-bottom hydrophone (OBH) recorders that were part of an underwater sound measurement program in the Chukchi Sea, approximately 140 km offshore the northwest coast of Alaska.[17] The program was originally designed to determine distances to specific sound-level thresholds from an airgun array used in seismic surveys to assess shallow hazards to drilling operations (e.g., near-surface gas) by Shell Oil Company. In addition to fulfilling the program objectives, the acoustic recordings of airgun pulses were found to be well suited for environmental inversion. This location is of significant interest because of potential hydrocarbon deposits and the presence of large numbers of marine mammals (e.g., bowhead and beluga whales, walrus, and several species of seals are commonly observed here). To my knowledge, there are no published geoacoustic properties to sufficient depth to accurately model low-frequency sound propagation at this location (surficial sediments are a mixture of sand, silt, and clay[54,55] but sediment properties can change dramatically with depth). One of the goals of this chapter is therefore to estimate site-specific environmental properties that can be used in future work to predict sound propagation for estimating sound-exposure levels as a function of range and for marine-mammal localization to help understand animal behaviour and mitigate anthropogenic effects on the animals.

2.2 Theory

2.2.1 Data processing

Small synchronously-fired airgun arrays produce low-frequency (below ∼500 Hz) impulsive sounds of durations short enough that all frequencies can be modelled as being emitted at the same instant for the purposes of analyzing dispersion measurements. The propagation of airgun pulses can be modelled using normal-mode theory.[19] Modes propagate with different group speeds that are dependent on the environment, i.e., water-column SSP and geoacoustic properties of the subbottom. The group speeds can be calculated using a normal-mode model.[56] The arrival time of mode m at frequency f for pulse p at a recorder at range r is

$$t_{mp}(f) = \tau_p + \frac{r_p}{v_m(f)}, \tag{2.1}$$

where τ_p is the time that the pulse was emitted from the source relative to an arbitrary time origin and $v_m(f)$ is the group speed. For this chapter, I analyze multiple pulses where the inter-pulse distance is fixed and known, i.e., $r_{p+1} - r_p = \Delta r \quad \forall\, p$.

The modal arrival times as a function of frequency can be determined from the TF representations of a pulse recorded at a single hydrophone. Previous studies have used a mode warping technique to improve the modal TF resolution from impulsive sources such as imploding light bulbs or explosive charges measured at close range.[21,44–47] Mode warping is a nonlinear resampling technique that transforms dispersive modes into constant-frequency tones. A band-pass filter (a Butterworth filter is used here) can then be used to isolate individual modes and the filtered signal transformed back into the time domain.

A signal $p(t)$ is transformed to the warped time domain as

$$q(w) = \sqrt{|w'(t)|}\, p[w(t)], \tag{2.2}$$

where $w(t)$ is the warping function with time derivative $w'(t)$ and $q(w)$ is the warped signal. The warped signal can be unwarped by using Eq. (2.2) with $w^{-1}(t)$ as the warping function and $q(w)$ as the signal. For an isospeed waveguide with rigid bottom and free surface, the warping function for dispersive modes is[20]

$$w(t) = \sqrt{t^2 + (r/c_w)^2}, \tag{2.3}$$

where r is the range and c_w is the water sound speed. This warping function was found suitable for low-frequency modes in several shallow-water environments despite violations of the ideal waveguide assumption.[21,44–47] A suitable value for the ratio r/c_w can be determined empirically by observing when modes become constant-frequency tones in a spectrogram of q. The warped pulse is filtered for each of M modes and unwarped, resulting in M mono-component signals $p_m(t)$. Figure 2.1 illustrates this procedure for the recording of an airgun pulse at 4 km range (described in Sec. 2.5). It is unknown why evidence of bubble pulses was not observed in the airgun recordings (to my knowledge, the airgun array was not tuned to cancel the bubble pulse and the source was sufficiently deep to expect a bubble pulse before the bubble breached the surface[57]).

For each filtered mode, a spectrogram is computed using a Hanning window with 99% overlap (Fig. 2.1 considers a 8192-point window for data sampled at 48 kHz). The mode arrival times are set to the time of maximum energy at each frequency. The bandwidth of each mode is limited by the environment in terms of the mode cutoff at low frequencies and modal attenuation at high frequencies. Near modal cutoff, the dispersion curves tail back around the slower Airy phase but the spectrogram resolution for these rapid TF changes is poor. In addition, the modal amplitude changes rapidly near the cutoff frequency which can bias the arrival-time estimate. Lower-frequency data are therefore limited to frequencies above the inflection point of the time vs. frequency curve. Modes at high frequencies arrive closely spaced in time due to their more similar modal group speeds. The spectrogram is not good at resolving such signals, so the modes are truncated if the arrival times for successive frequencies fall into the same time window.

2.2.2 Bayesian inversion

The picks of arrival time vs. frequency indicated on Fig. 2.1 (d)–(g) represent acoustic data which can be inverted for environmental parameters. The inversion carried out in this chapter uses a trans-D Bayesian formulation[58,59] which is briefly described here; a more detailed formulation is provided in the Appendix. The environmental model consists of a water column with unknown depth and SSP over a seabed consisting of an unknown number of homogeneous fluid layers (each layer characterized by thickness, sound speed, and density) overlying a fluid halfspace of unknown geoacoustic parameters. Mode group speeds are calculated for an environmental model

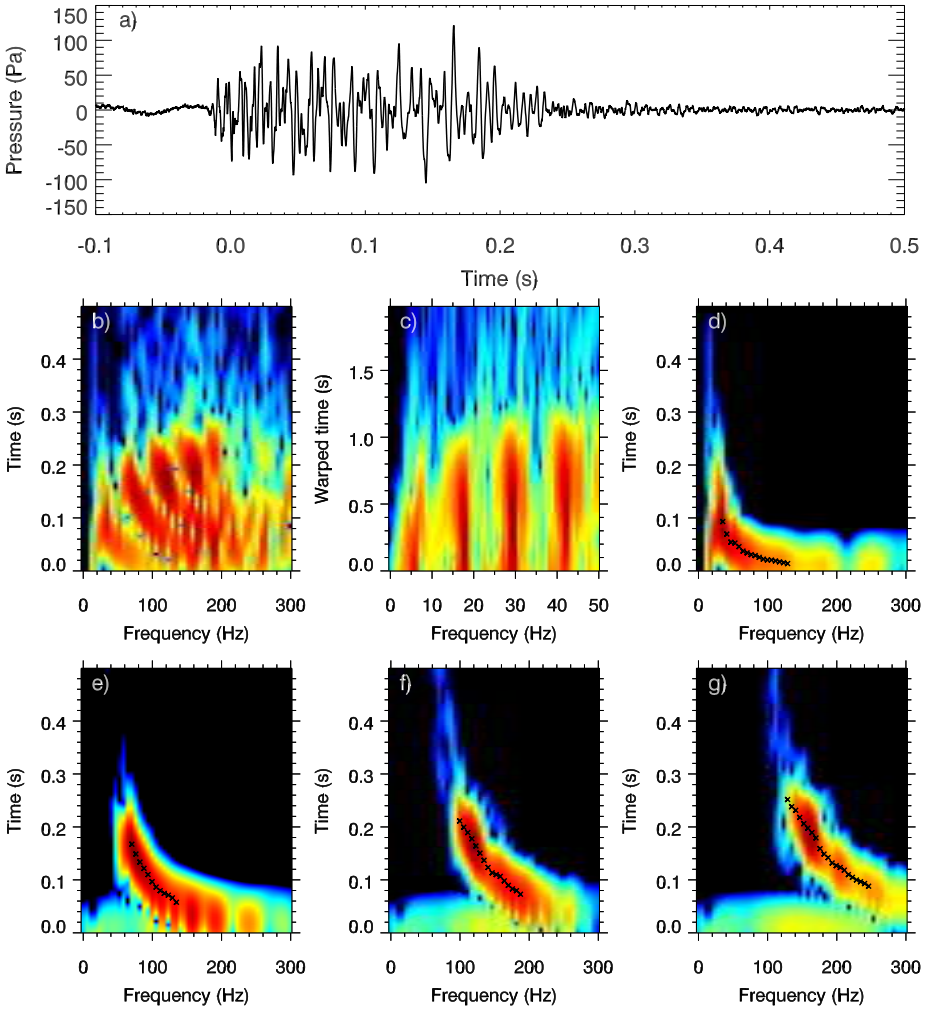

Figure 2.1: Example of warping TF analysis. (a) Measured airgun pulse waveform at 4 km range. (b) Unfiltered spectrogram. (c) Warped spectrogram showing four warped modes as approximate constant-frequency tones. (d)–(g) Filtered spectrograms with data picks (×) for modes 1–4, respectively. Note that higher-order modes are resolved to higher frequency than possible in the unfiltered spectrogram.

using the normal-mode code ORCA[56] and are converted to predicted modal arrival times using pulse time and range [Eq. (2.1)]. In a Bayesian formulation the solution is given by properties of the posterior probability density (PPD) of the model parameters given the measured data and prior information. A reversible-jump Markov-chain Monte Carlo algorithm is applied to sample the PPD over a trans-D model space in which the number of SSP nodes and seabed layers can change by probabilistically accepting transitions between model parameters/parameterizations according to the Metropolis-Hastings-Green criterion.[32] Model transitions to higher dimensions (in-

creased number of nodes or layers) are proposed from the prior rather than restricted to small perturbations to the current model to increase transition acceptance rate.[59] The transition acceptance probability depends on the prior, proposal, and likelihood ratios, with the likelihood defined by the assumption of Gaussian-distributed errors with unknown standard deviation and a trans-D auto-regressive process to represent possible error correlations[53] over frequency for each mode of each pulse (see the Appendix). Uniform prior probability densities are used for all model parameters, with an additional joint prior that constrains subbottom sound speed and density to physically realistic combinations.[25,26] The Markov chain samples over the number and parameters of SSP nodes, subbottom layers, and auto-regressive coefficients to estimate the trans-D PPD.

2.3 Simulation study

This section illustrates and verifies the data analysis and inversion methodologies in a realistic simulation study involving two pulses. The environmental model for the simulation has five subbottom interfaces and four water-column SSP nodes. The true parameter values and the bounds of the uniform prior probability density functions (PDF) assumed for all parameters are listed in Table 2.1, and the joint prior PDF for subbottom sound speed and density is described in the Appendix. Mode arrival times (the observed synthetic data) were generated in two ways to produce two simulated data sets to compare inversion results. First, data were simulated for two pulses using Eq. (2.1) with exact modal group speeds calculated by the normal-mode code ORCA,[56] i.e., I bypassed the TF data-processing step of identifying mode arrival times (Sec. 2.2.1). Gaussian-distributed errors were added to the synthetic data with standard deviations that were constant over frequency but varied between modes and between pulses from 2–4 ms, as given in Table 2.2. The second data set was created to represent a more realistic simulation that requires TF analysis to identify mode arrival times. Synthetic acoustic waveforms (time series) were modelled using Fourier synthesis of frequency-domain responses computed using ORCA from 5 to 500 Hz with 1-Hz frequency spacing. Two waveforms (A and B) for receivers at 3- and 4-km range at 3 m above the seafloor were computed assuming an impulse source function at time $\tau = 0$ and 2-m source depth. Mode arrival times were determined as described in Sec. 2.2.1 for five modes in each pulse and were limited to an upper frequency bound of 300 Hz. Random errors were not added to the picked data so the inversion results

Table 2.1: Model parameter values and prior bounds for the simulations. Note that subbottom sound speed and density were further constrained by the joint prior bound (see Sec. A.3).

Parameter	Unit	True value(s)	Prior
c_w at surface	m/s	1447	[1439,1455]
c_w at seafloor	m/s	1440	[1439,1455]
Water depth z_b	m	41	[38,45]
# SSP nodes	-	4	[0,15]
SSP node depths	m	[12.85,15,24,31]	[0,z_b]
SSP node $\boldsymbol{c}_w$	m/s	[1447,1442,1453,1440]	[1439,1455]
# subbottom interfaces	-	5	[0,10]
Interface depths	m	[2,5,10,20,40]	[0,50]
Layer speed $\boldsymbol{c}_b$	m/s	[1465,1555,1605,1730,2200]	[1460,2500]
Basement c_b	m/s	2300	[1460,2500]
Layer density $\boldsymbol{\rho}$	g/cm^3	[1.49,1.77,1.87,2.06,2.2]	[1.3,2.5]
Basement ρ	g/cm^3	2.3	[1.3,2.5]
Pulse A range	m	3000	[2950,3050]
Pulse A time	s	0	$[-1, 1]$
Pulse B time	s	0	$[-1, 1]$

Table 2.2: Error and residual standard deviations for the simulation with Gaussian (σ_G) and picked (σ_p) data sets, respectively.

Pulse	1	1	1	1	1	2	2	2	2	2
Mode	1	2	3	4	5	1	2	3	4	5
σ_G (ms)	2.0	3.0	4.0	4.0	4.0	2.0	3.0	4.0	4.0	4.0
σ_p (ms)	3.0	3.2	4.1	4.3	5.6	2.1	3.2	4.0	1.9	4.8

illustrate uncertainties resulting only from data processing limitations, which I believe are a major component of the errors for measured data. In practice, ambient noise may also contaminate mode arrivals; however, mode arrivals that have low signal-to-noise ratios can be discarded from the inversion during data processing. I refer to the first and second data sets as the Gaussian and picked data sets, respectively. For comparison with the Gaussian data set error statistics, residuals were computed from the difference between the exact (theoretical, noise-free) times and the picked data set. The resulting standard deviations are listed for each pulse and mode in Table 2.2. The Gaussian data set was limited to the same modes and frequencies that were resolved using the data processing method on the picked data set so the data information content is similar between data sets.

Inversions were performed on the two synthetic data sets with approximately 600 000 samples drawn from the PPD via the trans-D Bayesian inversion described in Sec. 2.2 and the Appendix. Fixed-length chain thinning[60] (described in Sec. A.1) restricted the number of samples that were saved to 250 000, and saved samples that survived the fixed-length thinning process from the first 100 000 samples were discarded as burn-in. Both inversions produced approximately Gaussian-distributed data residuals (not shown). Figure 2.2 shows the resulting marginal probability profiles for the SSP and geoacoustic parameters for the two data sets. To more clearly show the probability structure over a wide range of values, the probability profiles are normalized independently at each depth. The probability-ratio profiles, plotted to the right of each marginal profile, indicate the relative probability as a function of depth. This figure also shows the marginal profiles for the SSP-node and subbottom-interface depths. The SSP probability densities near the bottom of the water column are not smooth because the water depth prior bounds (discussed below) constrain the available depths of SSP nodes. The estimated SSP for the Gaussian data set is in excellent agreement with the true profile (dashed line) with reasonably small uncertainties. For the picked data set, the estimated SSP agrees closely with the true profile between 10- and 35-m depth. The speeds near the surface and bottom are somewhat overestimated; these discrepancies are discussed later in this section.

The geoacoustic probability profiles agree well with the larger-scale features of the true profile, although some small-scale features (e.g., layers as thin as 2 m) can not be resolved by the data and are averaged in the inversion results. For the Gaussian data set, the inversion resolves two layers above a halfspace and effectively averages the properties of the first three layers. Three layers are resolved above a halfspace for the picked data set. The shallowest layer is estimated to be somewhat too thick, and the three deeper layers are effectively averaged. The uncertainty in the profiles increases with depth and around layer interfaces for each data set. The increase in uncertainty with depth is due to the mode functions decaying exponentially into the seabed which decreases the data sensitivity to deeper structure (considered further in Sec. 2.5).

The inversion of the Gaussian data set accurately resolved the environmental profiles and did not introduce any spurious structure. Discrepancies between the true and estimated profiles are due to the noise (Gaussian errors) and the limited resolution of the data. For the picked data set, the inversion has higher subbottom resolution but introduces spurious SSP structure near the seafloor. I attribute the SSP discrepancies

to errors resulting from the inherent limitations of the data processing method. Such errors may not occur for all modal-dispersion data, but these discrepancies indicate the possibility even when residuals appear Gaussian distributed. Since data processing is required in all practical cases, for the remainder of this section I only consider the picked data set results.

Figure 2.3 shows the marginal distributions of the number of subbottom interfaces and SSP nodes sampled in the inversion. The most-probable number of interfaces is three, which again indicates that the data cannot resolve all five interfaces. The most-probable number of SSP nodes is six which overestimates the true number of nodes (4) and may be related to the spurious SSP structure in Fig. 2.2 (bottom).

Figure 2.4 shows the marginal probability densities for pulse times, ranges, and water depth (note that pulse B range is not an estimated parameter as it is fixed at 1 km larger than pulse A range for the simulation). The marginal PDF for pulse A range is essentially flat within the prior bounds indicating the data are not able to constrain this parameter. The pulse times are constrained well within their prior bounds of $[-1, 1]$ s. The joint marginal PDF between pulse A range and time indicates these parameters are strongly (negatively) correlated. Hence, the prior bounds on source range play an important role in constraining source times. The absolute value of the reciprocal slope of the joint PDF, approximately 1409 m/s, represents the average modal group speed weighted by the mode standard deviations. The water depth is resolved well within the prior bounds, restricting the SSP node depth marginal density and decreasing the SSP probability ratio near the seafloor (Fig. 2.2).

The fit to the data achieved in the inversion is shown in Fig. 2.5. The relative arrival times from the mode-filtered spectrograms (picked data) are shown with $\times$ symbols; marginal densities of the relative predicted arrival times, calculated from a random sample of 5000 models from the PPD, are shown as grey-scale bars (sometimes quite thin vertically), and the (error-free) theoretical relative arrival times calculated from Eq. (2.1) are shown with solid lines. Each marginal density is normalized individually for display purposes. The inversion sampled models that produce predicted times in excellent agreement with the picked times (i.e., the data that were inverted), but have worse agreement with the theoretical (true) times due to some correlated errors between the picked and theoretical times from data processing (e.g., mode 5). Figure 2.6 shows the error statistics for each mode and pulse, i.e., the marginal densities of the residual standard deviations, the fraction of time for which the AR process was required, and the marginal densities of the AR parameters when the AR process

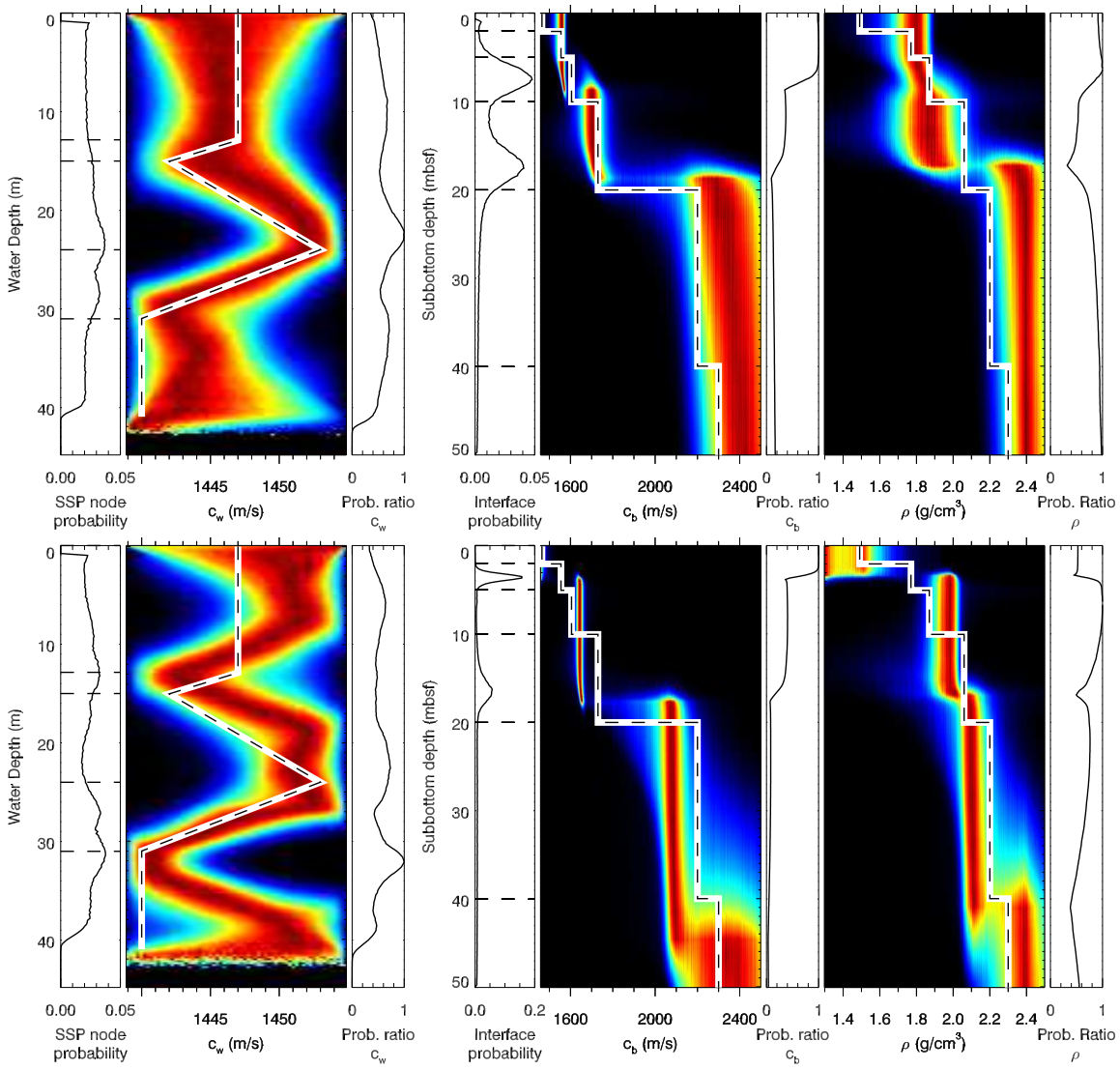

Figure 2.2: Marginal probability profiles for water SSP and subbottom sound speed and density, together with their corresponding node/interface depth profiles and depth normalization profiles. Top and bottom panels show results from inverting exact dispersion calculations with additive Gaussian noise and from data picked from synthetic waveforms (but no additive noise), respectively. Plot bounds are the prior bounds for SSP and geoacoustic parameters, though subbottom sound speed and density are further constrained by a joint prior PDF (see the Appendix). True parameter values are shown with dashed lines.

was required. The peaks of the residual standard-deviation densities are generally slightly less than the standard deviations between exact and picked data given in Table 2.2. The inversion required the AR process to be in effect for 30–70% of the samples, depending on the mode. These results show that the data processing method

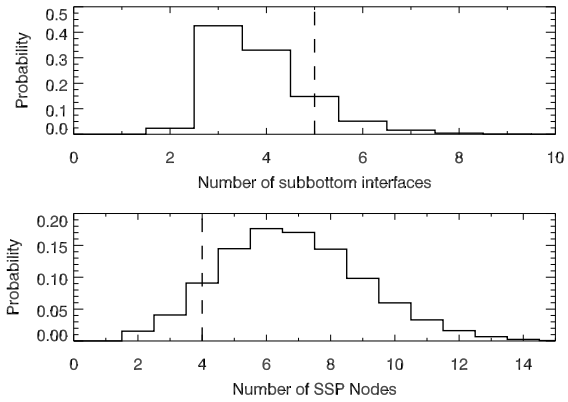

Figure 2.3: Probability distributions for the number of (top) subbottom interfaces and (bottom) SSP nodes for the picked-data simulation. True values are shown with dashed lines.

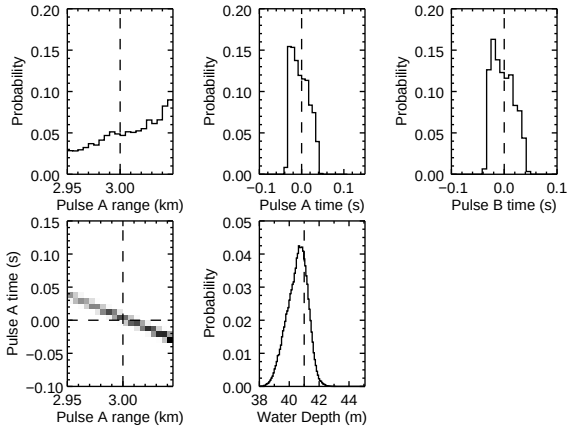

Figure 2.4: Marginal probability densities for pulse range, time, and water depth for the picked-data simulation. True values are shown with dashed lines. Pulse time axes are restricted within their prior bounds; all other axes ranges indicate prior bounds.

can result in errors which have both correlated and uncorrelated components.

2.4 Chukchi Sea survey

Underwater recordings of airgun array pulses were collected 16 August, 2009, during a seismic survey in the Chukchi Sea, Alaska, designed to assess shallow hazards for seabed drilling.[17] The recordings were made using two ocean-bottom hydrophone (OBH) recorders sampling at a 48 kHz sampling rate, each equipped with two hydrophones: Reson TC4043 (nominal sensitivity -201 dB re 1 V/μPa) and Reson

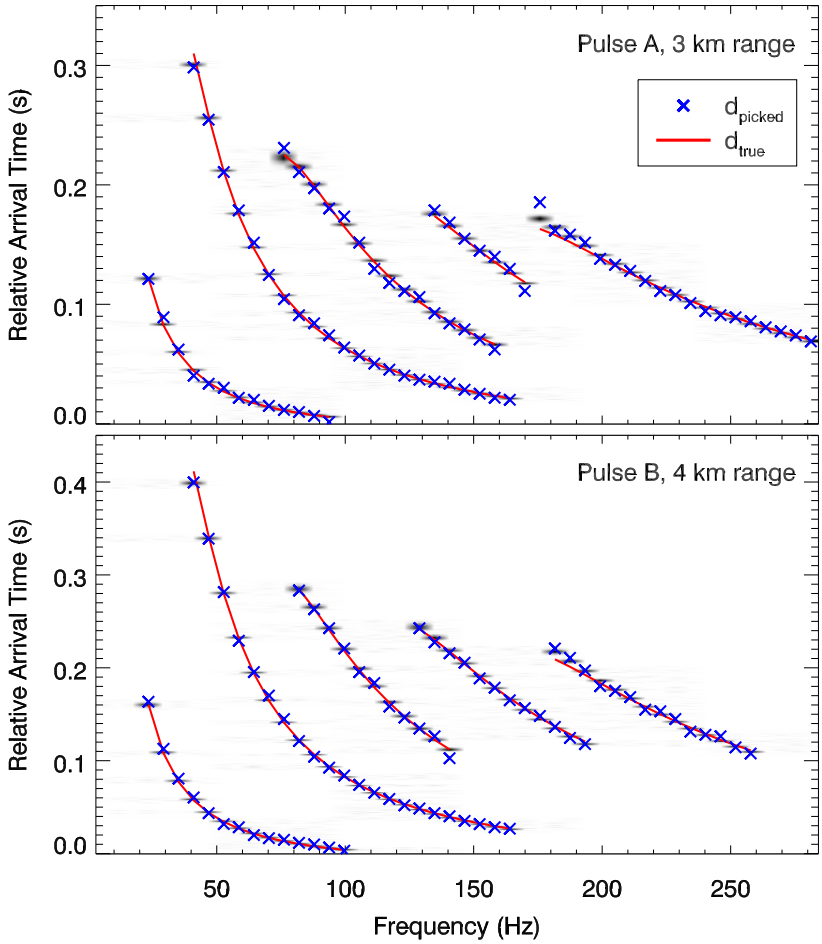

Figure 2.5: Mode relative arrival times for the two simulated pulses calculated from a random sample of models from the PPD (grey-scale PDFs sometimes quite thin), the arrival times picked from the synthetic pulses (×), and the true (error-free) arrival times (solid lines).

TC4032 (nominal sensitivity −166 dB re 1 V/μPa). The OBHs were deployed 200 and 1000 m off a survey line from the survey vessel *RV Mt. Mitchell*, and the deployment locations of the OBHs were recorded using a handheld GPS at 71°17.439'N, 163°38.115'W and 71°17.470'N, 163°39.436'W, with water depth measured using the ship's onboard echosounder at approximately 41 m. The bottom at this site is known to be very flat with seafloor slope on the order of 0.01%.

The source array consisted of four 10 in^3 airguns arranged in a 1-m long by 0.6-m wide rectangle which was towed at 2-m depth approximately 47 m behind the *RV Mt. Mitchell*. The airguns were fired synchronously every 15 m along a 25-km survey line. Airgun pulses were measured at ranges from 200 m to 20 km as the source was

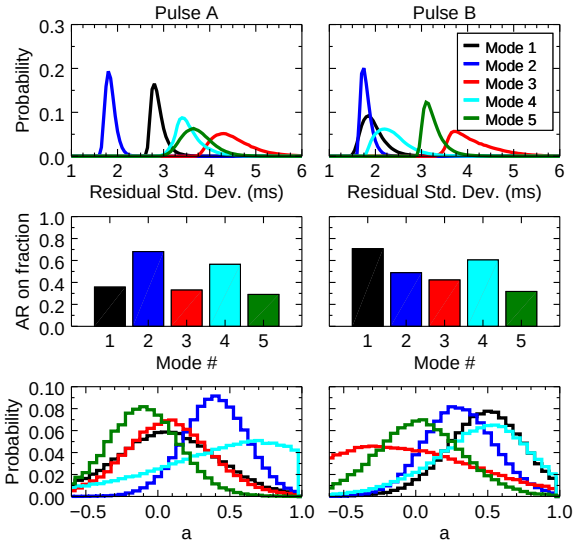

Figure 2.6: Error statistics for modes in simulated pulses (left) A and (right) B. Residual standard deviations, fraction of time the AR process was required (or "on"), and AR coefficient values are shown in the top, middle, and bottom panels, respectively.

towed past the recorders. The *RV Mt. Mitchell* logged its coordinates every second along the survey line, which were then translated into source coordinates of the airgun array by shifting the ship track by the tow distance.

The data used for the inversion were from pulses emitted south of the OBHs recorded on the more sensitive hydrophone of the 200-m offset recorder. Two pulses, A and B, spaced 66 pulses apart (i.e., $\Delta r = 15 \text{ m} \times 66 = 990 \text{ m}$) were used for the inversion. The range for pulse A was 2978 m according to GPS records, but to account for uncertainty in the OBH deployment position and airgun coordinates, this range is treated as an unknown parameter in the inversion with prior bounds ± 50 m from the estimated range. Knowing the 990-m pulse spacing between pulses A and B, the range for pulse B was set for each model based on the range for pulse A. These pulses were selected because the ranges are long enough that modal dispersion is easily measured, but not so long to reduce higher-order mode attenuation and potential environmental range-dependent effects. Accurate pulse times τ_s are not known because OBH clock drift desynchronized the acoustic recordings with the pulse logs. Pulse times are therefore treated as inversion parameters with prior bounds $[-3, 0]$ and $[-4, 0]$ s for pulses A and B, respectively, to allow physically realistic pulse times. Prior bounds other than for range and time are identical to those in Table 2.1. Relative arrival times were picked as described in Sec. 2.2.1 for 5 and 4 modes in pulses A and B,

respectively. Modes were required to have arrival times for at least 10 frequencies to estimate meaningful residual error statistics (see the Appendix). Within hours of the acoustic measurements, a conductivity-temperature-depth (CTD) cast was conducted 5.7 km north of the recorder site. Since the water-column conditions are expected to be quite stable in this region, the SSP calculated from the CTD cast provides reasonable "ground-truth" to compare with the SSP inversion results.

2.5 Results

The trans-D Bayesian inversion was applied to the measured data in a manner similar to that described for the simulation study with approximately the same number of models sampled from the PPD. Figure 2.7 shows the marginal profile densities for the SSP and geoacoustic parameters. Similar to the simulation study, the SSP marginal density near the seafloor is not smooth because the water depth prior bounds constrain the available depths of SSP nodes. The measured SSP (solid line overtop the corresponding PDF) shows a well-mixed (iso-speed) surface layer from 0 to 12 m and a second slower mixed-layer from 30 to 40 m, reaching the seafloor. Between these layers, the high sound speed from 17 to 30 m is likely due to a warm-water intrusion from the Bearing Sea, which is a common feature of the Chukchi Sea in August.[61] The SSP inversion result is in excellent agreement with the measured profile, closely tracking the depth-dependent structure with reasonably small uncertainties. Although the SSP marginal profile clearly resolves the structure of the measured SSP, the node-depth PDF is relatively uninformative. The marginal profiles for subbottom sound speed and density indicate well-resolved, near-constant values for an upper sediment layer which has relatively low density for its sound speed, although these parameter values are consistent with empirical studies.[25] The most probable interface depth is 14.6 mbsf, below which there is little resolved structure. The 95% credibility interval for interface depth is [11.6, 19.2] mbsf for single-interface models (credibility interval for interface depth for all models does not accurately quantify the dominant interface depth uncertainty because the PDF has heavy tails from other interfaces). The halfspace sound speed and density are not well constrained by the data.

Figure 2.8 shows the marginal distributions for the number of subbottom interfaces and SSP nodes. The most probable number of subbottom interfaces is one, supporting a single subbottom layer over a halfspace model. The most probable number of SSP nodes is six but the distribution is wider than those for seabed interfaces.

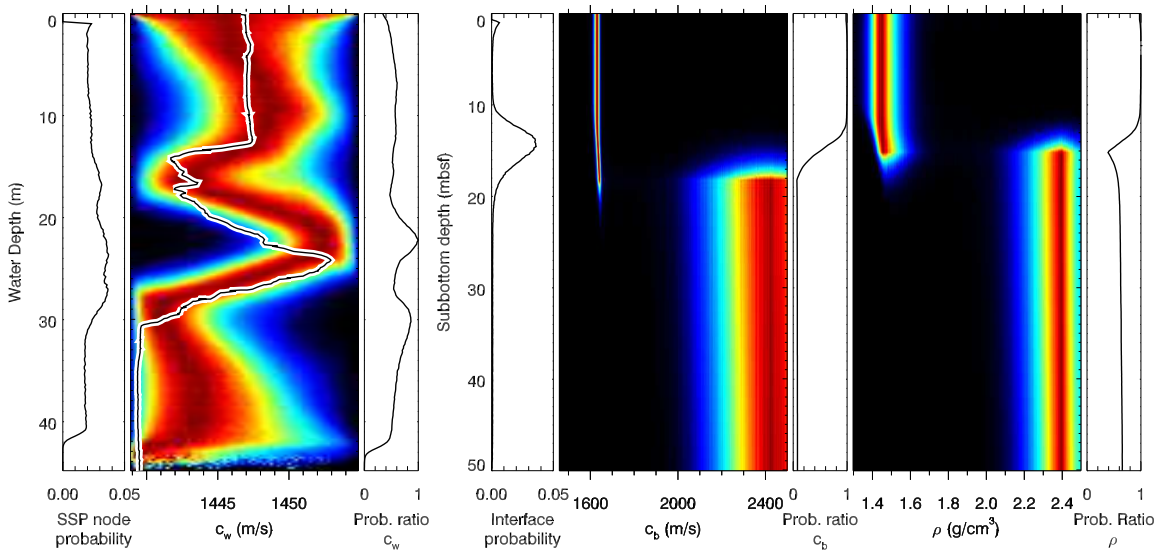

Figure 2.7: Marginal probability profiles for water SSP and subbottom sound speed and density, together with their corresponding node/interface depth profiles and depth normalization profiles. The solid line in the second panel shows the SSP measured 5.7 km from the OBH. Plot bounds are the prior bounds for SSP and geoacoustic parameters, though subbottom sound speed and density have been further constrained by a joint prior PDF (see the Appendix).

Figure 2.9 shows the marginal probability densities for pulse times, range, and water depth. Similar to the simulation study, the marginal density for pulse-A range is essentially the prior PDF. Pulse times are constrained well within their prior bounds. The slope of the joint PDF between pulse-A range and time corresponds to an average modal group speed of approximately 1428 m/s. The 95% credibility interval for water depth is [41.6, 43.3] m. The water depth at the OBH deployment site was measured with an echosounder to be 41 m which is just outside this interval. The discrepancy may be due to the vessel's draft not being taken into account for the water depth measurement (unfortunately this is unknown) or poor echosounder calibration. Water depth measurements in subsequent years near the measurement site were around 43 m. Bathymetric effects are not likely to be significant since the bottom is so flat at the study location; tides are also not significant at this location.

The fit to the data is shown in Fig. 2.10. The relative arrival times from the mode-filtered spectrograms (picked data) are shown with $\times$ symbols and marginal densities of the relative arrival times, calculated from a random sample of 5000 models from the PPD, are shown in grey-scale. There is generally good agreement for all modes, frequencies, and pulses, with some indication of correlated errors. Figure 2.11 shows

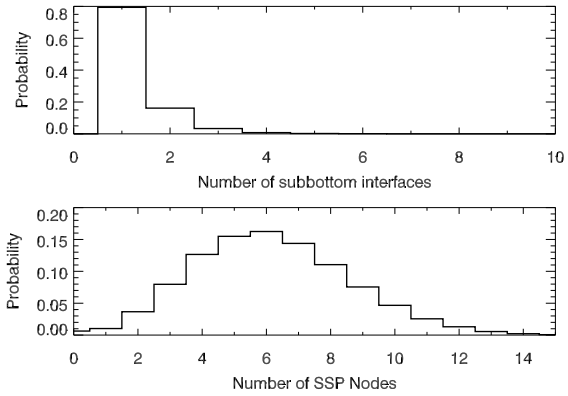

Figure 2.8: Probability distributions of the number of (top) subbottom interfaces and (bottom) SSP nodes.

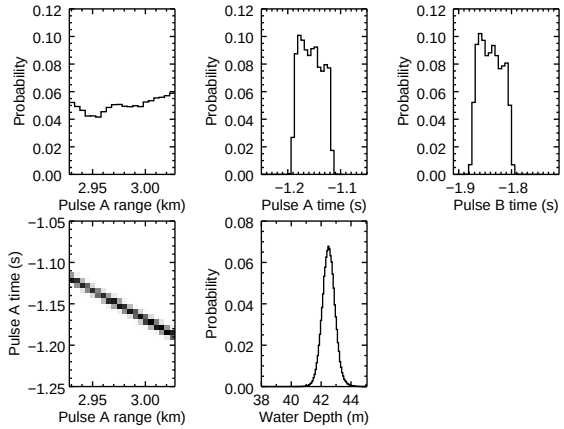

Figure 2.9: Marginal probability densities for pulse range, time, and water depth for Chukchi Sea data. Pulse time axes are restricted within their prior bounds; all other axes ranges indicate prior bounds.

the error statistics for each mode and pulse in the same format as presented earlier. The residual standard deviations generally increase with mode number. This may be due to higher-order modes being more sensitive to finer-scale environmental features that are less likely to be fully range independent. The AR process was required more often for higher-order modes and the AR coefficient a was generally positively correlated with the fraction of time the AR process was required. The standardized total residuals [Eq. (A.4)] from the same sample of models used for Fig. 2.10 were examined (not shown here) to check the validity of the error model assumptions and found to be approximately Gaussian distributed with zero mean and unit standard deviation, and had little autocorrelation between adjacent frequencies of each mode.

The marginal probability profiles for environmental parameters (Fig. 2.7) indi-

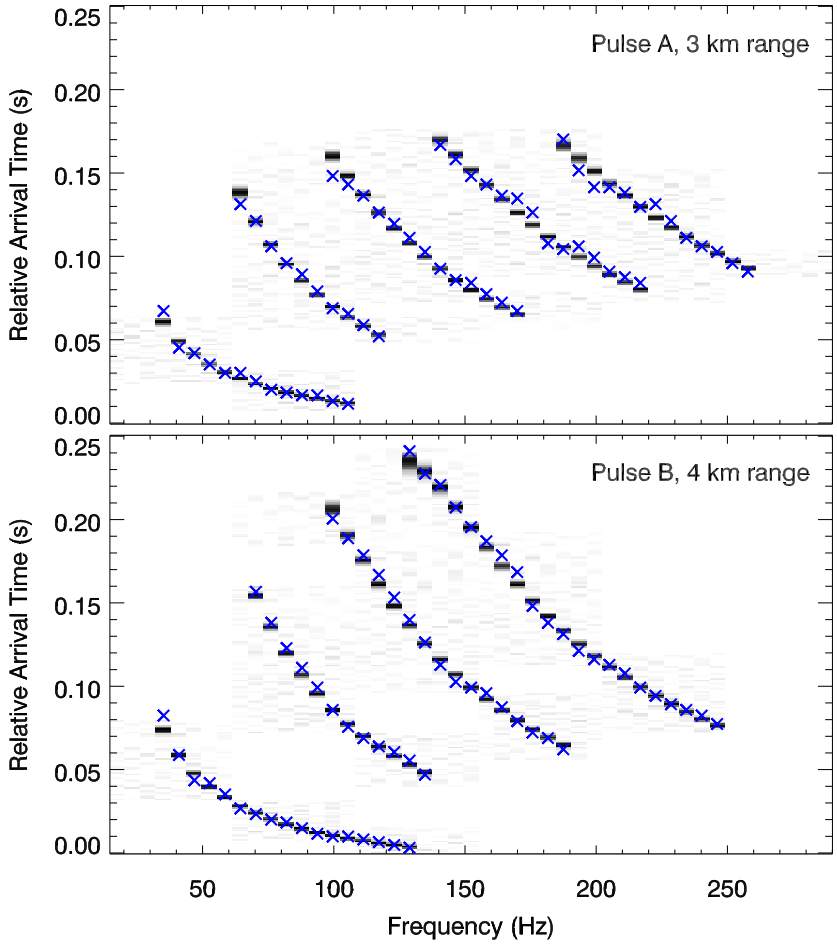

Figure 2.10: Mode relative arrival times for the two pulses calculated from a random sample of models from the PPD (grey-scale PDFs) and the arrival times picked from the measured pulses (×).

cate the sensitivity in terms of the probability density widths; however, it can also be insightful and complementary to investigate environmental sensitivity from a forward-modelling perspective. Figure 2.12 shows the mode functions and transmission loss (TL) computed for the environmental model with highest likelihood from PPD samples collected in the inversion. This model has six SSP nodes, 42 m water depth, and one subbottom layer with thickness 14.5 m, sound speed 1630 m/s, and density 1.45 g/cm^3. The halfspace sound speed and density are 2384 m/s and 2.32 g/cm^3, respectively. The mode functions are shown for the lowest and highest frequencies from each picked mode. TL was computed assuming uniform sediment attenuation of 0.1 dB per wavelength and a point source at 2 m depth (the airgun depth). The water depth and subbottom interface are shown on the plots as horizontal lines. The mode

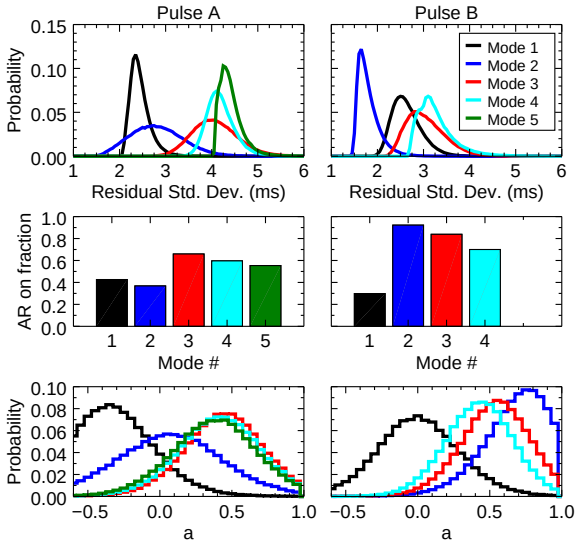

Figure 2.11: Error statistics for modes in pulses (left) A and (right) B. Residual standard deviations, fraction of time the AR process was required, and AR coefficient values are shown in the top, middle, and bottom panels, respectively.

functions show good subbottom penetration into the first ∼15 m of sediment, with lower frequencies penetrating deeper than higher frequencies. For the same frequency, higher-order modes penetrate deeper than lower-order modes (e.g., see the mode functions for the highest and lowest frequencies of modes 1 and 4, respectively, which are both for 128.9 Hz). Mode functions do not penetrate the halfspace well, which is consistent with the large uncertainties on estimated halfspace parameters. SSP resolution is more closely related to the mode function wavelength than the acoustic wavelength, i.e., higher-order modes are more important than higher frequencies for resolving finer-scale SSP features. It is also interesting to note that near the seafloor is an ideal depth for making dispersion measurements as all of the mode functions have relatively high amplitudes at this depth (a hydrophone placed at a mode function null would be insensitive to that mode). The TL plots at 35.2, 99.6, and 252.0 Hz show decreasing seafloor penetration with frequency, but adequate penetration in the upper sediment layer to 4 km range for these frequencies.

Figure 2.12 shows TL [which can be thought of as the absolute value of received level (RL) for a 0 dB source] for one sample of the PPD and therefore does not illustrate the TL uncertainties due to environmental uncertainties. RL uncertainties can be calculated using a set of environmental samples drawn either from the prior density (representing environmental information before the acoustic survey) or from

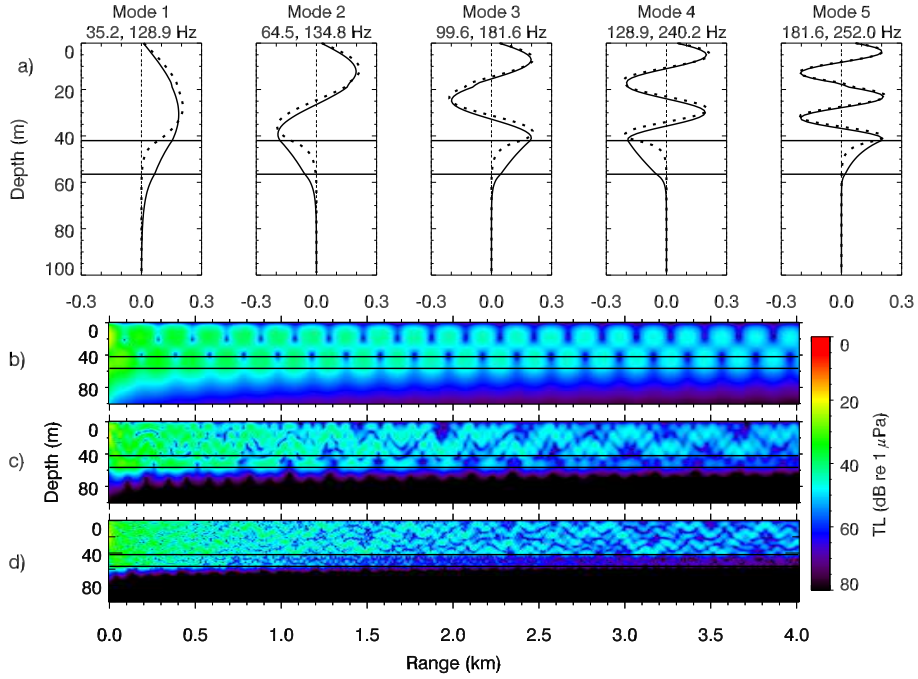

Figure 2.12: (a) Mode functions, and (b)–(d) TL for the maximum-likelihood environmental model. Solid horizontal lines indicate the water depth and subbottom layer interface depth. Mode functions for the lowest and highest frequencies picked from each mode are shown as solid and dashed curves, respectively (frequencies are indicated on each panel). TL is shown for 35.2, 99.6, and 252.0 Hz in (b)–(d), respectively.

the PPD (representing the improved environmental information gained by inverting the modal-dispersion data). In underwater noise environmental impact assessments, the maximum RL over all depths in the water column is often considered as a function of range to estimate distances to sound-level thresholds relevant to the protection of marine mammals. Figure 2.13 shows the normalized probability density for maximum-over-depth RL for a 0 dB source at 2 m depth for 70 Hz using environmental samples drawn from the prior and posterior environmental probability densities (sediment attenuation for all layers and the halfspace in each sample were independently chosen from a uniform distribution bounded by 0 and 0.2 dB per wavelength). The information content of the data has significantly constrained the predicted RL at any given range, and, more importantly, the range at which RLs are reached.

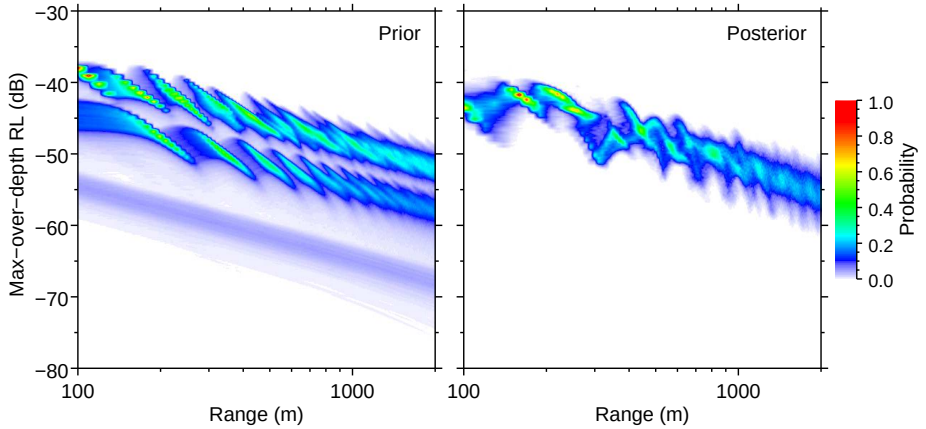

Figure 2.13: Normalized probability densities for predicted maximum-over-depth RL vs. range using environmental samples from the (left) prior and (right) posterior. Source depth is 2 m, source level is 0 dB, and the frequency is 70 Hz.

2.5.1 Headwave inversion

To further corroborate the modal dispersion inversion results for this Chukchi Sea location, I performed an independent analysis of headwave arrival times to estimate the seafloor sound speed. Headwaves are longitudinal waves that travel along the seafloor or subbottom interfaces at the compressional-wave speed of the lower layer. They are excited by compressional waves incident on an interface at the critical angle, and as they propagate they generate upward-propagating compressional waves at the critical angle in the media above the interface.[36] These waves may arrive at a receiver before the direct waterborne acoustic wave if the source-receiver range is sufficiently large. Assuming uniform water and bottom sound speeds c_w and c_b, the arrival times for the waterborne wave and headwave are[36]

$$t_w = \sqrt{r^2 + (h_s - h_r)^2}/c_w \simeq r/c_w, \text{ for } r \gg h_s - h_r, \tag{2.4}$$

$$t_h = \frac{r}{c_b} + (h_s + h_r)\frac{\sqrt{c_b^2 - c_w^2}}{c_b c_w}, \tag{2.5}$$

where r is the source-receiver range, and h_s and h_r are the heights of the source and receiver above the seafloor, respectively. The arrival time difference between the waterborne path and headwave is

$$\Delta t \simeq r\left(\frac{1}{c_w} - \frac{1}{c_b}\right) - (h_s + h_r)\frac{\sqrt{c_b^2 - c_w^2}}{c_b c_w}. \tag{2.6}$$

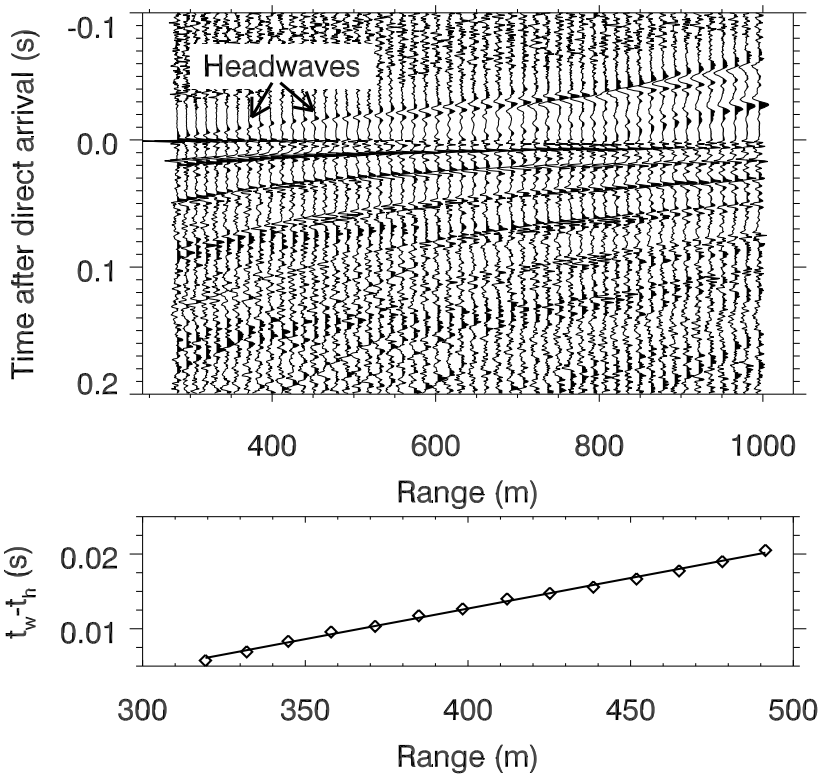

Figure 2.14: Top and bottom plots show stacked pulse waveforms aligned by the direct path arrival and time-of-arrival difference between the direct and headwave arrivals, respectively. AGC has been applied to the waveforms to show headwave arrivals.

This equation is linear with range and the slope of a Δt vs. r plot can be used to calculate the seafloor sound speed if the water sound speed is known.

Low-frequency headwaves ($\sim$140 Hz) were observed in the Chukchi Sea data before the direct-path arrival for pulses measured beyond approximately 250-m range. To determine accurate arrival times, pulse waveforms were stacked by manually time-aligning the direct-path arrivals. The low-frequency, low-amplitude headwaves were amplified by applying an automatic gain control (AGC) filter over the waveforms with a 0.02 s gate (Fig. 2.14, top). The headwave arrival times were picked from the peak arrival time for ranges between 320 and 490 m. A linear fit was calculated for the time difference between the direct and headwave arrivals (Fig. 2.14, bottom). Using Eq. (2.6) and an average water sound speed of 1443 m/s, the slope of the line and its uncertainty correspond to a seafloor sound speed of 1636 m/s and 95% credibility interval of [1629, 1643] m/s. Based on the modal dispersion inversion results, the most-probable subbottom sound speed from the PPD for the top 5 mbsf is 1633 m/s

and the 95% credibility interval is [1612, 1647] m/s, which is in excellent agreement with the headwave results. Analysis of headwave arrival times can provide estimates of layer thicknesses and of sound speeds of deeper layers if headwaves off deeper layer interfaces can be detected in the acoustic data. Headwaves corresponding to the subbottom interface indicated in Fig. 2.7 at ∼10–20 mbsf were not discernable in the acoustic time series, so the thickness of the upper layer and sound speed of the halfspace in the modal inversion results could not be corroborated in this way.

2.6 Summary and conclusion

This chapter presented trans-dimensional Bayesian inversion of modal-dispersion data (both simulated and measured) at a single hydrophone. Mode arrival times were determined from time-frequency analysis of pulses after filtering individual modes using a warping procedure. The arrival times were then used in the inversion to estimate the water sound-speed profile, subbottom properties, and parameters of the survey which were not precisely known (pulse ranges and times). A trans-D framework was applied in three ways for: the water-column SSP, subbottom layering and geoacoustic properties, and first-order auto-regressive error model.

The simulation study characterized the ability of the inversion to estimate environmental and experimental parameters. Limitations of the data processing method were shown through discrepancies in portions of the SSP. Dispersion data predicted using models from the PPD were shown to match the times estimated from synthetic time series via the data processing method. Autocorrelated errors between picked arrival times and the true times from theoretical dispersion curves are attributed to time-frequency data processing limitations which can be a major component of the errors.

Inversion results for the Chukchi Sea survey showed excellent agreement between the estimated SSP and the measured profile. The inversion resolved all significant features of the SSP, often requiring six or more sound-speed nodes to define the profile. The estimated geoacoustic profile showed less structure (two layers) but was well resolved for the shallowest layer. An independent headwave analysis for the seafloor sound speed agreed well with the modal-inversion estimates. The basement properties were less well resolved although the depth of the acoustic basement was well resolved. The ability to resolve SSP and seabed parameters via modal dispersion inversion agreed well (qualitatively) with forward-modelling sensitivity analysis of the

predicted mode functions and transmission loss. A comparison of marginal probability densities for received level vs. range using environmental samples from the prior and PPD showed uncertainties of the distances to received levels are greatly reduced by the information content of the modal-dispersion data. The estimated geoacoustic properties can be used to model sound propagation for noise-exposure estimation or marine-mammal localization at the measurement location.

Overall, modal-dispersion data and the trans-D inversion approach are shown to be capable of estimating water SSP and subbottom sound speed and density profiles to about 10–20 m below seafloor with accuracy sufficient for many scientific purposes. The inversion results here from only two airgun array pulses provided useful profiles. The results are expected to be representative of the average properties over a 3–4 km path and are less susceptible to small-scale variations that could influence spot measurements. Synchronized clocks for the source and receiver could remove the requirement to invert for absolute timing. Pulses could be produced by an autonomous system, so long-term measurements could be possible. An extension to this work could be to apply a trans-D formulation in source-receiver range to estimate range-dependent environmental properties using data from several pulses.

Chapter 3

Bowhead whale localization using asynchronous hydrophones in the Chukchi Sea

This chapter estimates bowhead whale locations and uncertainties using nonlinear Bayesian inversion of their modally-dispersed calls recorded on asynchronous recorders in the Chukchi Sea, Alaska. Bowhead calls were recorded on a cluster of seven asynchronous ocean-bottom hydrophones that were separated by 0.5–9.2 km. A warping time-frequency analysis is used to extract relative mode arrival times as a function of frequency for nine frequency-modulated whale calls that dispersed in the shallow-water environment. Each call was recorded on multiple hydrophones and the mode arrival times are inverted for: the whale location in the horizontal plane, source instantaneous frequency (IF), water sound-speed profile, seabed geoacoustic parameters, relative recorder clock drifts, and residual error standard deviations, all with estimated uncertainties. A simulation study shows that accurate prior environmental knowledge is not required for accurate localization as long as the inversion treats the environment as unknown. Joint inversion of modal-dispersion data from multiple recorded calls is shown to substantially reduce uncertainties in location, source IF, and relative clock drift. Whale location uncertainties are estimated to be 30–160 m and relative clock drift uncertainties are 3–26 ms.

3.1 Introduction

Acoustic localization of vocalizing marine mammals is important for characterizing their spatial distributions, movement behaviours and grouping, and for source level measurements. This chapter develops a Bayesian approach to localize bowhead whales in the Chukchi Sea based on modal dispersion of their calls, including a quantitative uncertainty analysis that accounts for unknown environmental parameters, call source signal, and recorder clock drifts. Several studies have employed localization methods to examine bowhead whale movement and behaviour changes in the Chukchi and Beaufort Seas due to exposures to anthropogenic underwater noise, mainly associated with offshore oil and gas exploration activities.[8,62–64]

The western arctic bowhead whale population migrates annually between wintering areas in the Bering Sea and summer feeding areas off the Mackenzie Delta in the Beaufort Sea. Their fall migration occurs from September through November along the Beaufort coast and through the central northeastern Chukchi Sea.[1,65,66]

Oil and gas exploration and increased shipping has occurred spatially and temporally coincident with bowhead summer feeding and fall migration. There is concern that anthropogenic noise from these activities could affect the whale's use of sounds for critical life functions such as navigating, avoiding predators, and maintaining group structure. A recent study has found bowheads modify their calling behaviour in the presence of quite low levels of seismic survey noise.[8] There is further concern that anthropogenic noise exposures during or prior to subsistence whale hunting could modify bowhead swimming behaviours, potentially making the hunts more difficult;[67] however, the relationship between noise exposure and effects is poorly understood.

A common strategy to reduce marine mammal exposures to anthropogenic noise is to carry out anthropogenic activities during times when animals are not present and at locations away from high animal densities. This approach requires knowledge of the temporal and spatial distributions of animals. Passive acoustic monitoring, based on listening for natural sounds produced by animals, is an increasingly popular method for measuring temporal and spatial distributions that causes no disturbance to the animals (e.g., compared to tagging).

Bowhead whales make a variety of sounds including frequency-modulated (FM) sweeps, moans, amplitude-modulated pulsive calls, and songs.[66,68] During the fall migration, most bowhead calls are moans and low frequency (< 400 Hz) FM sweeps. Recordings of these calls can be used to localize the whales.

Several approaches have been developed for localizing whales using low-frequency calls. Distributions of directional autonomous seafloor acoustic recorders (DASARs) have been used in the Beaufort Sea to triangulate whale locations using the bearing estimates from multiple recorders.[69–71] Clark and Ellison[72] used a linear omnidirectional (time-synchronized) hydrophone array deployed along an ice ridge to estimate whale locations from call arrival time differences. Several studies have used (synchronized) vertical line arrays to exploit sound propagation effects for low-frequency calls in shallow water.[71,73,74] These studies used normal-mode propagation in a variety of ways (e.g., matched-field and matched-mode processing) to estimate source locations. Sei whales, which also make low-frequency calls, have been tracked in three dimensions by using normal-mode models to back-propagate calls recorded on synchronized horizontal and vertical arrays.[75]

There has been some effort to obtain range estimates for whales using a single hydrophone because of the relative simplicity and low cost of the equipment required. In particular, range estimation based on low-frequency right whale and bowhead whale calls has been achieved by exploiting the frequency-dependence of acoustic normal mode group speeds in shallow-water environments.[22,76] In shallow water, the environment supports a limited number of propagating modes, each of which supports a continuum of frequency bands that do not overlap. The frequency- and mode-dependence of modal group speeds (which I collectively refer to as *modal dispersion* in this chapter) is well modelled with normal-mode theory.[19] Signals disperse as they propagate, with higher frequencies generally travelling faster than lower frequencies within a mode, and higher-order modes generally travelling slower than lower-order modes for a given frequency. This frequency-dependence affects mode arrival times in proportion to the source-receiver range (within the range-independent assumption) so dispersion measurements can be made by analyzing signals recorded at a single hydrophone using time-frequency (TF) methods. However, modal arrival times also depend on environmental properties [e.g., water-column sound-speed profile (SSP) and seabed geoacoustic parameters] and on the TF characteristics of the acoustic signal emitted by the source [the instantaneous frequency[77] (IF) function], which are usually not well known in marine mammal applications, complicating localization. Resolving mode arrival times in the TF plane requires sufficient signal bandwidth and is also dependent on the difference in modal group speeds and the signal-processing techniques applied. For relatively short-duration FM calls received at long ranges, modes are well separated in time and arrival times can be determined from the mag-

nitude of a short-time Fourier transform (STFT). At close ranges, mode arrivals are difficult to separate in the TF plane. Mode-warping techniques used to improve the TF resolution of modes for close-range dispersion measurements of impulsive sounds[21] have recently been modified and successfully applied to FM bowhead whale calls.[22] This chapter applies the modified mode-warping technique to FM calls or portions of calls that monotonically increase or decrease in frequency with time.

The single-hydrophone range-estimation studies using normal-mode theory[22,76] parameterized the acoustic environment with a range-independent model consisting of a water layer over a fluid halfspace. Wiggins *et al.*[76] fixed environmental parameter values using historical information and assessed sensitivity of modal group speeds by varying the mean water sound speed and seafloor sound speed independently for a few parameter perturbations. Bonnel *et al.*[22] used a Pekeris waveguide with fixed water sound speed from conductivity-temperature-depth (CTD) measurements and varied the seafloor sound speed over a discretized interval. In that study, the bathymetry was strongly range-dependent; however, independent DASAR measurements showed the single-hydrophone range estimates were reasonably accurate despite the violation of the range-independent assumption. It is difficult to assess the uncertainty of range estimates using these approaches in general without additional information because the fixed environmental parameterization (e.g., Pekeris waveguide) and constrained parameter values may not provide an appropriate level of model complexity that corresponds to the information content of the data. Hence, these approaches could underparameterize the environmental model which could, in turn, lead to underestimation of range uncertainty.

This chapter estimates bowhead whale locations and their uncertainties in the horizontal plane from the dispersion of normal modes recorded with multiple non-synchronized omni-directional hydrophones in a shallow-water (approximately) range-independent environment. I use a general model for the unknown environment to rigorously quantify its effect on localization uncertainties (the general idea of accounting for environmental uncertainty in localization is sometimes referred to as focalization[78]). In particular, a trans-dimensional (trans-D) Bayesian inversion approach is applied for the water SSP and for the subbottom to allow the data to estimate how much environmental structure is appropriate.[35] The SSP has a $1/c_w^2$ piecewise-linear gradient (c_w is water sound speed) defined by an unknown number of depth/sound-speed nodes. The subbottom consists of an unknown number of homogeneous sediment layers, each having unknown thickness, sound speed, and density,

overlying a halfspace. The trans-D algorithm samples over the number of SSP nodes and subbottom layers and their parameter values so the range estimates and their uncertainties account for realistic environmental uncertainty.

A standard time-difference-of-arrival (TDOA) localization approach is not applicable here because the recorders were not synchronized due to clock drift after deployment. Using arrival time differences between modes from multiple asynchronous recorders could be used as data in a combined localization/environmental inversion, but this ignores information contained in calls or portions of calls that have only one detectable mode. Utilizing this information requires treating as unknowns the source IF (a function of frequency to be estimated) and the relative recorder clock drifts, and inverting arrival times (as opposed to arrival time differences). While this approach involves more unknown parameters, it allows more data information to be used, providing whale locations based on recorded calls composed of as few as one detectable mode. Additionally, the source IF and its uncertainty are quantitatively estimated using this approach, which may be of biological significance. I use this approach to invert the modal arrival times measured at each recorder relative to a reference recorder clock. Range information in the data for multiple distributed recorders constrains the whale location in the horizontal plane. The data also constrain the relative clock drifts, providing information to synchronize the recorders. I apply the new algorithm to single and multiple whale calls and show that localization and synchronization results are significantly improved if arrival times from multiple calls are inverted jointly. The Bayesian inversion developed here estimates parameter values and uncertainties for whale location, source IF, water SSP (including effective water depth), subbottom layering and geoacoustic parameters, relative recorder clock drift (synchronization), and residual error statistics. To my knowledge, whale localization based on inversion of modal-dispersion data from FM whale calls from asynchronous recorders has not been reported previously. This method can be applied to data collected by relatively inexpensive recorders that are easy to deploy (compared to synchronized hydrophone arrays or directional sensors).

This method is limited to shallow-water, range-independent environments, with low-frequency FM calls that disperse as they propagate. The source-receiver range has to be large enough such that mode dispersion is quantifiable (the minimum range is generally dependent on the TF characteristics of the call and the environmental properties) but not so large that range-dependent effects violate the range-independent approximation. Mode amplitudes are not required except in the sense that they

must be higher than background noise such that accurate mode arrival times can be determined. I applied a threshold of approximately 5 dB for this chapter.

Whale depth is not required or estimated using this approach; however, a whale calling at the depth of a mode-function node will not excite that mode. In general, a missing mode will not necessarily preclude successful localization, particularly in multi-call inversions. However, if a missing mode leads to misidentification of the mode (e.g., mode 3 is identified as mode 2), the localization will likely fail. Applying the inversion to multiple whale calls may increase the robustness if the call depths differ, as wrongly-identified mode arrivals would likely be fit poorly and could be reassigned in a subsequent inversion.

The trans-D Bayesian inversion is applied to acoustic data collected from August to October 2013 using seven autonomous ocean-bottom hydrophone (OBH) recorders which were part of an underwater sound measurement program in the Chukchi Sea, Alaska.[18] The program was originally designed to determine ambient noise levels, quantify sound levels from oil and gas exploration activities, and investigate spatial and temporal distributions of marine mammals based on their calls. The seven OBHs recorded thousands of bowhead whale calls including low-frequency FM sweeps. Many of these sweeps showed significant dispersion in the TF plane and were recorded on multiple OBHs. In this chapter I apply the Bayesian focalization algorithm in a simulation study to investigate the impact of varying degrees of environmental knowledge on localization and then to nine bowhead whale calls recorded within 3.25 minutes on multiple OBHs.

3.2 Theory

3.2.1 Data processing

Bowhead whale calls include low-frequency moans and sweeps that can excite several propagating modes in shallow waters, which can be modelled using normal-mode theory.[19] Modes propagate with different group speeds that are dependent on the environment, i.e., the water-column SSP and geoacoustic properties of the subbottom. At long ranges, mode arrivals (for a fixed frequency) are well separated in time and can be determined from the TF representations of a recorded call. A recent study used a mode warping technique to improve the modal TF resolution of non-impulsive bowhead whale calls[22] based on a similar technique used previously

for impulsive sounds.[21] To apply mode warping to non-impulsive signals,[22] the received signal is first deconvolved with an approximate (empirical) source IF designed to decrease the received signal duration for subsequent mode warping. In practice the empirical source IF is manually estimated by an IF function that has a shape that is similar to, but precedes, the mode 1 arrival. The deconvolved signal is then warped using standard methods and transformed into the warped-TF domain using a STFT. Each mode is filtered in the warped-TF domain, transformed back into the warped-time domain using an inverse STFT, unwarped into the original time domain using standard methods, and transformed into the TF domain with a STFT. The mode arrival times (picks) are determined from the time of maximum energy of the deconvolved filtered mode in the TF domain and then corrected using the empirical source IF. The inversion is not sensitive to the empirical source IF because this correction undoes the effect of the initial source IF-based deconvolution. For impulsive sounds in an approximately range-independent waveguide, warping transforms the dispersed modes into near-constant frequency tones that can be band-pass filtered to separate the modes. For frequency sweeps, deconvolution and warping separates the modes, but it is often difficult to achieve sufficient separation such that a band-pass filter isolates individual modes. Hence, warped modes are filtered using a TF mask (a manually defined polygon in TF space) and transformed back into the time domain using an inverse STFT. This process improves the accuracy of estimated mode arrival times and extends the bandwidth over which modes are resolved. Figure 3.1 illustrates the data processing procedure for a bowhead whale call recorded in the Chukchi Sea (described further in Sec. 3.4).

For each filtered mode, a spectrogram (magnitude of STFT) is computed using a Hanning window with 99% overlap (Fig. 3.1 considers a 16 384-point window for data sampled at 64 kHz). The mode arrival time data are limited to frequencies where mode arrivals have high enough levels such that the arrival times are not significantly influenced by background noise. In practice this can be difficult to determine *a priori*; however, poor data can often be identified by performing a preliminary inversion to detect outliers (i.e., data residuals that lie several standard deviations outside of the assumed Gaussian probability density). Those data can then be discarded and the inversion rerun on the reduced data set.

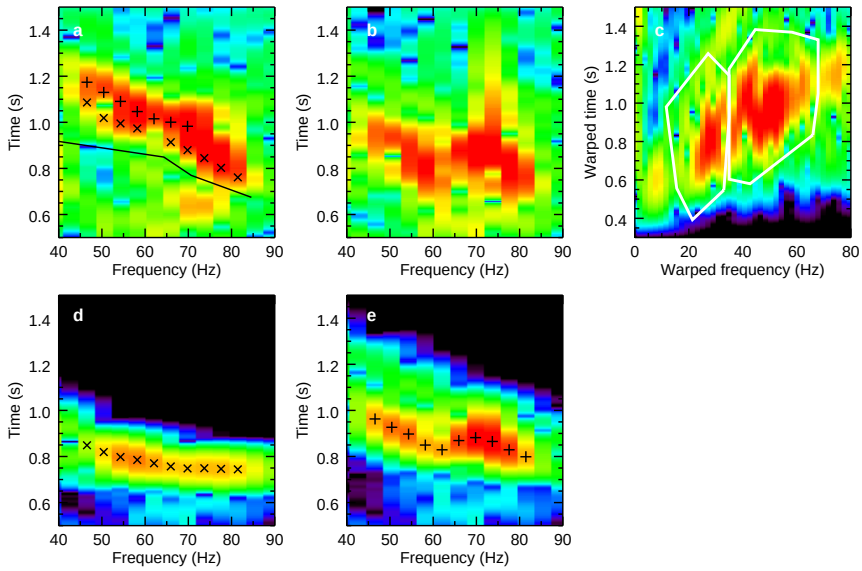

Figure 3.1: Example of warping TF analysis. (a) Recorded bowhead whale call spectrogram and empirical source IF (solid line). (b) Spectrogram after deconvolution by source IF. (c) Warped spectrogram showing two modes and the inverse TF masks (white polygons). (d) and (e) Filtered spectrograms with deconvolved data picks ($\times$ and $+$) for modes 1 and 2, respectively. Reconvolved picks are shown on panel (a), where some picks have been removed due to insufficient signal level.

3.2.2 Bayesian inversion

The mode arrival-time picks indicated on Fig. 3.1(a) are dependent on the whale location, source IF, environment, and relative recorder clock offsets. The arrival time of mode m at frequency f for whale call w at recorder a is

$$t_{wam}(f) = \tau_w(f) + \frac{\sqrt{(x_w - X_a)^2 + (y_w - Y_a)^2}}{v_m(\mathbf{e}, f)} + \Delta_a, \tag{3.1}$$

where $\tau_w(f)$ is the source IF [i.e., $\tau_w(f)$ is the time that frequency f was emitted by whale w], x_w and y_w are the easting and northing coordinates of the whale, X_a and Y_a are the coordinates of the recorder (considered known), $v_m(\mathbf{e}, f)$ is the mode group speed which depends on the environmental model $\mathbf{e}$, and Δ_a is the recorder clock offset relative to a reference recorder. The inversion uses a trans-D Bayesian formulation which is briefly described here (see Warner *et al.*[35] for details). The range-independent environmental model $\mathbf{e}$ consists of a water column with unknown depth and SSP over a seabed consisting of an unknown number of homogeneous layers (each layer characterized by unknown thickness, sound speed, and density)

overlying a halfspace of unknown geoacoustic parameters. Mode group speeds are calculated for an environmental model using the normal-mode code ORCA[56] and are converted to predicted modal arrival times using the whale source IF and location, as well as the relative recorder clock offset [Eq. (3.1)], all of which are unknown model parameters to be estimated in the inversion (the model also includes error standard deviations, see Sec. 3.2.3). In a Bayesian formulation the solution consists of properties of the posterior probability density (PPD) of the model parameters given the measured data and prior information. A reversible-jump Markov-chain Monte Carlo[32] algorithm is applied to sample the PPD over a trans-D model space in which the number of SSP nodes and seabed layers can change by probabilistically accepting transitions between model parameters/parameterizations according to the Metropolis-Hastings-Green criterion.[32] The transition acceptance probability depends on the prior, proposal, and likelihood ratios, with the likelihood defined by the assumption of Gaussian-distributed errors with unknown standard deviation for each whale call (discussed below in Sec. 3.2.3). Uniform bounded priors are used for all model parameters, with an additional joint prior that constrains subbottom sound speed and density to physically realistic combinations.[25,26] The Markov chain samples over the number and parameters of SSP nodes and subbottom layers to estimate the trans-D PPD. Parallel tempering[40–43] is applied to increase the dimension-jump acceptance rate. Fixed-dimensional parameters (i.e., source IF, whale location, and relative clock offset) were found to be highly correlated and perturbations to these parameters had to be applied in principal-component (rotated) space[38] to achieve convergence.

3.2.3 Likelihood

The likelihood function is defined by the residual error probability density function (PDF). These errors result from measurement, data-processing, and theory errors, the statistics of which are often unknown. The data residuals for model $\mathbf{m}_k$ are given by $\mathbf{d} - \mathbf{d}(\mathbf{m}_k)$, where $\mathbf{d}$ and $\mathbf{d}(\mathbf{m}_k)$ are the measured and predicted data (i.e., mode arrival times in seconds), respectively, and k indexes possible model parameterizations (number of SSP nodes and subbottom layers). In this chapter, the residual errors are assumed independent and Gaussian distributed; the validity of this assumption is checked *a posteriori*. For N data with independent Gaussian-distributed errors, the

likelihood function is

$$L(k, \mathbf{m}_k) = \frac{1}{(2\pi)^{N/2}|\mathbf{C}_d|^{1/2}} \exp\left[-\frac{1}{2}(\mathbf{d} - \mathbf{d}(\mathbf{m}_k))^T \mathbf{C}_d^{-1}(\mathbf{d} - \mathbf{d}(\mathbf{m}_k))\right], \tag{3.2}$$

where $\mathbf{C}_d$ is a diagonal data covariance matrix. Some previous modal-dispersion inversions have assumed different error standard deviations between modes[35,47] but this requires many data (arrival times) for each mode to constrain each standard deviation. The whale calls analyzed for this chapter have relatively few modes and frequencies per mode so applying such a granular error parameterization could over-parameterize the problem and result in overestimated parameter uncertainties (and also increase the computational expense of the inversion). I therefore assume error standard deviations (σ_w) that vary only between whale calls so σ_w is constant over recorder, mode, and frequency. Let $\mathbf{d}_{wam}$ represent a vector of modal arrival times at N_{wam} frequencies. The likelihood function for uncorrelated noise is the product

$$L(k, \mathbf{m}_k) = \prod_{w=1}^{W} \prod_{a=1}^{A} \prod_{m=1}^{M_{wa}} \frac{1}{(2\pi\sigma_w^2)^{N_{wam}/2}} \exp\left[-\frac{|\mathbf{d}_{wam} - \mathbf{d}_{wam}(\mathbf{m}_k)|^2}{2\sigma_w^2}\right], \tag{3.3}$$

where W is the total number of whale calls considered, A is the total number of recorders that detected at least one call, and M_{wa} is the number of modes considered for call w on recorder a. For recorders that do not detect a particular whale call the term within the products is replaced by unity. Substituting Eq. (3.1) into this equation and optimizing over inter-recorder clock offset (i.e., setting $\partial L/\partial \Delta_a = 0$) leads to a maximum-likelihood estimate for the inter-recorder clock offset Δ_a:

$$\hat{\Delta}_a(\mathbf{m}_k) = \frac{\sum_w^W \sum_m^{M_{wa}} \sum_f^{N_{wam}} \left[d_{wam}(f) - \tau_w(f) - |\mathbf{r}_{wa}|/v_m(f)\right]/\sigma_w^2}{\sum_w^W \sum_m^{M_{wa}} N_{wam}/\sigma_w^2}, \tag{3.4}$$

where $\mathbf{r}_{wa}$ is $(x_w - X_a, y_w - Y_a)$. Equation (3.4) provides an expression for Δ_a in terms of the data and the other unknown parameters which can be used to sample implicitly over Δ_a by sampling explicitly over the other parameters.[79] This formulation assumes the relative recorder clock offset does not change significantly between the first and last inverted whale calls.

3.3 Simulation study

This section illustrates and verifies the inversion methodology in a simulation study based on recordings of bowhead whale calls from the Chukchi Sea (described in Sec. 3.4). This study considers calls from five whales at different locations about a cluster of seven asynchronous recorders, labeled A–G. The recorder locations for the simulation are taken from coordinates of a deployed recorder cluster.[18] The source IF are linear frequency up- or down-sweeps and the relative clock offsets are constant between calls. The environmental model for the simulation has two subbottom layers (one interface) and two water-column SSP nodes (in addition to unknown water sound speeds at the surface and bottom). The true parameter values and the bounds of the uniform prior PDFs assumed for all environmental parameters are listed in Table 3.1 (Quijano *et al.*[26] describes the joint prior PDF for subbottom sound speed and density used here). The easting and northing prior bounds on the whale locations are ±10 km from recorder A, the source IF prior bounds are 10 s prior to the call arrival time on the reference recorder (recorder A for all calls except call 3 which had reference recorder D), and the error standard deviation prior for each whale call is uniform from 1 to 100 ms. Mode arrival times at seven frequencies for modes 1 and 2 were simulated using Eq. (3.1) for each call with exact modal group speeds calculated by the normal-mode code ORCA.[56] Data were simulated for a minimum of two and up to all seven recorders, depending on the call. Gaussian-distributed errors were added to the synthetic data with standard deviations that were constant over recorders, modes, and frequencies but varied between whale calls from 12 to 17 ms. Table 3.2 lists the recorders that detected each call and the corresponding error statistics.

Inversions for nine scenarios were performed on the synthetic data. Scenarios 1–5 invert individual calls 1–5, respectively; scenario 6 jointly inverts all five calls (environmental parameters are inverted for in each scenario). Scenarios 7–9 are variations on scenario 1 that investigate the effect on localization uncertainties of knowing the SSP and/or geoacoustic parameters: scenario 7 considers known SSP but unknown geoacoustics, scenario 8 considers known geoacoustics but unknown SSP, and scenario 9 considers known SSP and geoacoustics. Inversions were performed on the synthetic data sets with approximately 500 000 samples drawn from the PPD via the trans-D Bayesian inversion and fixed-length chain thinning[60] restricted the number of samples that were saved to 100 000. All inversions were found to produce approximately

Table 3.1: Environment parameter values and prior bounds for the simulations. Note that subbottom sound speed and density were further constrained by a joint prior bound.

Parameter	True value(s)	Prior
c_w at surface (m/s)	1450	[1435,1455]
c_w at seafloor (m/s)	1440	[1435,1455]
Water depth z_b (m)	41	[38,50]
# SSP nodes	2	[0,5]
SSP node depths (m)	[20,24]	[0,z_b]
SSP node $\boldsymbol{c}_w$ (m/s)	[1450,1440]	[1435,1455]
# subbottom interfaces	1	[0,6]
Interface depths (m)	[14.5]	[0,50]
Layer speed c_b (m/s)	[1630]	[1460,2500]
Basement c_b (m/s)	2384	[1460,2500]
Layer density ρ (g/cm^3)	[1.45]	[1.3,2.5]
Basement ρ (g/cm^3)	2.32	[1.3,2.5]

Table 3.2: Simulated whale call parameters.

Call	Recorders	x_w (km)	y_w (km)	σ_w (ms)
1	A–G	3	3	14
2	A–D	7	4	14
3	D, E	8	2	17
4	A–D, F, G	−2	−1	12
5	A–D, F, G	−4	3	15

Gaussian-distributed data residuals (not shown).

Figure 3.2 shows the two-dimensional marginal probability densities for whale locations in scenarios 1–9. Each call marginal density is normalized by its maximum value to more clearly illustrate the density shapes. The true whale locations are shown as the intersection of the dashed lines (lines for scenario 6, which includes all sources, are omitted to reduce clutter) and the recorders that detected calls are shown with × symbols. Inset plots at 3 times magnification are shown in some panels to illustrate small marginal density shapes. The extents of the marginal densities show the estimated uncertainty of the whale locations. The probability contours for scenarios 1, 4, and 5 are approximately elliptical. Scenarios 2 and 3 have relatively high uncertainties because the simulated calls were not detected on recorders off the cluster's main axis (approximately NE–SW), resulting in symmetric but non-elliptical probability

contours. The localization results for scenario 6 (i.e., calls from scenarios 1–5 inverted collectively) show substantial improvement over all corresponding individual whale call inversions. The marginal location PDFs for calls 1, 4, and 5 are much narrower than those of their corresponding single-call inversions. The symmetric PDF for call 3 is well constrained but multi-modal about the axis of the receivers D and E on which it was recorded (see scenario 3 result). Parallel tempering was found to be essential for sampling these multi-modal PDFs and achieving PPD convergence. Scenario 6 clearly shows the localization improvements from joint inversion of modal-dispersion data from multiple whale calls. Resolution of other parameters (especially relative recorder clock offset) are also greatly improved by joint inversion and are discussed later in this section. The localization results for scenarios 7 and 8 are very similar to those of scenario 1, indicating that precise prior knowledge of the SSP and/or geoacoustic parameters does not significantly improve localization results, given that the environmental parameters are included in the inversion. Scenario 9 shows minor localization improvement when both SSP and geoacoustic parameters are known, but the improvement is much less than that from joint inversion over multiple whale calls. Table 3.3 quantifies the localization results with two-standard deviation (2SD) uncertainties of the easting and northing estimates for the simulated calls.

Figure 3.3 shows the normalized marginal probability densities for source IF 1–5 in scenarios 1–6. The left panels show source IF for calls in scenarios 1–5 (inverted individually) and the right panels show the source IF for the same calls in scenario 6 (inverted jointly). Note that scenario 3 [panel (c)] had reference recorder D (since only recorders D and E detected the call). To compare source IF probability densities for this scenario with scenario 6, which had reference recorder A, estimated and true times for scenario 3 were adjusted to account for the difference in reference recorders using the true relative clock offset (-8.2 s). In all scenarios the shape of the source IF is well resolved and most of the mismatch is associated with a frequency-independent time shift that is due to uncertainties of the relative recorder clock offsets and/or source locations. The time shifts are more accurately constrained in scenario 6 due to the smaller uncertainty on source locations and clock offsets (the latter is discussed later in this section).

Figure 3.4 shows the marginal probability profiles for the SSP and geoacoustic parameters for scenarios 1 and 6 (corresponding results for scenarios 2–5 are similar to those of scenario 1 and are omitted for brevity). To more clearly show the probability structure over a wide range of values, the probability profiles are normalized inde-

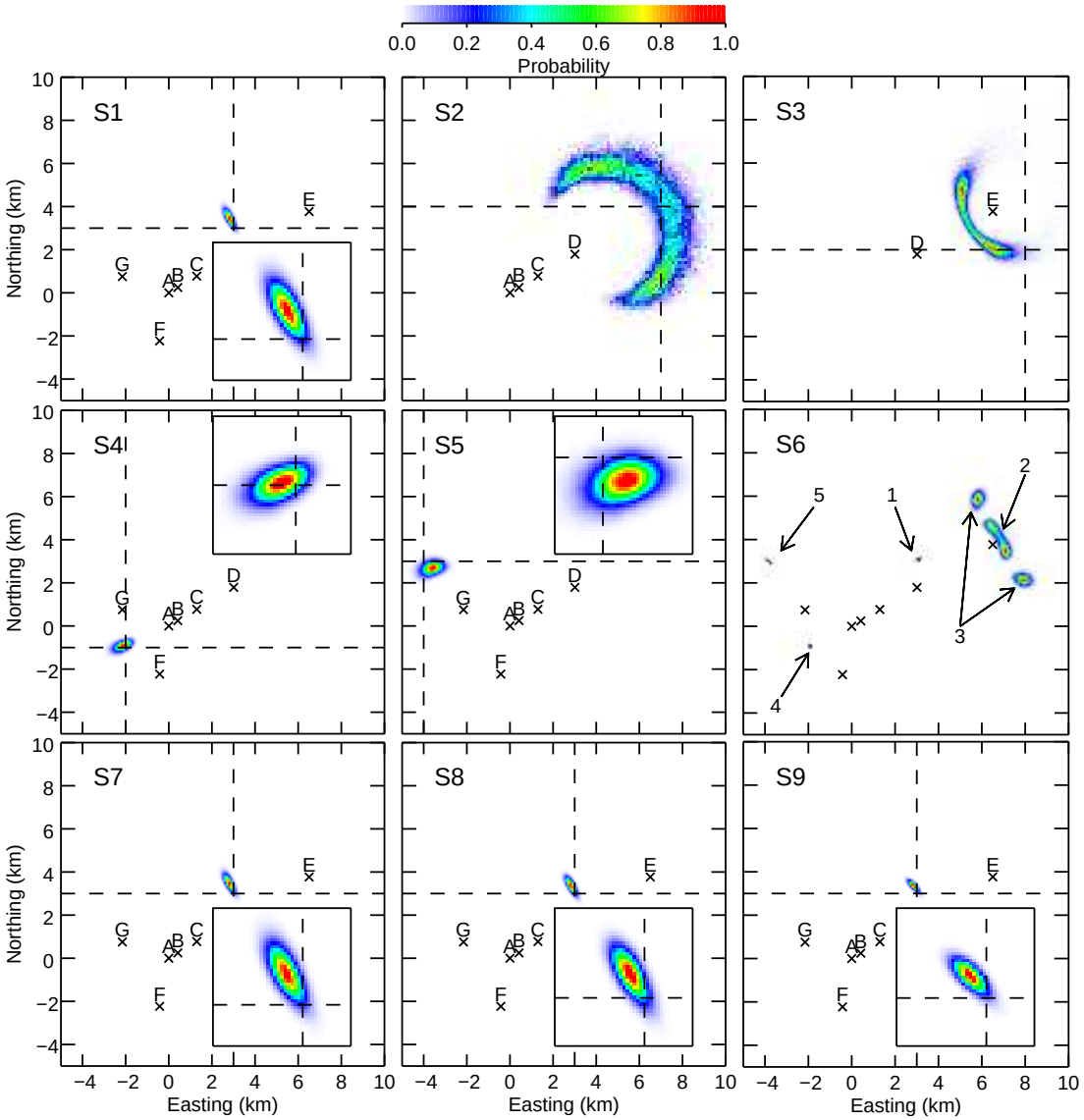

Figure 3.2: Marginal probability densities for whale location(s) in simulated scenarios 1–9 (described in text). True whale locations are shown with dashed lines (except scenario S6), and receivers that recorded the call(s) in each scenario are indicated with × symbols. Inset plots show the corresponding marginal densities at 3 times magnification.

pendently at each depth. The probability-ratio profiles, plotted to the right of each marginal profile, indicate the relative probability as a function of depth. This figure also shows the marginal profiles for the SSP-node and subbottom-interface depths.

The marginal SSP probability density is relatively uniform over depth in scenario 1, indicating that little structure is resolved by the data. The node depth PDF

Table 3.3: Localization results and mean residual error standard deviations ($\overline{\sigma}_w$) for inverted simulated calls. Mean location and 2SD are given as easting and northing pairs. Note that the marginal probability density contours for whale locations for calls 2 and 3 are not elliptical so results for these calls should be considered in the context of the marginal location probability densities (see Fig. 3.2)

Call	Scenario	Mean Location (km)	2SD (km)	$\overline{\sigma}_w$ (ms)
1	1	2.77,3.40	0.32,0.53	11.2
1	6	3.01,3.01	0.13,0.11	11.7
1	7	2.75,3.44	0.32,0.54	11.6
1	8	2.78,3.32	0.32,0.51	11.8
1	9	2.79,3.29	0.30,0.32	11.9
2	2	5.98,3.61	3.34,4.40	15.3
2	6	6.76,3.95	0.65,1.03	15.6
3	3	5.92,3.46	2.01,2.93	18.7
3	6	6.83,3.94	2.13,3.72	19.5
4	4	−2.23,−0.98	0.53,0.34	12.4
4	6	−2.00,−0.99	0.02,0.02	12.4
5	5	−3.70,2.64	0.67,0.44	14.0
5	6	−3.92,2.94	0.13,0.08	14.6

is uniform over most of the water column but decreases to zero near the bottom (over the prior bounds for water depth). The marginal distribution for the number of SSP nodes and PDF for the water depth are approximately uniform (not shown). Higher-order modes, which have smaller mode function wavelengths (in depth), are required for resolving finer-scale SSP structure.[35] The geoacoustic probability profiles agree well with the true profile given their uncertainties. Subbottom sound speed and density are resolved within their prior bounds; however, the resolution for density within the prior bounds is primarily due to the joint prior bound with sound speed.

The corresponding results for scenario 6 show some narrowing of the SSP probability density in the lower portion of the water column but the overall shape of the SSP is not resolved. The geoacoustic profiles are similar to those of scenario 1. This suggests there is little benefit to inverting dispersion data from multiple whale calls in terms of environmental resolution; however, there could be more benefit if multiple whale calls cover different frequency ranges and/or more modes are present.

Table 3.4 lists the mean recorder clock offsets relative to reference recorder A and the estimated (2SD) uncertainties. The single call inversions (scenarios 1–5, and 7–9) provide estimated clock offsets with uncertainties that vary between 8 and 739 ms.

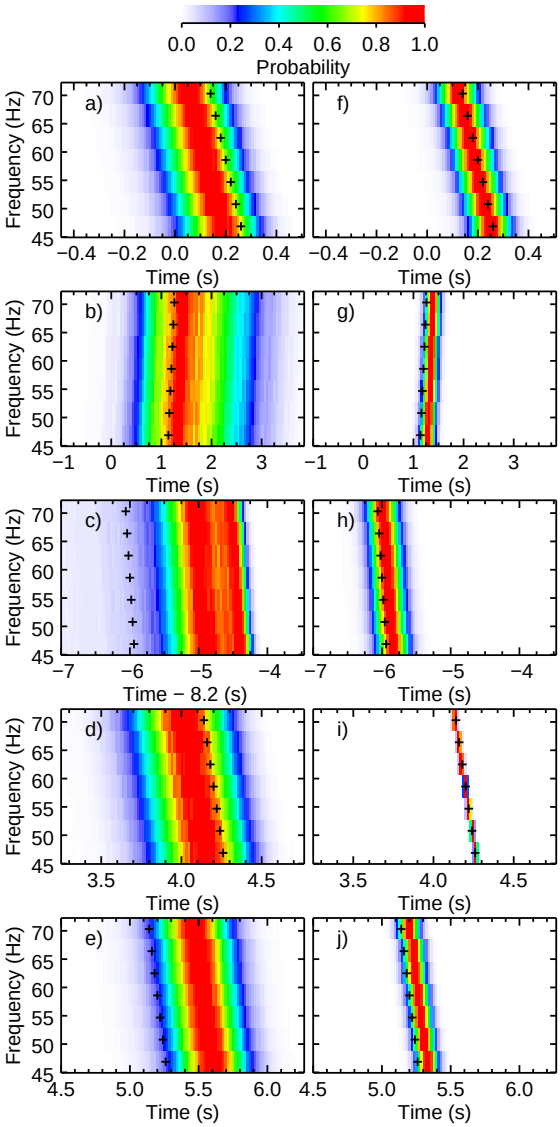

Figure 3.3: Normalized marginal probability densities for simulated whale call source IF in scenarios 1–5 (panels a–e) and scenario 6 (f–j). True source IF are shown with + symbols.

Clock offset uncertainties are correlated with distance from the reference recorder (e.g., offset uncertainties for B, the closest recorder to A, were typically lowest) and anticorrelated with the number of recorders that detected the call. Each detection provides a source-receiver range estimate, and having more range estimates better constrains the whale location, which in turn improves clock offset estimates. The multi-call inversion (scenario 6) produced significantly reduced clock offset uncertainties compared to the single-call inversions. Each whale call constrains the clock offsets

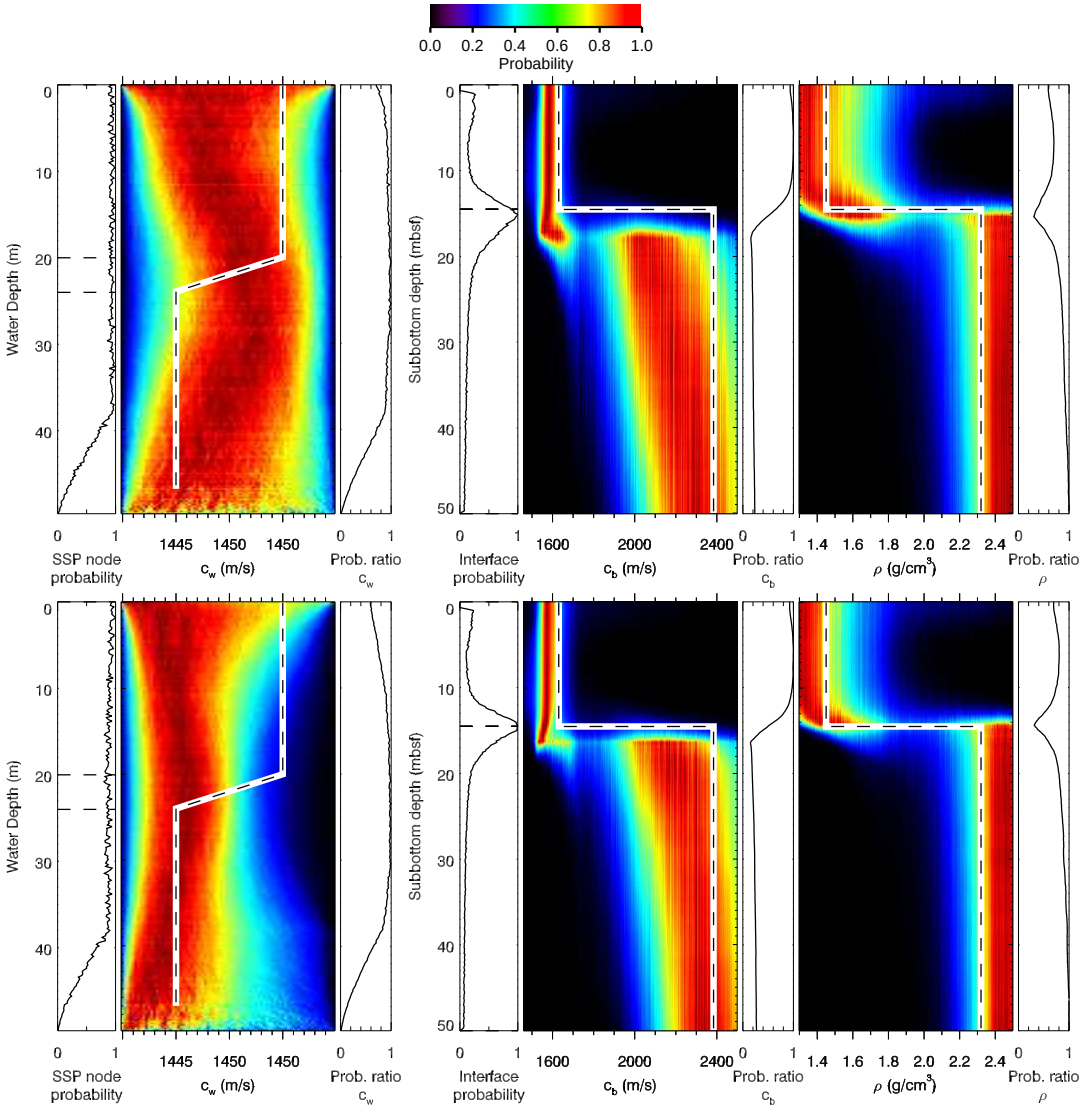

Figure 3.4: Marginal probability profiles for water SSP and subbottom sound speed and density, together with their corresponding node/interface depth profiles and depth normalization profiles. Top and bottom panels show results from simulation scenarios 1 (single whale call) and 6 (multiple whale calls), respectively. Plot bounds are the prior bounds for SSP and geoacoustic parameters, although subbottom sound speed and density are further constrained by a joint prior PDF. True parameter values are shown with dashed lines.

in different ways and to different degrees. The multi-call inversion requires that all data are fit simultaneously, which requires an effective averaging of the clock offset estimates. The benefit comes from having multiple whale calls at locations spread out among the hydrophone cluster (inverting multiple calls from a single location

Table 3.4: True and estimated mean relative recorder clock offsets (relative to recorder A) and 2SD uncertainties (s) for the simulation scenarios. Note that estimated clock offset for scenario 3 has been adjusted to account for the difference in reference recorders (D vs. A in scenarios 3 and 6, respectively) using the true relative clock offset (−8.2 s) to allow direct comparison with results in other scenarios.

Scenario	Δ_B	Δ_C	Δ_D	Δ_E	Δ_F	Δ_G
True	14.1	18.3	8.2	-2.3	-20.8	-3.4
1	14.09,0.018	18.25,0.065		-2.32,0.252	-20.85,0.063	-3.27,0.162
2	14.08,0.042	18.22,0.157	7.88,0.569			
3				-2.88,0.739		
4	14.11,0.008	18.31,0.014	8.22,0.025		-20.80,0.253	-3.25,0.283
5	14.10,0.039	18.28,0.105	8.14,0.184		-20.78,0.166	-3.39,0.117
6	14.10,0.004	18.30,0.004	8.20,0.010	-2.27,0.227	-20.80,0.014	-3.40,0.009
7	14.09,0.018	18.24,0.067		-2.31,0.258	-20.86,0.063	-3.26,0.165
8	14.09,0.017	18.25,0.063		-2.35,0.252	-20.84,0.066	-3.29,0.159
9	14.09,0.014	18.26,0.049		-2.36,0.227	-20.85,0.054	-3.30,0.117

would not improve clock offset estimates to this extent). The clock offset uncertainty reduction from a multi-call localization approach increases with the number of calls detected on a given recorder provided the magnitude of the offset uncertainties for single-call inversions are relatively consistent. For example, the uncertainty for Δ_C decreases by a factor of 3.5 (relative to the smallest uncertainty from the single-call inversions) but the uncertainty for Δ_E, which is only estimated in scenarios 1 and 3, only decreases by a factor of 1.1; data in scenario 3 do not add much information because uncertainty is significantly higher than that in scenario 1. The clock offset uncertainties for scenarios 7–9 show some improvement compared to scenario 1, but the improvement is much less than that from joint inversion. This indicates that prior environmental knowledge does not significantly improve clock offset estimates, provided the baseline inversion treats the environment as unknown.

Figure 3.5 shows the fit to the data achieved in scenario 1 including the synthetic (noisy) arrival times, 5th and 95th percentiles for predicted arrival times calculated from a random sample of 5000 models from the PPD, and the (error-free) theoretical arrival times calculated from Eq. (3.1). The inversion sampled models that produce predicted times in good agreement with the synthetic noisy arrival-time data. Fits to the data for other scenarios were similar and are not shown here for brevity; however, the mean standard deviations for residuals in all simulated scenarios are summarized in Table 3.3 and were within 2.8 ms of the true values in Table 3.2.

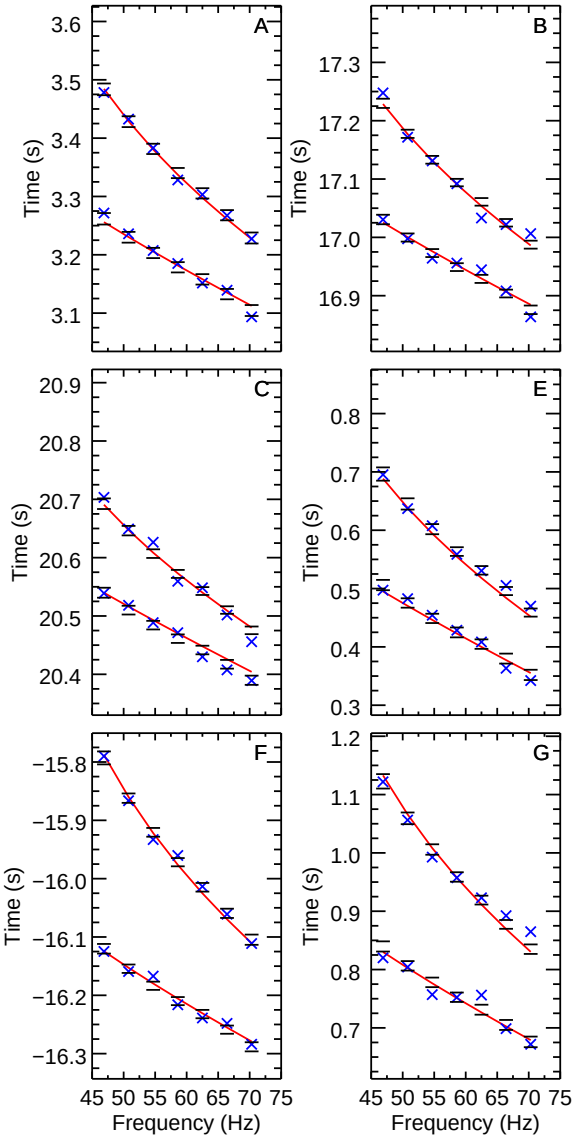

Figure 3.5: Mode arrival times for simulated whale call 1 on recorders A–C, and E–G (the call was not detected on recorder D in scenario 1). True (error-free) arrival times (solid curves), noisy synthetic data (×), and the 5th and 95th percentile predicted arrival times calculated from a random sample of models from the PPD (solid horizontal lines) are shown for each recorder.

3.4 Bowhead whale-call data

Long-term underwater acoustic recordings were collected by JASCO Applied Sciences from August to October 2013 as part of an acoustic measurement program designed, in part, to record marine-mammal calls over a large area of the Chukchi

Sea.[18] The recordings were made using 28 of JASCO's Autonomous Multichannel Acoustic Recorders (AMARs), each equipped with a single Geospectrum M8E hydrophone (nominal sensitivity -164 dB re 1 V/μPa). Most of the recorders were spaced tens of kilometres apart; however, a cluster of closely-spaced recorders was centred around Shell's 2012 drilling location to quantify sound levels from oil and gas exploration activities. Seven recorders (denoted by JASCO as BGA–BGE, BGH, and BGJ, but herein renamed as A–G, respectively) were deployed within 8 km of the drill site (71°18.5'N, 163°12.7'W) at nominal distances of 0.5, 1, 2, 4, and 8 km (three AMARs were deployed at 2-km range at different azimuths) and recorded 24-bit samples at a 64 kHz sampling rate. The water depths at the seven AMAR locations ranged between 46.0 and 48.7 m, so based on this relatively flat bathymetry, the environment is approximated as range-independent with an unknown (effective) water depth.

Bowhead whales passed the AMAR cluster during their annual fall migration from the Beaufort and Chukchi Seas to the Bering Sea. The AMARs recorded thousands of bowhead calls and many of the calls were detected on multiple AMARs in the cluster. Some of these calls were at low frequencies (35–97 Hz) and contained significant energy in at least two dispersive modes. For this study, mode arrival times for nine bowhead calls recorded on up to all seven AMARs (A–G) were estimated as described in Section 3.2.1. The same call was identified by listening to the recordings and observing similar TF characteristics of the call. The calls spanned a 3.25 min period on 11 October; I do not expect the relative AMAR clock offsets to change significantly over this short period. Table 3.5 lists the recorders, frequency ranges, and number of mode arrival times (N) over all recorders, modes, and frequencies for each call. Figure 3.6 shows spectrograms of the nine calls and Fig. 3.7 shows spectrograms for call 1 for recordings on all seven AMARs. The relative modal dispersion that is clearly visible in Fig. 3.7 indicates that the whale was closest to AMAR D or E (since these recordings show the least dispersion).

Whale call inversions used the same environmental prior bounds as in the simulation study (see Table 3.1), except the effective water depth bounds were expanded to [35, 55] m and water sound speed bounds were [1439, 1465] m/s based on historical SSP measurements in the area.[80] Location, source IF, and error standard deviation prior bounds were the same as in the simulation study.

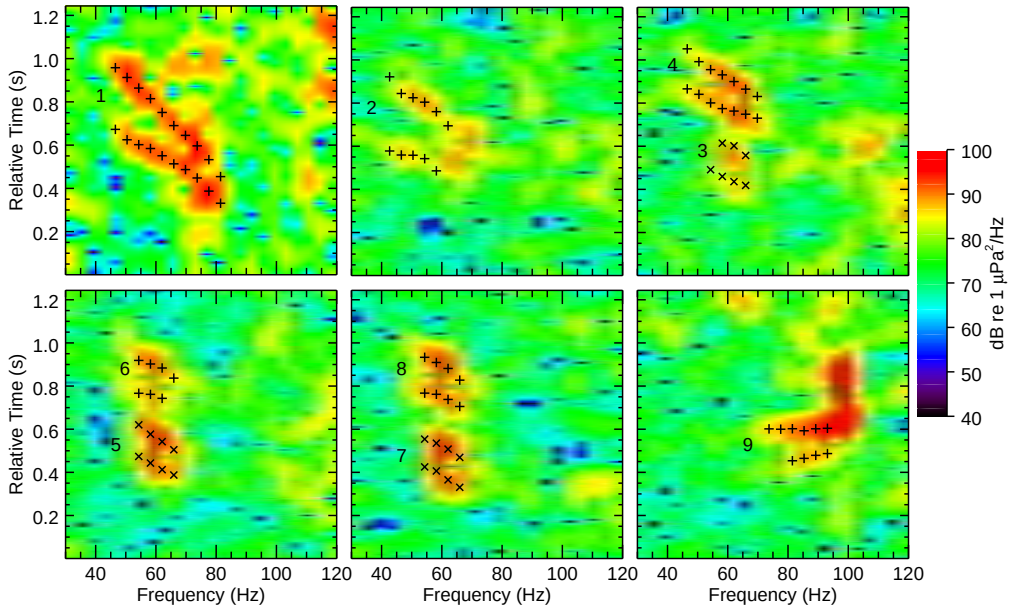

Figure 3.6: Spectrograms of bowhead whale calls recorded on AMAR A for all calls considered. Call numbers are vertically centred to the left of modes 1 and 2 of each call. Data picks (see method described in Sec. 3.2.1 and illustrated in Fig. 3.1) are shown with + and × symbols. Note that calls 3–8 are received within an ∼8 s period.

3.5 Inversion results

The trans-D Bayesian inversion was applied to each of the nine bowhead whale calls independently (scenarios 1–9) and then jointly for one multi-call inversion (scenario 10). The inversions were carried out on a parallel computer cluster with each inversion using 32 (2.1 GHz) central processing unit cores. The independent inversions took approximately 24 hours to reach convergence and the joint inversion, with many more parameters to estimate, took approximately 72 hours. Figure 3.8 shows the two-dimensional marginal probability densities for whale locations for all scenarios, with the recorders that detected calls shown with × symbols. Each call probability density is normalized by its maximum value to more clearly illustrate the density shapes. Inset plots at 3 times magnification are shown in some panels to illustrate small probability density shapes. Most probability contours are approximately elliptical; however, the PDF in scenario 9 is curved and wider than the others. The probability densities for calls 3–8 overlap substantially, so it is not possible to conclude if the calls are coming from a single whale or multiple whales. The PDFs for the multi-call inversion are substantially narrower than their corresponding single-call inversion PDF, similar

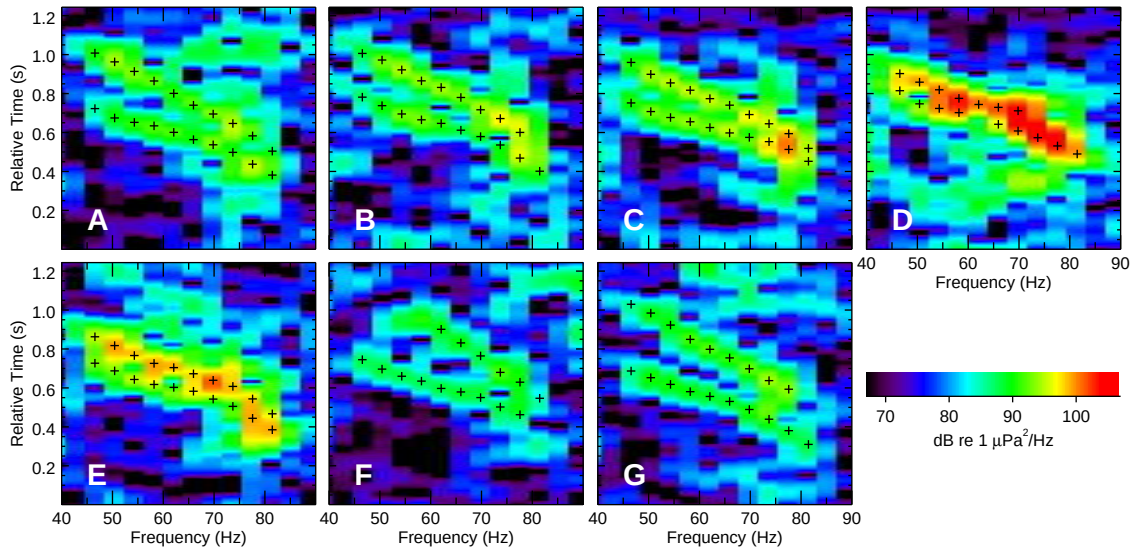

Figure 3.7: Spectrograms of bowhead whale call 1 recorded on each AMAR. Data picks are shown with + symbols.

to findings in the simulation study. The most-probable locations for calls 1–8 are consistent (within uncertainties) between the single- and multi-call inversions, but the location for call nine moves a few kilometres from the peak of the single-call inversion PDF; this is discussed below with respect to the relative recorder clock offsets. Table 3.6 lists the localization results and uncertainties for all bowhead whale calls considered.

Figure 3.9 shows the normalized marginal probability densities for the source IF. The left panels show source IF for the individual-call inversions and the right panels

Table 3.5: Inverted Bowhead whale call parameters.

Call	AMARs	Frequency range (Hz)	N
1	A–G	47–81	129
2	A–D, F, G	35–85	101
3	A, B, D–G	54–70	41
4	A–G	43–70	90
5	A, B, D–G	54–66	39
6	A–G	50–66	53
7	A, B, D–G	54–66	45
8	A–G	50–66	56
9	A–C, E–G	74–97	54

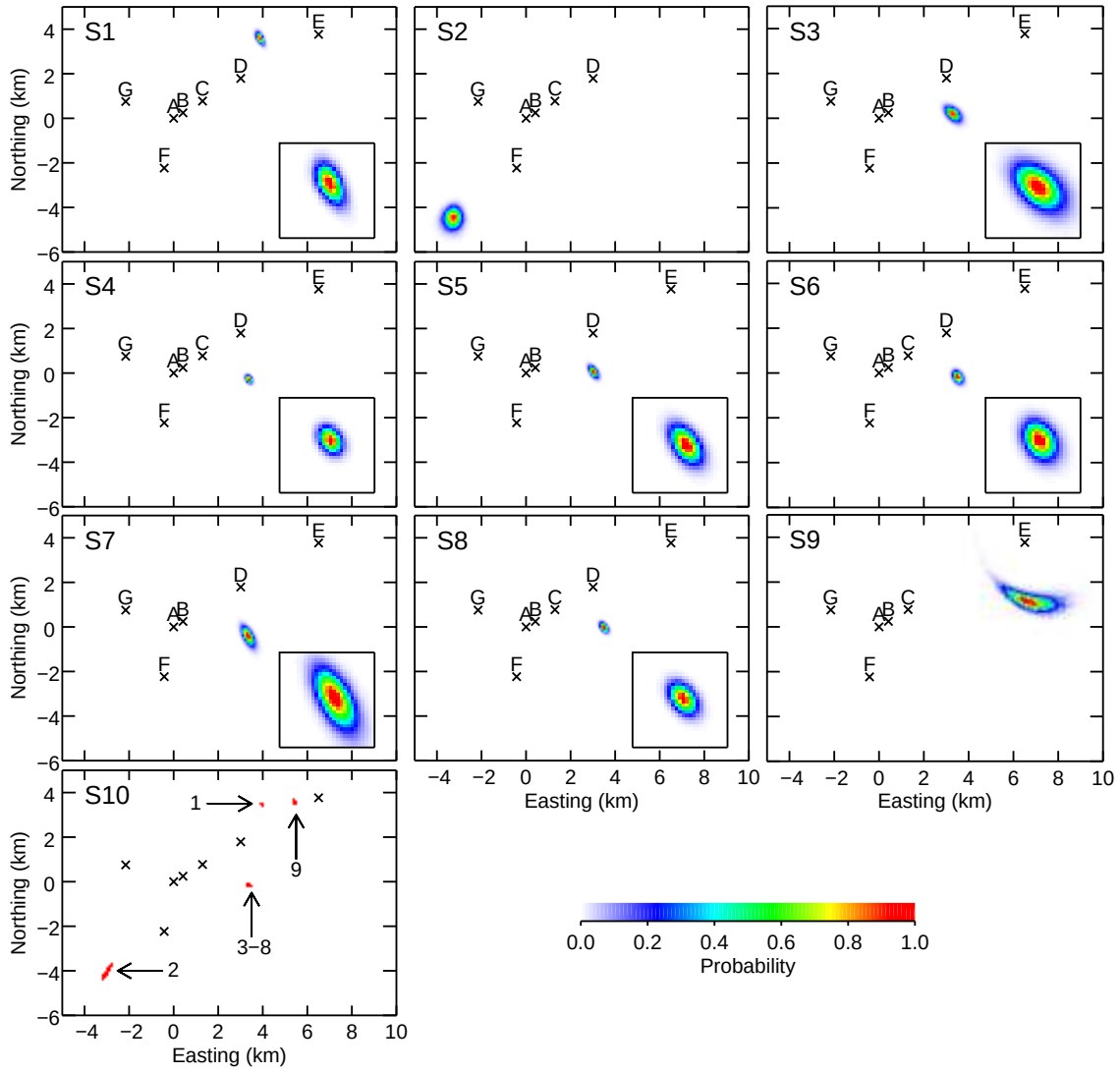

Figure 3.8: Marginal probability densities for bowhead whale location(s) for scenarios 1–10 (described in text). Probability densities for scenario 10 are compact and are shown as a binary image for clarity. Receivers that recorded the call(s) in each scenario are indicated with × symbols. Inset plots show the corresponding probatility densities at 3 times magnification.

show the corresponding source IF for the joint inversion. The shapes of the source IF are well resolved for all calls and most of the mismatch is attributed to uncertainty in whale location and relative recorder clock offset which produces strongly correlated source IF over frequency. The probability densities are much more tightly constrained in the joint inversion due to the smaller uncertainty of whale location and relative clock offset (the latter is discussed later in this section).

Table 3.6: Localization results and mean residual error standard deviations ($\overline{\sigma}_w$) for inverted bowhead calls. Mean location and 2SD are given as easting and northing pairs.

Call	Scenario	Mean Location (km)	2SD (km)	$\overline{\sigma}_w$ (ms)
1	1	3.83,3.58	0.21,0.33	10.9
1	10	3.93,3.42	0.03,0.02	12.0
2	2	−3.38,−4.57	0.52,0.63	12.7
2	10	−3.07,−4.12	0.08,0.14	16.8
3	3	3.28,0.15	0.42,0.41	10.5
3	10	3.32,−0.21	0.03,0.02	10.0
4	4	3.33,−0.33	0.17,0.21	9.5
4	10	3.33,−0.21	0.03,0.02	11.4
5	5	2.97,0.01	0.25,0.33	9.7
5	10	3.33,−0.22	0.03,0.02	9.7
6	6	3.49,−0.24	0.28,0.33	10.9
6	10	3.33,−0.23	0.03,0.02	16.2
7	7	3.31,−0.50	0.36,0.55	11.7
7	10	3.31,−0.22	0.03,0.02	11.6
8	8	3.43,−0.08	0.22,0.26	8.3
8	10	3.33,−0.21	0.03,0.03	19.6
9	9	6.80,1.16	1.56,0.77	7.0
9	10	5.38,3.53	0.03,0.04	11.2

Figure 3.10 shows the marginal probability profiles for the SSP and geoacoustic parameters for scenarios 1 and 10. The corresponding results for single-call inversions 2–9 (not shown) are similar to those of scenario 1 but vary somewhat in the upper sediment layer thickness and sound speed (although the profiles are consistent within their estimated uncertainties).

In scenario 1, little SSP structure is resolved by the data and the distribution of the number of SSP nodes is uniform (not shown). The limited SSP resolution, particularly with depth, is likely due to the large wavelengths of the low-order mode functions. The node depth PDF is uniform over the water column but decreases to zero over the prior bounds for effective water depth. The marginal distribution for the number of subbottom interfaces (not shown) is peaked at zero and decreases for increasing numbers of interfaces; little subbottom structure is resolved by the single-call data. Subbottom sound speed and density are resolved within their prior bounds; however, the resolution for density is only due to the joint prior bound with sound speed.

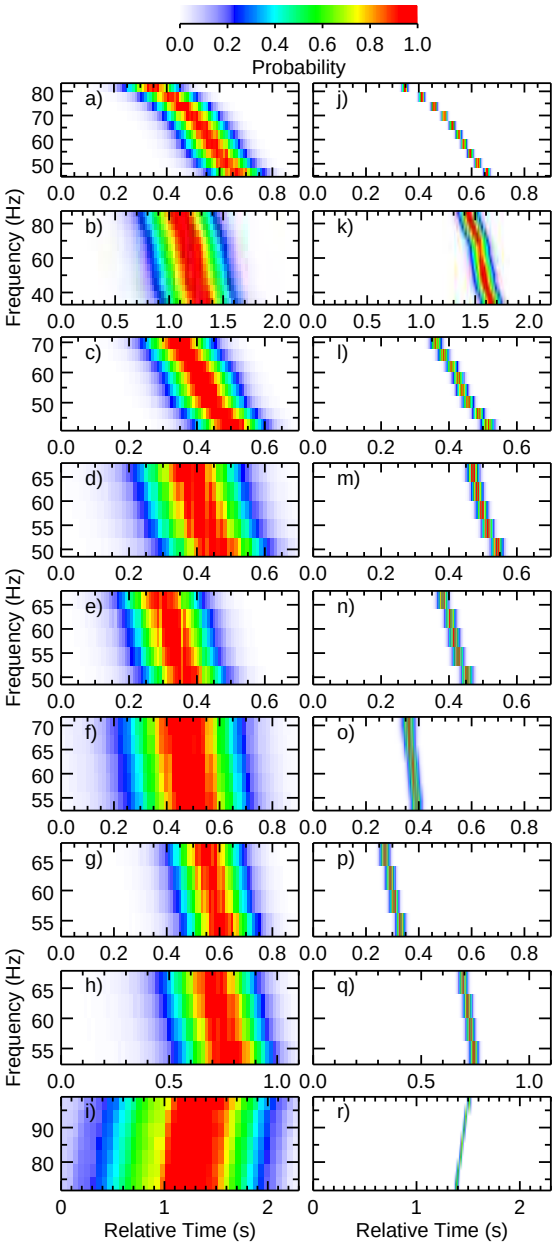

Figure 3.9: Normalized probability densities of source IF for calls 1–9 inverted independently (a–i) and jointly (j–r).

The corresponding results for the multi-call inversion suggest some SSP structure, though the upper and lower portions of the profile are very uncertain. Considering the simulation study did not include any data processing or theory error and found that data were not able to resolve even relatively simple SSP structure, it is unlikely that the relatively fine SSP structure suggested in Fig. 3.10 is real. A non-Gaussian error

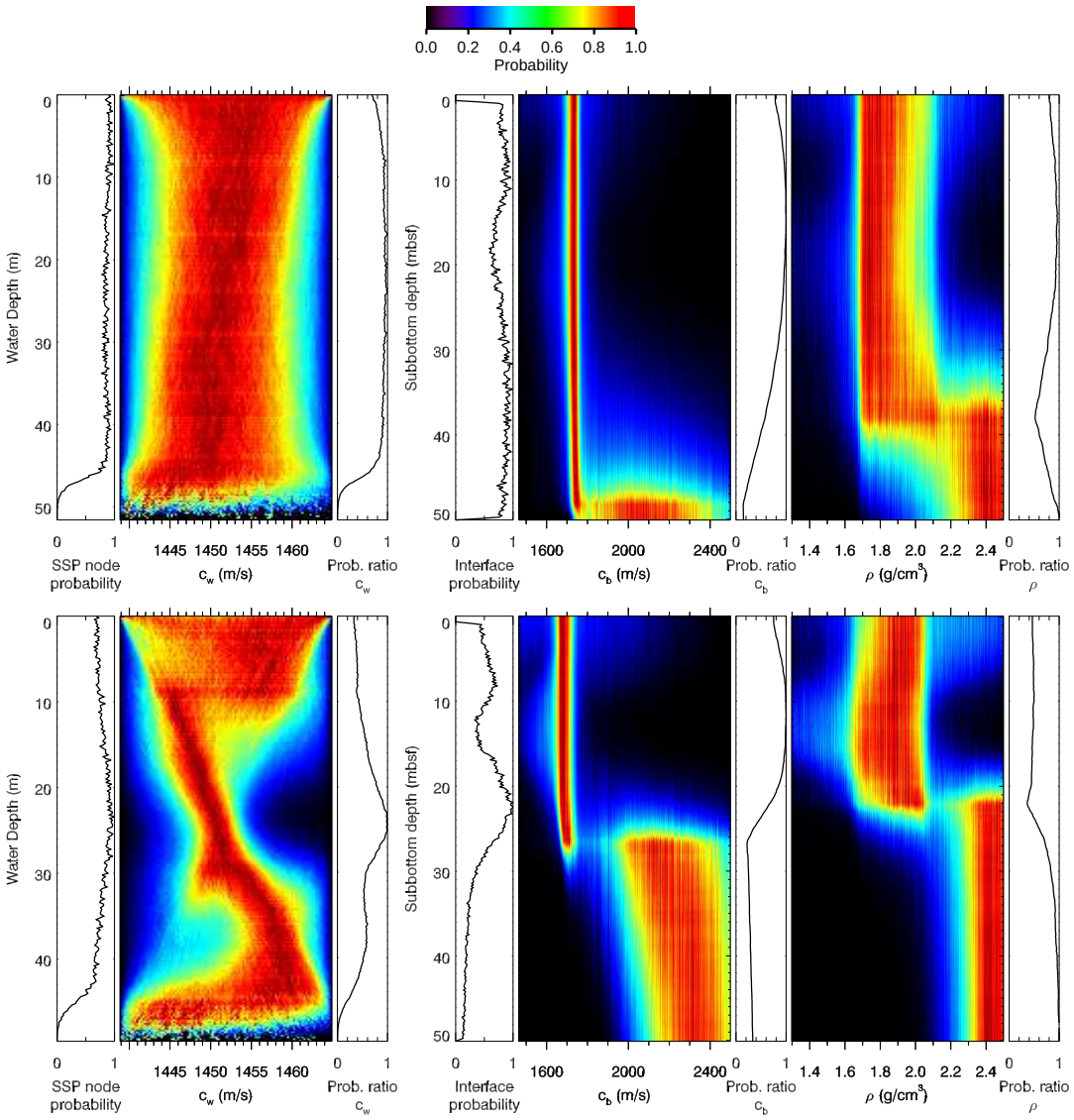

Figure 3.10: Marginal probability profiles for water SSP and subbottom sound speed and density, together with their corresponding node/interface depth profiles and depth normalization profiles. Top and bottom panels show results from scenarios 1 (call 1) and 10 (calls 1–9), respectively. Plot bounds are the prior bounds for SSP and geoacoustic parameters, though subbottom sound speed and density are further constrained by a joint prior PDF.

process might have contributed to the fine-scale SSP result. Still, the sound speed at mid-depth in the water column is approximately 1450 m/s which is reasonable for this Arctic region in the fall.[81] The geoacoustic profiles are similar to those of call 1 but the prominent interface depth is constrained between approximately 15

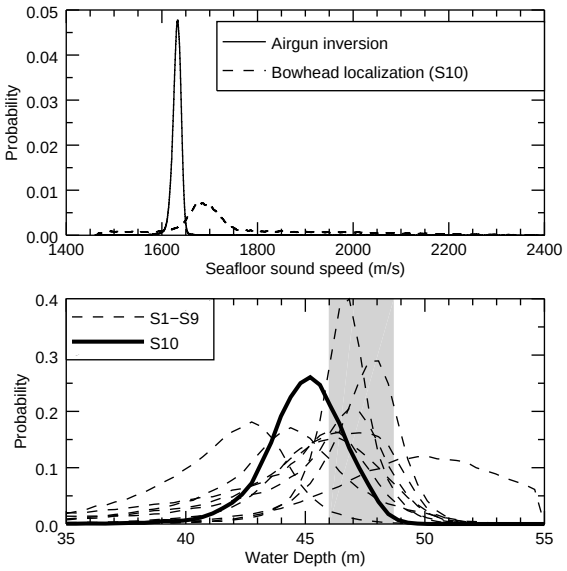

Figure 3.11: Top: Marginal PDF for subbottom sound speed in the top 5 mbsf from inversion of airgun modal dispersion[35] and bowhead whale-call data (scenario 10). Bottom: Marginal PDF for effective water depth from separate (S1–S9) and joint (S10) inversions, with the water depths measured during AMAR deployments indicated by the shaded region.

and 28 m below the seafloor (mbsf), below which the parameters are very uncertain. Figure 3.11 compares the top 5 mbsf subbottom sound speed PDF from scenario 10 to that from a recent geoacoustic inversion based on dispersion of airgun signals (with 5 modes) at a site ∼16 km away from AMAR A.[35] The probability densities peak at different bottom sound speeds but the PDF from the bowhead whale call inversion has heavy tails that overlap with the higher-resolution PDF from the airgun modal dispersion inversion.

Figure 3.11 also shows the marginal probability densities for effective water depth and the shaded region indicates the range of water depths measured during AMAR deployments. The probability densities for scenarios 1–9 overlap with the water depth measurements but vary in width and most-probable depth. The PDF for scenario 10 is more constrained than the ensemble of probability densities from single-call inversions and has standard deviation of 1.7 m.

The environmental properties estimated in the inversion can be used to predict received levels (RL) which are useful in the context of underwater noise environmental impact assessments. In such assessments, the maximum RL over all depths in the water column is often considered as a function of range to estimate distances

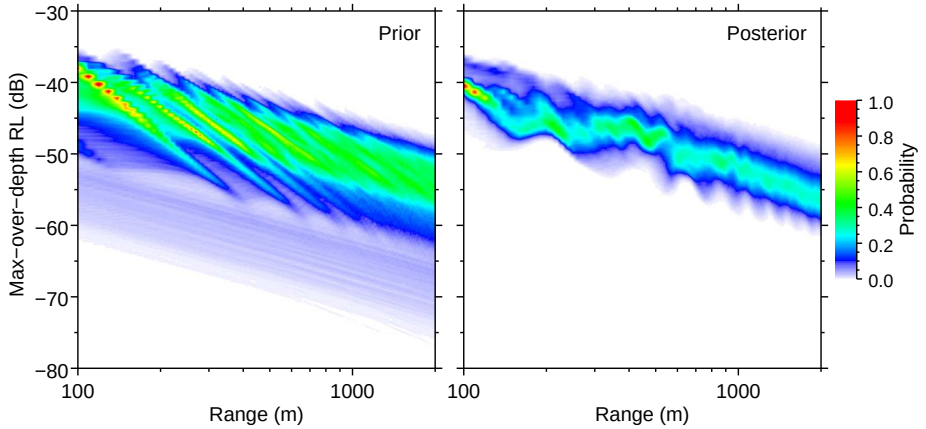

Figure 3.12: Normalized probability densities for predicted maximum-over-depth received level vs. range using environmental samples from the (left) prior and (right) posterior of scenario 10. Source depth is 2 m, source level is 0 dB, and the frequency is 70 Hz.

to sound-level thresholds relevant to the protection of marine mammals. RL can be calculated using environmental parameters from either the prior or posterior probability densities, and the RL uncertainty differences illustrate the information gained by inverting the modal-dispersion data. Figure 3.12 shows the normalized probability density for maximum-over-depth RL for a 0 dB source at 2 m depth for 70 Hz using environmental samples from the prior and posterior environmental probability densities of scenario 10 (sediment attenuation for all layers and the halfspace in each sample were independently chosen from a uniform distribution bounded by 0 and 0.2 dB per wavelength). The information content of the data has significantly constrained the predicted RL at any given range, and, more importantly, the range at which levels are reached.

Table 3.7 lists the mean relative AMAR clock offsets (to reference AMAR A) and the estimated uncertainties. The single call inversions provide estimated clock offsets with uncertainties that varied between 8 and 728 ms. Clock offset uncertainties are correlated with distance from the reference recorder and strongly reflect localization uncertainty (e.g., offset uncertainties on AMARs F and G for call nine are relatively large which is reflective of the large position uncertainty perpendicular to the main axis of the AMAR cluster). The multi-call inversion (scenario 10) produced significantly reduced clock offset uncertainties compared to the corresponding single-call inversions with estimated uncertainties of 3 to 26 ms (a reduction of up to 96%).

The fit to the data achieved in scenario 1 is shown in Fig. 3.13 including the picked

Table 3.7: Estimated relative AMAR clock offsets and 2SD uncertainties (s) for the bowhead whale call inversions.

Scenario	Δ_B	Δ_C	Δ_D	Δ_E	Δ_F	Δ_G
1	24.04,0.008	97.84,0.022	53.49,0.090	54.34,0.214	53.13,0.046	45.91,0.079
2	24.07,0.015	97.86,0.034	53.59,0.065		53.19,0.105	45.92,0.153
3	24.04,0.028		53.75,0.284	54.50,0.432	52.99,0.177	45.88,0.047
4	24.04,0.015	97.80,0.054	53.47,0.135	54.34,0.188	53.20,0.090	45.86,0.018
5	24.05,0.024		53.47,0.203	54.09,0.254	53.03,0.149	45.88,0.034
6	24.04,0.023	97.84,0.081	53.62,0.218	54.56,0.308	53.18,0.136	45.87,0.027
7	24.04,0.038		53.33,0.259	54.22,0.313	53.27,0.240	45.84,0.029
8	24.05,0.017	97.88,0.063	53.70,0.161	54.59,0.224	53.12,0.108	45.90,0.025
9	24.02,0.016	97.75,0.054		53.60,0.728	53.62,0.203	45.54,0.101
10	24.04,0.003	97.84,0.003	53.54,0.009	54.39,0.026	53.16,0.007	45.87,0.005

arrival times and the 5th and 95th percentiles for estimated arrival times, calculated from a random sample of 5000 models from the PPD. The inversion sampled models that produce predicted times in excellent agreement with the picked times. Fits to the data for other scenarios were similar and are not shown here for brevity; however, the standard deviations for the residuals in all scenarios are quantified in Table 3.6. The call standard deviations generally increased somewhat for the multi-call scenario because all calls had to be fit with a single environmental model and set of relative clock offset parameters.

3.6 Summary and conclusion

This chapter presented Bayesian inversion of low-frequency bowhead whale-call modal-dispersion data (both simulated and measured) received at a cluster of asynchronous hydrophones. Mode arrival times were determined from time-frequency analysis of calls after filtering individual modes using a modified warping procedure that accounted for a non-impulsive source. The arrival times were then used in the inversion to estimate the whale location, source instantaneous frequency, water sound-speed profile, subbottom geoacoustic properties, and relative recorder clock offsets, all with estimated uncertainties. A trans-dimensional framework was applied for the water-column SSP and subbottom geoacoustic layering properties to account for uncertainty in model parameterization that would be difficult to account for in a fixed-dimensional inversion (particularly for the SSP).

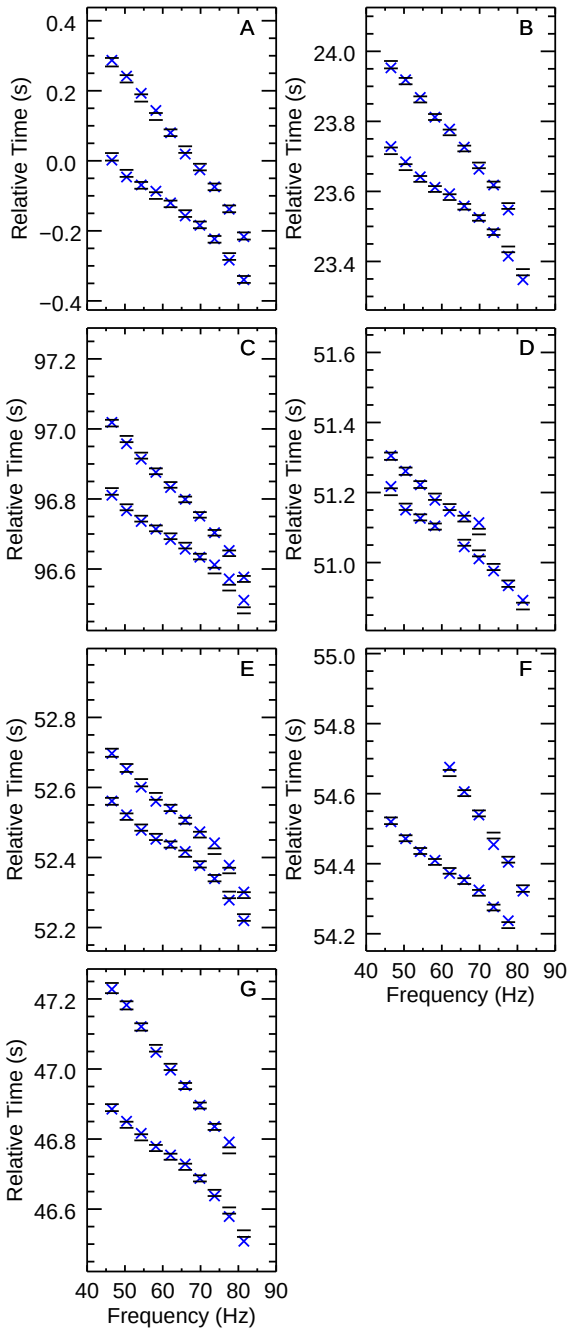

Figure 3.13: Mode arrival times for whale call 1 (× symbols) on recorders A–G, and the 5th and 95th percentile predicted arrival times calculated from a random sample of models from the PPD (horizontal lines).

A simulation study characterized the ability of the inversion to estimate the unknown parameters. Joint inversion of modal-dispersion data from multiple calls was found to substantially decrease whale location and recorder clock offset uncertainties

compared to single-call inversions. Exact prior knowledge of the SSP and/or geoacoustic properties was found to produce a relatively small improvement in localization and clock offset uncertainties. The inverted data provided little information on the SSP and water depth which may be due to the low frequencies and low-order modes (1 and 2) used for the simulation. The estimates of the geoacoustic profiles, whale call source IF, and relative recorder clock offsets were consistent with the true values within the estimated uncertainties.

Inversion results for bowhead whale calls recorded in the Chukchi Sea showed similar effects to the simulation study. The localization and relative recorder clock offset results improved substantially when including multiple calls in the same inversion. The SSP and subbottom density were not resolved but the estimated effective water depth was constrained in the multi-call inversion and agreed with water depth measurements. The resolution of seabed sound speed was much less than that found in a previous Chukchi Sea study of modal dispersion inversion of airgun data which exploited the impulsive nature of the source and involved a higher modal content (up to five modes compared to only two in the whale-call data). Nevertheless, the environmental information provided by the bowhead whale-call modal-dispersion data was found to significantly reduce uncertainty in predicted received levels (transmission loss) for the measurement location by applying environmental knowledge from the PPD rather than from the prior.

Overall, modal-dispersion data and the trans-D inversion approach are shown to be capable of estimating locations of bowhead whales several kilometres from an asynchronous hydrophone cluster to accuracies of 30–160 m in an uncertain range-independent environment. This localization accuracy is sufficient for determining if marine mammals are exposed to sound levels above specific thresholds (so that mitigation strategies can be implemented). The inversion also resolved relative recorder clock offset to uncertainties less than 30 ms. This synchronization is sufficient for localizing marine mammals using other types of calls that are not suitable for mode arrival time estimation (e.g., using time-difference-of-arrival data). Whale tracking and marine mammal density estimation may be possible using such an approach since it can be applied to a much larger data set of marine mammal vocalizations. Performing modal dispersion-based localization and synchronization at multiple times throughout a long-duration recording could provide information on relative recorder clock drift rates.

Chapter 4

Bowhead whale localization using time-difference-of-arrival data from asynchronous recorders

This chapter estimates bowhead whale locations and uncertainties using nonlinear Bayesian inversion of the time-difference-of-arrival (TDOA) of whale calls recorded on onmi-directional asynchronous recorders in the Chukchi Sea, Alaska. A Y-shaped cluster of seven autonomous ocean-bottom hydrophones, separated by 0.5–9.2 km, was deployed for several months over which time their clocks drifted out of synchronization. Hundreds of recorded whale calls are manually annotated with time-frequency bounds and associated between recorders. The TDOA between all hydrophone pairs are calculated from filtered waveform cross-correlations and depend on the whale locations, hydrophone locations, relative recorder clock offsets, and effective waveguide sound speed. The inversion estimates all of these parameters and their uncertainties as well as data error statistics. The problem is highly nonlinear and a linearized inversion did not produce physically-realistic results. Whale location uncertainties can be low enough to allow tracking of migrating whales that vocalize repeatedly over several minutes. Estimates of clock drift rates are obtained from inversions of TDOA data over two weeks and agree with corresponding estimates obtained from long-time averaged ambient noise cross-correlations. The inversion is computationally efficient and suitable for application to large data sets of manually- or automatically-detected whale calls.

4.1 Introduction

Localizing marine mammals is important for estimating their distributions and movement. Passive acoustic monitoring can be used to infer the presence and location of vocalizing marine mammals over long time periods using autonomous underwater recorders to record calls from animals over large areas. Many localization techniques rely on recorder synchronization but the clocks in low-power underwater recorders are often susceptible to temperature changes and tend to drift out of synchronization with respect to each other over long-duration deployments. This chapter presents a nonlinear Bayesian inversion for localizing bowhead whales in the Chukchi Sea using call time-difference-of-arrival (TDOA) data derived from calls recorded on asynchronous seabed recording systems.

TDOA localization methods have been developed and used extensively for synchronized recorders.[9–11,72,82–88] The localization problem is more difficult with unsynchronized recorders and difficulties are further compounded if the recorder locations and/or water sound speed are uncertain.[89] A linear clock drift between deployment and recovery is often assumed,[90] but this may not accurately reflect the true clock drift especially during periods of rapid temperature change (e.g., upon deployment and recovery). Sabra *et al.*[91] showed that ambient noise can be used to synchronize and locate array elements using cross-correlations if the local sound speed is known and the noise sources are distributed uniformly in azimuth. This technique has been successfully applied to small-aperture arrays;[73] however, the large averaging times required for wide-aperture arrays can preclude synchronization if the clocks drift significantly over the duration required to build the time-domain Green's function (derivative of the cross-correlation between receivers). Equipping recorders with global positioning system (GPS) devices can provide accurate timing and position information[92–95] but requires a GPS receiver at the sea surface which may not be practical/possible in all environments (e.g., ice-covered waters). Recorders with chip-scale atomic clocks can stay adequately synchronized but have been expensive and require more power.

A previous study involving an unsynchronized wide-aperture array used a nonlinear Bayesian inversion to estimate bowhead whale locations and recorder clock offsets using modal-dispersion data.[37] That approach was based on extracting dispersion data (arrival times as a function of frequency) for multiple water-borne acoustic modes using a warping time-frequency analysis,[22] and inverting the data for whale

locations, clock offsets, the instantaneous frequency function of each whale call, and environmental models (sound-speed profile of the water column and sound-speed and density profiles of the seabed). Sound propagation was modelled using a normal-mode code and the inversion used trans-dimensional Markov-chain Monte Carlo sampling[32] to account for the unknown number of points and layers in the sound-speed profile and seabed, respectively. Although that method was quite accurate, the computational expense of the propagation model and environmental inversion (as well as the manual effort in data processing) prohibited the method from being applied to large numbers of whale calls. In this chapter, I use a much simpler and faster (but less accurate) propagation/environmental model and a nonlinear Bayesian inversion to estimate bowhead whale locations using whale-call TDOA data (the inversions were two to four orders of magnitude faster per whale localization). Acoustic propagation is modelled as straight acoustic paths in the horizontal plane with an unknown effective sound speed. The nonlinear inversion considers the whale locations, relative recorder clock offsets, sound speed, and recorder locations as unknown parameters (with varying levels of prior information) that are all estimated simultaneously. The inversion also rigorously estimates residual error statistics and quantitative uncertainties for all parameters. I note that a corresponding linearized Bayesian inversion I developed was even faster but often did not produce physically-realistic results, indicating that the inverse problem is strongly nonlinear.

The nonlinear inversion is applied here to batches of bowhead whale-call TDOA data (both simulated and measured) occurring over time periods which are short enough that the clocks do not drift significantly (approximately 30 minutes). A simulation study investigates how uncertainty probability density functions (PDF) for whale locations change with the number of recorders that detected each call and the source-receiver geometry, as well as the degree to which the other parameters are constrained. The measurement study considers bowhead whale-call TDOA data obtained from recordings of an underwater sound measurement program in the Chukchi Sea, Alaska.[18] Although the low-frequency bowhead calls propagate as normal modes in the shallow-water environment, dispersive (call spreading) effects are of much less significance than the propagation time from source to receiver. Hundreds of bowhead whale calls were manually annotated and associated from recordings of seven seabed-mounted recorders. The inversion results showed the recorder geometry was suitable for bowhead whale localization and estimating relative recorder clock offsets including long-term drift rates. Whale location uncertainties are often small enough to asso-

ciate calls with distinct whales and track repetitively-calling whales (or whale groups) with reasonable swim speed. I also show an example of possible whale responses to hearing another whale's call (a known behaviour of bowhead whales[96,97]).

4.2 Bowhead whale-call data

Long-term underwater acoustic recordings were collected by JASCO Applied Sciences from August to October, 2013, as part of an acoustic measurement program designed, in part, to record marine-mammal calls over a large area of the Chukchi Sea.[18] The recordings were made using 28 of JASCO's Autonomous Multichannel Acoustic Recorders (AMARs) which drifted out of synchronization with each other over the deployment period. Each recorder was equipped with a single Geospectrum M8E hydrophone (nominal sensitivity -164 dB re 1 V/μPa) and recorded 24-bit samples at a 64 kHz sampling rate. Most recorders were spaced tens of kilometres apart; however, a cluster of closely-spaced recorders was centred around Shell's 2012 drilling location to quantify sound levels from oil and gas exploration activities. Seven recorders (denoted by JASCO as BGA–BGE, BGH, and BGJ, but herein renamed as A–G, respectively) were deployed within 8 km of the drill site (71°18.5'N, 163°12.7'W) at nominal distances of 0.5, 1, 2, 4, and 8 km (three AMARs were deployed at 2-km range at different azimuths). Approximate AMAR locations were recorded upon deployment using GPS. The water depths at the seven AMAR deployment locations varied between 46.0 and 48.7 m.

Bowhead whales passed the AMAR cluster during their annual fall migration from the Beaufort and Chukchi Seas to the Bering Sea. The AMARs recorded thousands of bowhead calls (mostly at frequencies below 400 Hz) and many of the calls were detected on multiple AMARs in the cluster. The bowhead whale calls and other acoustic events (e.g., seismic pulses) were used to approximately synchronize the recorders by listening to the recordings and observing time-frequency characteristics of the events. Bowhead whale calls were detected manually and assigned start and end times relative to the corresponding recorder's clock, as well as lower and upper frequencies. For this study, I manually made 1926 annotations of 347 unique bowhead whale calls recorded on AMARs A–G during six half-hour time windows between 27 September and 11 October. The same call was identified on multiple AMAR recordings by listening to the recordings and observing corresponding spectrograms of the call. For each call, corresponding detections on all recorders were associated

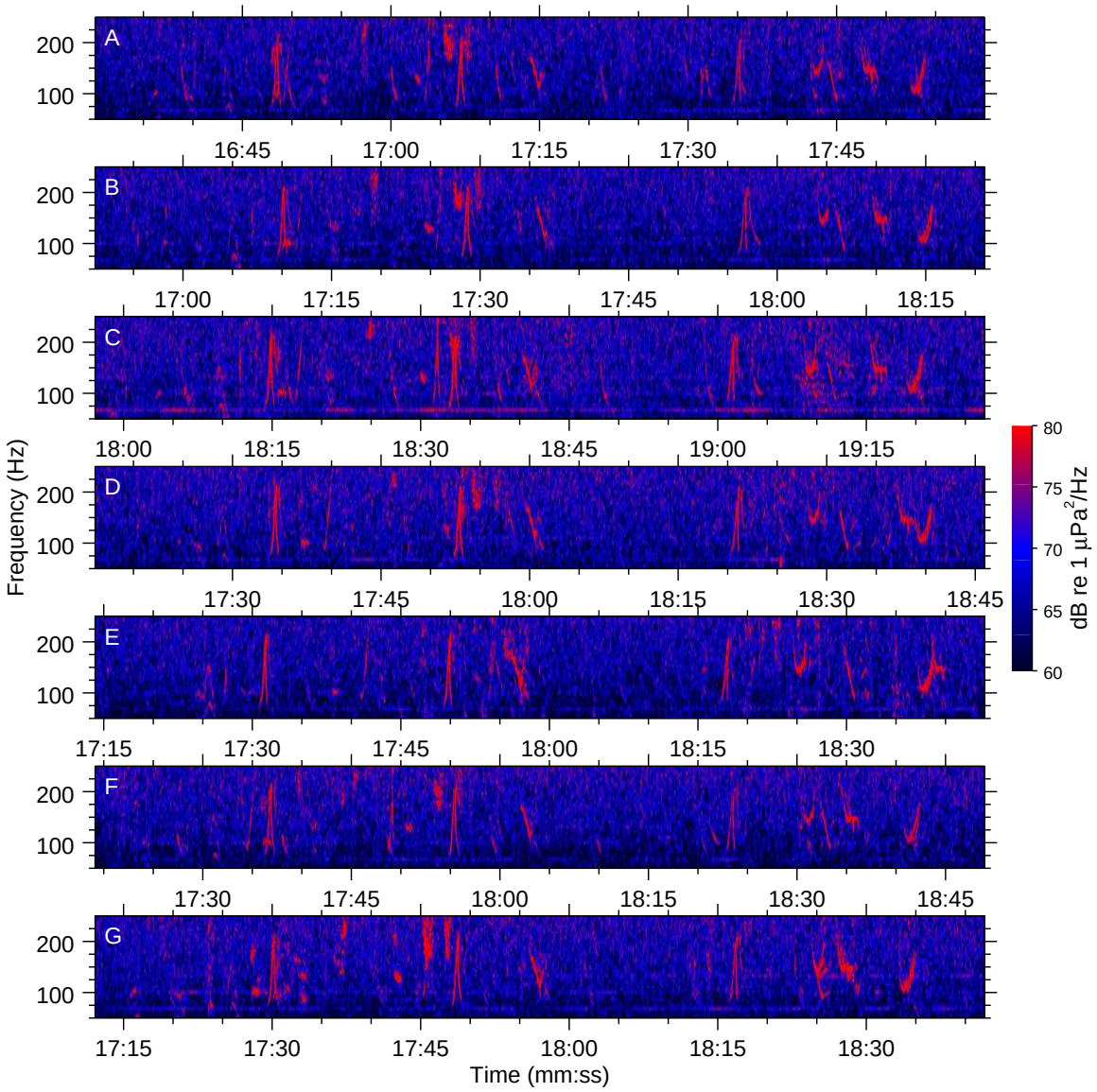

Figure 4.1: Spectrograms of bowhead whale calls recorded on AMARs A–G on 3 Oct. Times are given in minutes and seconds after midnight for each AMAR clock. Note that the relative recorder clock offsets are much larger than any physically-realistic propagation effect but it is still possible to (approximately) time-align the recordings.

by assigning the same unique call name to each annotation. Figure 4.1 shows an example of spectrograms from each AMAR during a 90-s period on 3 October.

4.3 Theory

4.3.1 Data processing

Call waveforms were band-pass filtered within their lower and upper frequencies and then cross-correlated with detections of the same call from other recorders. In this chapter, I consider whale calls recorded at up to seven recorders which yields up to 21 cross-correlation functions per call. The envelopes of the normalized cross-correlation functions were computed (most calls were 0.5–2.1 s long) and the TDOAs were determined by the time delay of the envelope's maximum.[87] The TDOAs were sorted in descending order by the maximum values of the envelopes (typically in the range 0.3–0.8) and the first two and up to six linearly independent TDOAs were saved for the inversion (linearly dependent TDOAs were discarded). This was done because using linearly dependent TDOA is inconsistent with the assumptions of independent data errors (described in Sec. 4.3.3) and could result in underestimating uncertainties in the whale locations. It also reduced the influence of call dispersion on TDOA data (not accounted for in the propagation model), as higher cross-correlation maxima favoured similarly dispersed calls which yielded more-accurate TDOA data.

4.3.2 Bayesian inversion

The call arrival times depend on the whale and receiver locations, time of the call, and relative recorder clock offsets. Using a simple straight-path time-of-flight propagation model, the arrival time for call w at recorder i is

$$t_{wi} = \tau_w + \frac{\sqrt{(x_w - X_i)^2 + (y_w - Y_i)^2}}{c} + \Delta_i, \tag{4.1}$$

where τ_w is the time of the whale call, x_w and y_w are the easting and northing coordinates of the whale, X_i and Y_i are the coordinates of the recorder, c is the effective waveguide sound speed (discussed below), and Δ_i is the recorder clock offset relative to a reference recorder. The bowhead whale calls analyzed for this chapter propagate as normal modes in the shallow-water environment. The sound speed c is therefore an effective average modal group speed (less than the water sound speed) weighted by the frequency and modal content of the calls (the latter is also dependent on source depth). Considering TDOAs for a whale call recorded at receivers i and j

removes the dependence on whale call time, as given by

$$t_{wi} - t_{wj} = \frac{\sqrt{(x_w - X_i)^2 + (y_w - Y_i)^2}}{c} - \frac{\sqrt{(x_w - X_j)^2 + (y_w - Y_j)^2}}{c} + \Delta_i - \Delta_j. \quad (4.2)$$

The Bayesian inversion estimates the unknown model parameters $\mathbf{m} = [x_1, \ldots, x_W, y_1, \ldots, y_W, X_1, \ldots, X_R, Y_1, \ldots, Y_R, \Delta_2, \ldots, \Delta_R, c]^{\mathrm{T}}$, where W is the number of whale calls, R is the number of recorders (with recorder 1 as the reference recorder so $\Delta_1 = 0$). In addition, the error standard deviation is also considered unknown and treated as described in Sec. 4.3.3. The inversion is carried out by sampling the posterior probability density (PPD) of the model parameters given the measured data and prior information with Metropolis-Hastings sampling,[28,29] a Markov-chain Monte Carlo algorithm. Parallel tempering[40–43] and parameter rotation[38] are used to efficiently sample potentially multi-modal PPD structure which involve highly-correlated parameters. Parameter rotation is implemented for all model parameters using eigenvalue decomposition of the model covariance matrix (estimated using all previous MCMC samples) and perturbing the current model along a randomly-selected eigenvector using symmetric Gaussian proposal densities with variance given by corresponding eigenvalues. The model transition acceptance probability is applied after perturbing the current model and depends on the prior, proposal, and likelihood ratios. Uniform (bounded) prior probability densities are used for all model parameters and symmetric (Cauchy) probability densities are used for the proposals, reducing the model transition acceptance probability to the likelihood ratio (Sec. 4.3.3).

The upper (prior) bound for sound speed was set to be the maximum expected water sound speed in the area during September and October.[80,98,99] The minimum sound speed was approximately the lowest group speed of mode 3 as estimated using environmental properties from a previous inversion of bowhead whale modal-dispersion data recorded on the same hydrophones.[37] Mode 3 was the highest-order mode observed in all annotated calls. Recorder locations (easting and northing) were allowed to vary by up to 50 m from their GPS-based deployment locations to account for recorder location uncertainty. The intent is not so much to localize the recorders as to quantitatively account for deployment location uncertainties in the whale localization uncertainties. Relative recorder clock offsets were allowed to vary by up to 5 s from the median of all TDOAs for each recorder.

4.3.3 Likelihood

The likelihood function is defined by the residual error PDF. Measurement, data-processing, and theory errors comprise residual errors and their PDFs are often unknown. Residual errors for model $\mathbf{m}$ are given by $\mathbf{d} - \mathbf{d}(\mathbf{m})$, where $\mathbf{d}$ and $\mathbf{d}(\mathbf{m})$ are the measured and predicted (TDOA) data, respectively. I assume residual errors are independent and Gaussian-distributed in this chapter, the validity of which is checked *a posteriori*. For N data, the corresponding likelihood function is

$$L(\mathbf{m}) = \frac{1}{(2\pi)^{N/2}\sigma^N} \exp\left[-\frac{|\mathbf{d} - \mathbf{d}(\mathbf{m})|^2}{2\sigma^2}\right], \tag{4.3}$$

where σ is the error standard deviation. Setting $\partial L/\partial\sigma = 0$ leads to a maximum-likelihood estimate for the error standard deviation σ:

$$\hat{\sigma}(\mathbf{m}) = [|\mathbf{d} - \mathbf{d}(\mathbf{m})|^2/N]^{1/2}. \tag{4.4}$$

Equation (4.4) expresses σ in terms of the data and other unknown model parameters, allowing implicit sampling of σ by sampling explicitly over the parameters in $\mathbf{m}$.[79]

4.4 Simulation study

This section illustrates the capabilities and limitations of the TDOA localization in a simulation study based on bowhead whale recordings in the Chukchi Sea (described in Sec. 4.2). The simulation considered 12 calls recorded on up to seven asynchronous recorders (A–G). The recorder locations were taken from coordinates of the deployed recorder cluster[18] to investigate how the source-receiver geometry affects location uncertainty. TDOAs were simulated using Eq. (4.2) with true model parameters listed in Table 4.1. Data were simulated for a minimum of three and up to all seven recorders, depending on the call, and linearly-dependent data (combinations of receiver pairs) were removed on the basis of larger path length differences from source to receiver. This was done to simulate the expected effect of decreasing peak cross-correlation values between recorded calls in a dispersive waveguide. Gaussian-distributed independent zero-mean random errors with standard deviation 0.12 s were added to the true TDOA data. The synthetic (noisy) data were inverted for the unknown parameters with prior bounds listed in Table 4.1. Approximately 400 000 samples were drawn from the PPD via Metropolis-Hastings sampling, after a suitable

burn-in period.

Table 4.1: True model parameters and corresponding prior bounds for the simulation study. Priors given with ± indicate bounds relative to the true parameters.

Parameter	True value(s)	Prior bounds
c (m/s)	1400	[1300,1465]
Δ_{B-G} (s)	$[-51, -53, -5, 31, 11, -59]$	± 5
x_w (km)	See Fig. 4.2	$[-30, 30]$
y_w (km)	See Fig. 4.2	$[-30, 30]$
X_{A-G} (m)	See Fig. 4.2	± 50
Y_{A-G} (m)	See Fig. 4.2	± 50

Figure 4.2 shows the two-dimensional (2D) marginal probability densities for whale locations and the true locations for all 12 simulated calls. The localization results depend strongly on the whale location relative to the receivers that recorded its call (indicated by filled diamonds). The probability densities are constrained in both easting and northing for calls 1, 4, 7, 10, and 12 whereas PDFs for calls 2, 3, 8, 9, and 11 are constrained in bearing but not range from the recorders. The probability densities for calls 3 and 6 are the least constrained, being symmetric about the main recorder axis since the off-axis recorders F and G did not receive these calls. Generally, the location uncertainty decreases with the number of recorders that detected the call. The PDF for call 12 is multi-modal with the southeastern mode having higher-probability than the northwestern mode; however, the true call location is within the northwestern mode. Resolving this multi-modal PPD structure illustrates the usefulness of the uncertainty analysis provided by the nonlinear Bayesian inversion approach. A linearized inversion would miss the northwestern mode, and multi-modal marginal distributions for other calls.

Figure 4.3 shows normalized marginal probability densities for effective waveguide sound speed, relative recorder clock offsets, and residual error standard deviation. In all cases the marginal densities are peaked near the true values. The sound speed is not particularly well resolved within the prior bounds but the relative recorder clock offsets are estimated with uncertainties of a few tenths of seconds. Marginal probability densities for recorder locations were approximately uniform (not shown), indicating that the data do not resolve recorder locations within the prior bounds; however, recorder location uncertainties are accounted for in the whale location uncertainties.

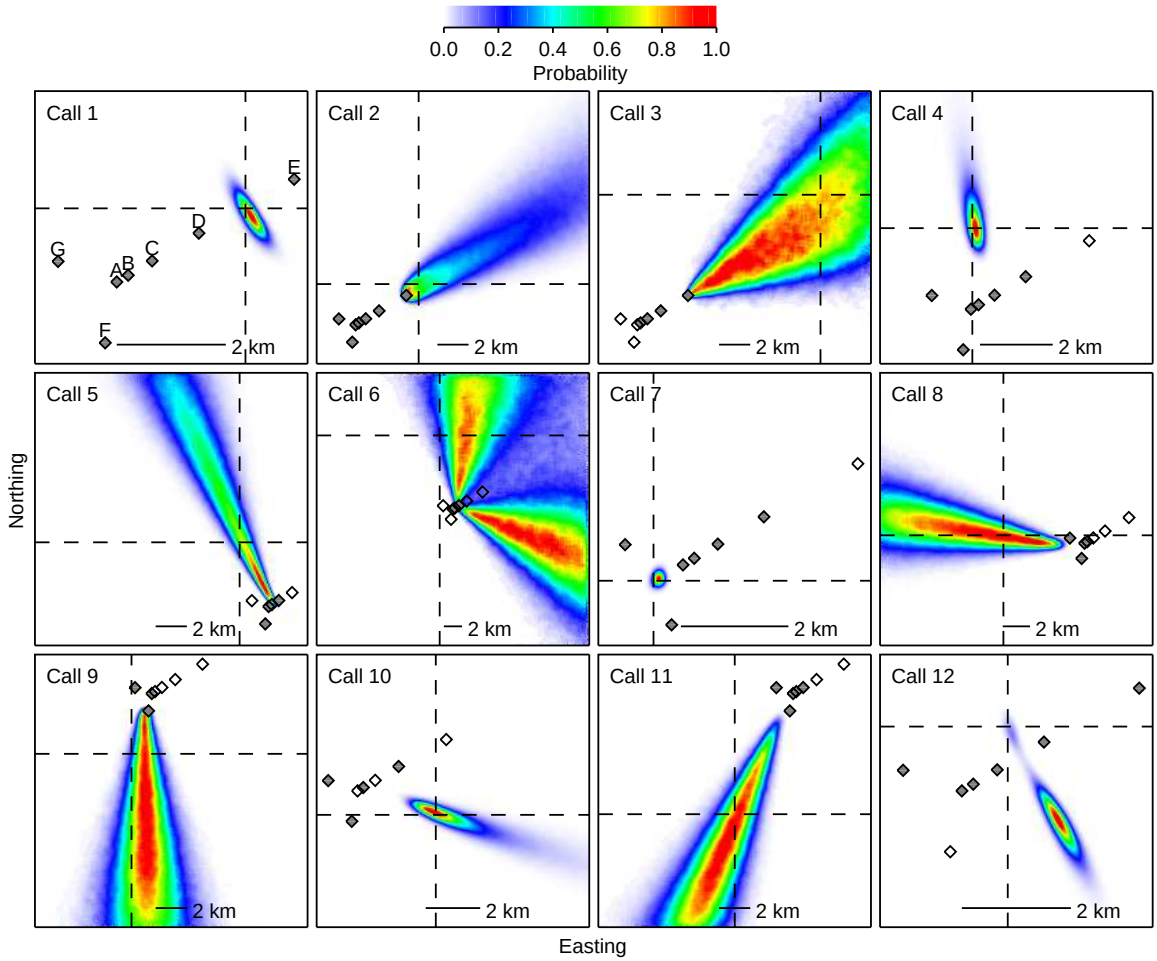

Figure 4.2: Normalized marginal probability densities of simulated whale locations for calls 1–12. *A priori* recorder locations (simulated GPS deployment positions) are shown with diamond symbols; filled diamonds indicate recorders with TDOA data, open diamonds represent recorders without an associated call. The intersection of the dashed lines indicates true whale locations. Receivers A–G are identified for call 1.

Figure 4.4 shows a sample of the fit to the data for the first four calls with the synthetic (noisy) TDOA data and the 5th and 95th percentiles for estimated TDOAs, calculated from a random sample of 5000 models from the PPD. The data index on the x-axis represents TDOA data from different recorder pairs. The observed and estimated TDOAs were reduced by the difference of the clock offset estimates [taken from the most-probable or maximum *a posteriori* (MAP) model sample] so the percentile differences were perceptible. The inversion sampled models that produced predicted TDOA data in excellent agreement with the measured data. The data fits

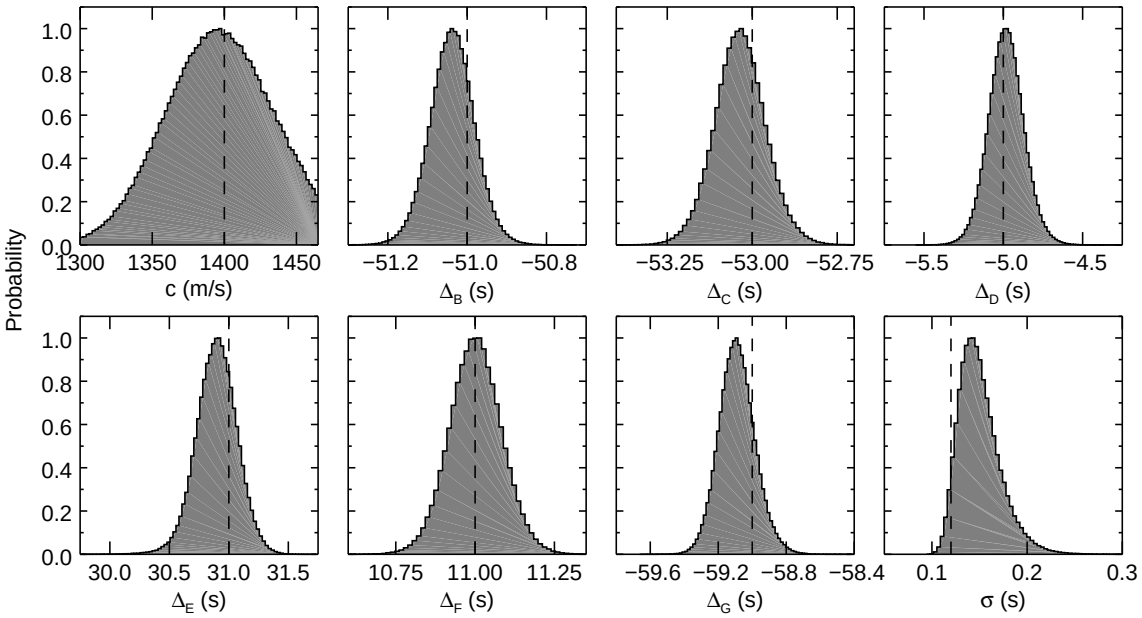

Figure 4.3: Normalized marginal probability densities for effective sound speed, relative recorder clock offsets, and residual error standard deviation for the simulation. True values are indicated with dashed lines.

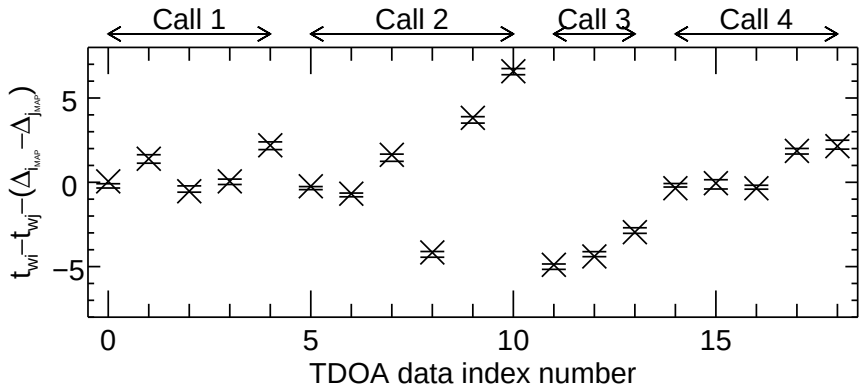

Figure 4.4: Simulated (×) and predicted (−) TDOA data (s) for simulated whale calls 1–4, reduced by the difference in relative recorder clock offsets from the MAP model. Predicted data are shown for the 5th and 95th percentiles of TDOA data from a random sample of the PPD.

to other calls were qualitatively similar and are not shown for brevity.

4.5 Chukchi Sea whale localization results

The Bayesian inversion was applied to six batches of bowhead whale-call TDOA data from different half-hour periods of the recordings (referred to as scenarios S1–S6, Table 4.2). I do not expect the relative recorder clock offsets to change significantly over the half-hour periods. The inversions were carried out on a desktop computer using a single 4.4 GHz central processing unit. Convergence was reached after collecting approximately 200 000 PPD samples which took between 1 and 10 hr depending on the scenario. The inversions were found to produce approximately Gaussian-distributed data residuals (Fig. 4.5) that were independent of time.

Table 4.2: Start dates and times for the six half-hour time windows analyzed for Chukchi Sea bowhead whale calls.

Scenario	Start Date	Start Time
S1	2013-09-27	00:30:00
S2	2013-09-27	01:00:00
S3	2013-09-27	01:30:00
S4	2013-10-03	00:00:00
S5	2013-10-06	00:00:00
S6	2013-10-11	03:39:00

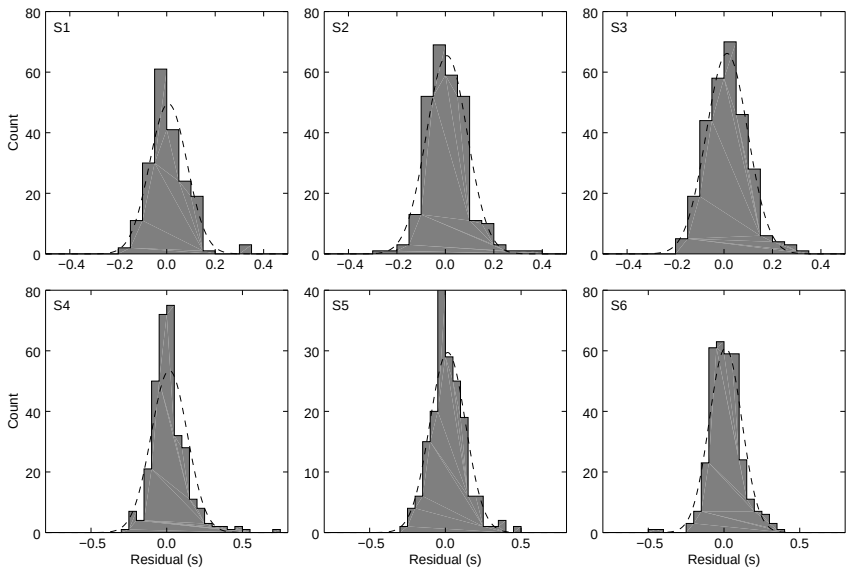

Figure 4.5: Histograms of residuals $[\mathbf{d}-\mathbf{d}(\mathbf{m})]$ for scenarios 1–6. Dashed lines indicate Gaussian distributions that are scaled by the residual standard deviation and the number of data for the corresponding scenarios.

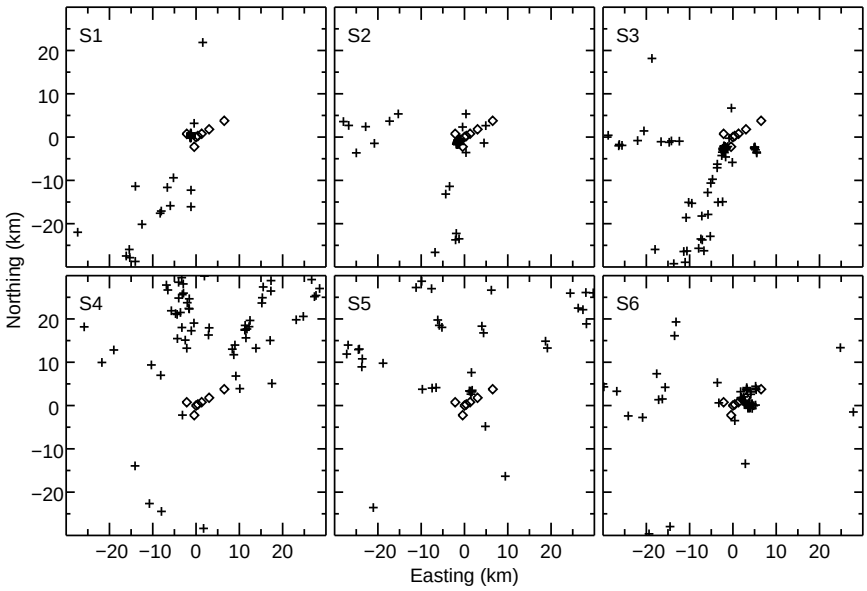

Figure 4.6: Bowhead whale locations (+ symbols) from the MAP models of each scenario. *A priori* AMAR locations (GPS deployment positions) are shown with diamond symbols.

Figure 4.6 shows the MAP whale locations for the six scenarios. Many of the 2D marginal probability densities for whale locations overlap, making them difficult to display on the same plot. For brevity, I only show a few (12) examples of localization marginals to illustrate the variety of PDF shapes in Fig. 4.7. Location uncertainty tends to increase with distance from the centre of the AMAR cluster. When the off-axis recorders do not record a call, the probability densities are symmetric about the cluster axis (panels d, j, and l). These three PPDs illustrate the potentially strong non-linearity of the inverse problem. Furthermore, the marginal densities can be multi-modal (panel d); resolving such probability densities required parallel tempering to provide sufficient sampling of all modes. The direction of arrival for calls at long ranges (panels b and h, and to a lesser degree, panels e, f, and i) is adequately determined but the range to the cluster is poorly constrained.

Although true whale locations are unknown, the nine whale calls analyzed using modal dispersion data in Chapter 3 were also analyzed using TDOA data in S6 for this chapter, so the localization results can at least be compared. Figure 4.8 shows the marginal PDFs for the whale locations in S6 that correspond to the nine calls in Chapter 3 (Fig. 3.8). In general, the TDOA-based locations agree and have uncertainties comparable to or larger than those of the modal dispersion-based estimates. One ex-

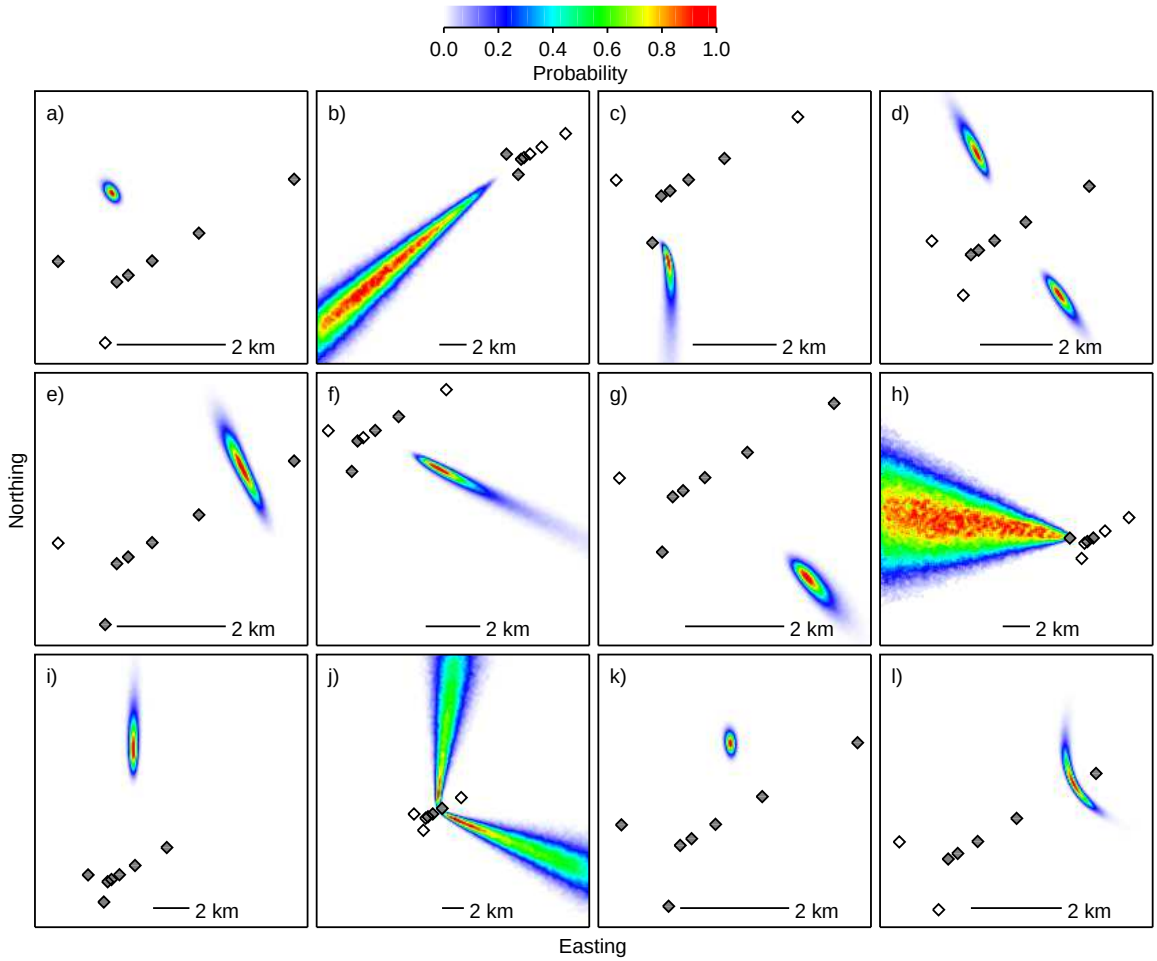

Figure 4.7: Normalized marginal probability densities of bowhead whale locations for 12 selected calls. *A priori* AMAR locations (GPS deployment positions) are shown with diamond symbols; filled diamonds indicate AMARs with corresponding annotations, open diamonds represent AMARs without associated call annotations.

ample where the TDOA data provides significantly less location information is for call 2; the range to the array is uncertain here but is well resolved by the modal-dispersion data in Fig. 3.8. Also note that the TDOA-based location for call 9 corresponds best with the dispersion-based location from the joint (multi-call) inversion.

The numerous whale location estimates close to AMARs A, F, and G in S1–3 shown in Fig. 4.6 form a roughly north–south oriented line. The call times can be estimated by rearranging Eq. (4.1) for τ_w using the call annotation time for t_{wi}, resulting in slightly different estimates from each AMAR. For the following analysis, I set the times for each call to the mean of the call times estimated from each AMAR. Figure 4.9 shows the whale easting and northing vs. time for S1–3. The locations

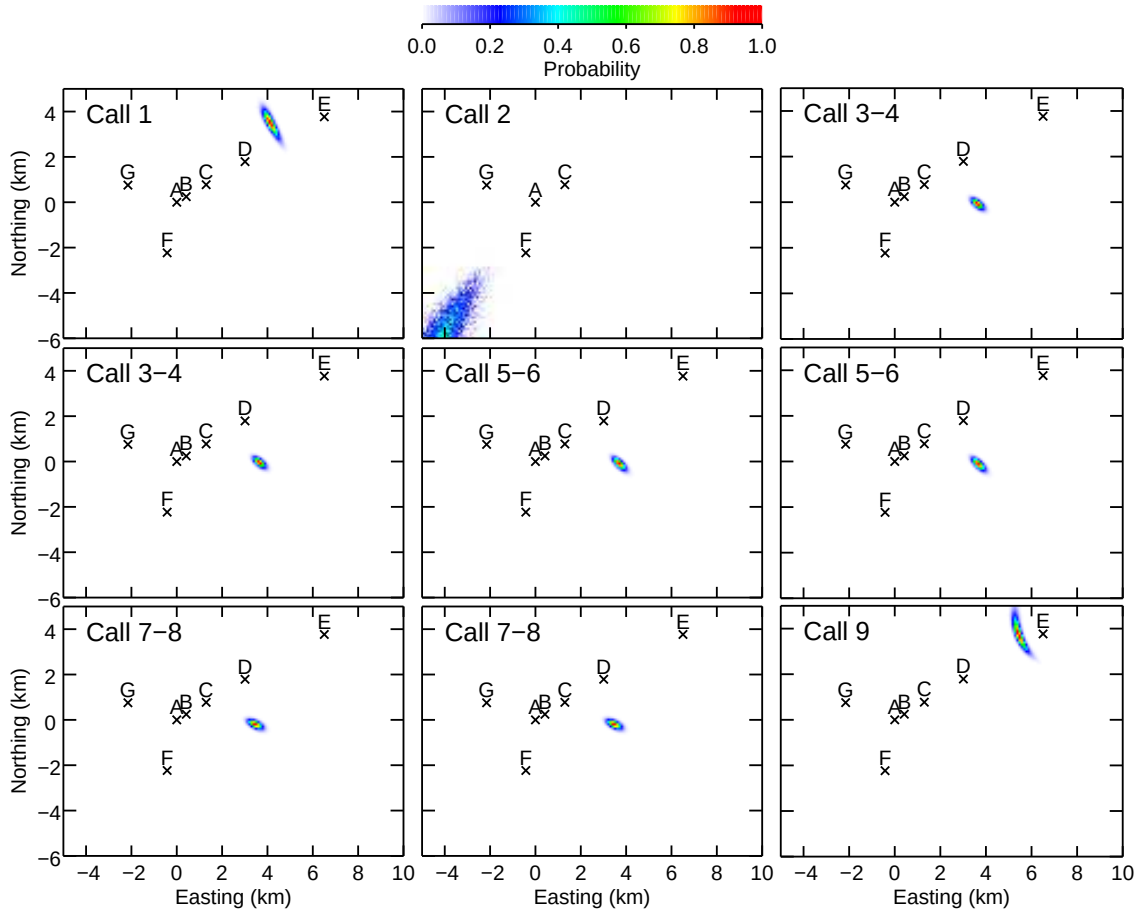

Figure 4.8: Normalized marginal probability densities of bowhead whale locations from S6 for the same calls as analyzed using modal dispersion data in Chapter 3. Call numbers on each panel correspond to call numbers in Chapter 3. Marginal densities for pairs of calls (3-4, 5-6, 7-8) are duplicated here because the annotations for the TDOA analysis encompassed both calls, treating the call pairs as single calls. The easting and northing extents are identical to those in Fig. 3.8 to allow direct comparison between the figures. Note that the marginal density for call 2 extends away from the AMARs to the boundary formed by the minimum easting and northing prior (-30 km).

estimated from periodic bursts of calls may indicate a whale (or whale group) travelling southward at approximately 3 km/hr, a reasonable (although somewhat slow) speed for migrating bowhead whales.[66]

The estimated whale locations, call times, and sound speed can be used to examine possible whale response to receiving other calls (i.e., a responder whale that makes a call after hearing a caller whale's call). I illustrate two examples of this with different levels of uncertainty in Fig. 4.10. The left panels show normalized 2D probability

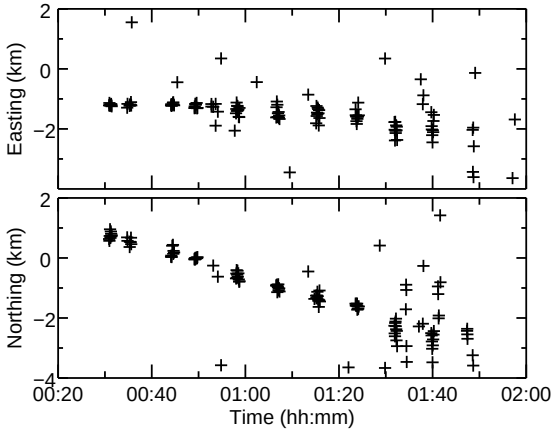

Figure 4.9: Whale easting and northing vs. time (on 27 Sept., 2013) from the MAP models in S1–3. The clusters of whale locations are likely from a whale (or whale group) travelling at approximately 3 km/hr.

densities for the acoustic wavefront location of the caller's call at the time of the responder's call. Contours of the whale location probability densities and *a priori* recorder locations are also shown. The right panels show the normalized probability densities for the response delays (i.e., response call time after receiving the initial call). The upper panels show a caller/responder pair where the response delay is well constrained to just over 1 s. The lower panels show a caller/responder pair where the response delay PDF peaks at a few seconds but is quite wide and extends to negative delays, indicating that the responder may have called before hearing the first call. Most of the potential caller/responder calls I examined had relatively large uncertainties in response delays (larger than those in the lower panels of Fig. 4.10) which precluded a probabilistic analysis of the response delay for large numbers of call pairs.

Table 4.3 lists the mean sound speed, relative recorder clock offsets, and residual error standard deviations with uncertainties for S1–6, as well as clock offset estimates from a modal-dispersion inversion[37] for a shorter time window within that of S6. Figure 4.11 shows the corresponding marginal probability densities for S6 (corresponding figures for S1–5 are omitted for brevity). The average effective waveguide sound speed and two-standard deviations (2SD) were 1403 and 35 m/s, respectively. The sound speed corresponds approximately with the average mode group speeds expected for the measurement environment for the frequencies of the annotated bowhead whale calls (1436 and 1383 m/s for modes 1 and 2, respectively). The clock drifts are approximately linear over the scale of days (also see Fig. 4.12). The estimated clock offsets

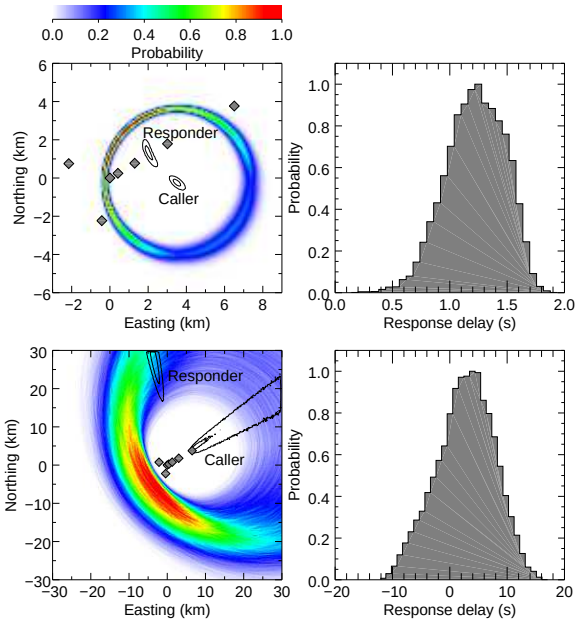

Figure 4.10: Normalized PDFs for (left) wavefront location from a caller whale at the time a (potential) responder makes a call, and (right) response delay of the responder. Contours of the marginal PDFs for whale locations are also shown on the left panels. Top and bottom rows show examples from pairs of calls in S6 and S4, respectively.

in S6 are similar to but not consistent (within uncertainties) with those in Warner *et al.*[37] using whale-call dispersion inversion. The latter estimates are likely more accurate because the normal-mode modelling of dispersive propagation is more accurate and dispersion data are more informative than the straight-path time-of-flight model and TDOA data used in this chapter.

Figure 4.12 shows the mean clock offset estimates from the whale call inversion vs. time compared with point estimates obtained from cross-correlations of ambient noise.[91] For the latter, long-time (1–4 days) ambient noise cross-correlation functions (NCF) were estimated by averaging NCFs calculated from sequential five-minute recordings. Such long time-averages were required to build the NCF due to the relatively large recorder separations; however, over these long durations, the clocks drifted relative to each other. To account for this, relative clock drift rates were estimated from the clock offset inversion results (they varied from approximately 11 to 54 ms/hr) and the cross-correlations were calculated after delaying each five-minute noise segment of the non-reference recorder using drift rates of approximately ± 10 ms/hr from the inversion estimates with 1 ms/hr increments. The acoustic noise segments were band-pass filtered between 50 and 250 Hz and clipped to reduce the

Table 4.3: Estimated effective waveguide sound speed, relative AMAR clock offsets, and residual error standard deviations, all with corresponding 2SD uncertainties for the bowhead whale call inversions. Clock offset estimates from a previous study (Warner *et al.*[37]) during a smaller time window of S6 are also included.

Scenario	c (m/s)	Δ_B (s)	Δ_C (s)	Δ_D (s)	Δ_E (s)	Δ_F (s)	Δ_G (s)	σ (s)
1	1454,18	20.42,0.055	79.70,0.074	44.17,0.098	42.45,0.162	42.20,0.088	37.93,0.159	0.10,0.010
2	1421,49	20.42,0.052	79.66,0.058	44.01,0.098	42.19,0.347	42.35,0.092	37.96,0.097	0.10,0.009
3	1322,42	20.42,0.055	79.54,0.069	43.87,0.116	42.32,0.431	42.70,0.090	38.19,0.082	0.13,0.035
4	1422,25	21.93,0.058	87.30,0.051	48.05,0.068	47.35,0.100	46.94,0.058	41.33,0.063	0.13,0.007
5	1429,45	22.73,0.069	91.24,0.075	50.18,0.113	50.08,0.178	49.33,0.101	43.10,0.075	0.14,0.012
6	1370,31	24.09,0.043	97.97,0.046	53.79,0.097	54.76,0.202	53.37,0.063	46.01,0.047	0.13,0.011
Ref. [37]	N/A	24.04,0.003	97.84,0.003	53.54,0.009	54.39,0.026	53.16,0.007	45.87,0.005	N/A

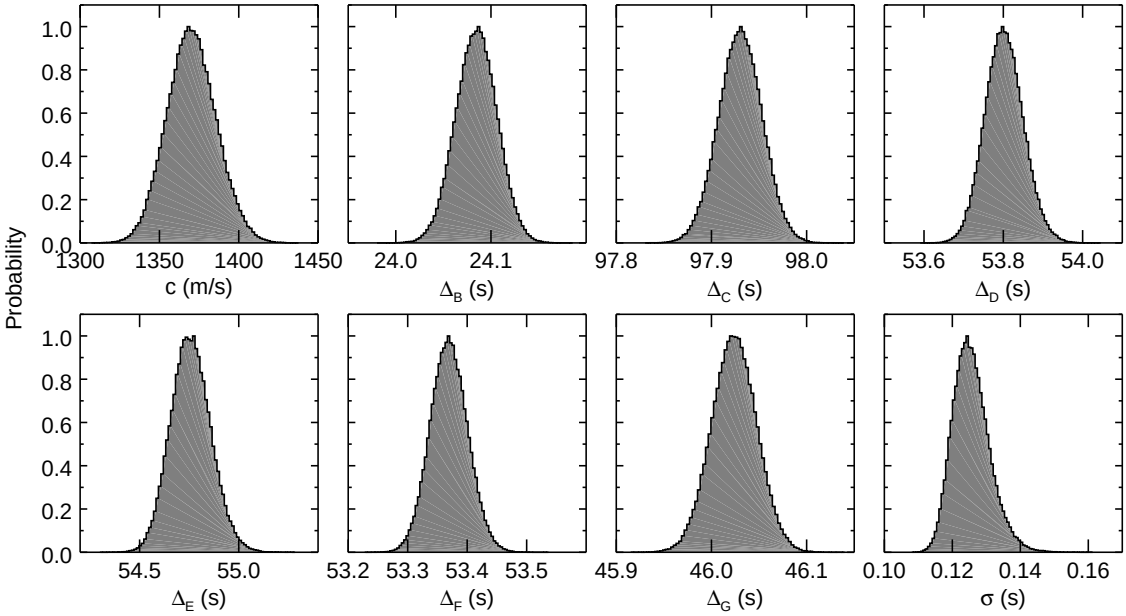

Figure 4.11: Normalized marginal probability densities for effective sound speed, relative recorder clock offsets, and residual error standard deviation estimated from the bowhead-whale call TDOA data in S6.

influence of transient noise events (e.g., bowhead whale calls). Only some NCFs (time period and drift rate combinations) showed the expected double-peak structure (at $\pm$ the acoustic travel time between receivers) and were suitable for estimating clock offset, likely because vessel noise significantly violated the uniform noise source distribution assumption for some time segments. For each time period that resulted in the double-peak structure, only the NCF with strongest double peaks over all trial drift rates was saved for analysis. Clock offset estimates were obtained from the average of the lags corresponding to the two peaks of the derivative of the NCF.

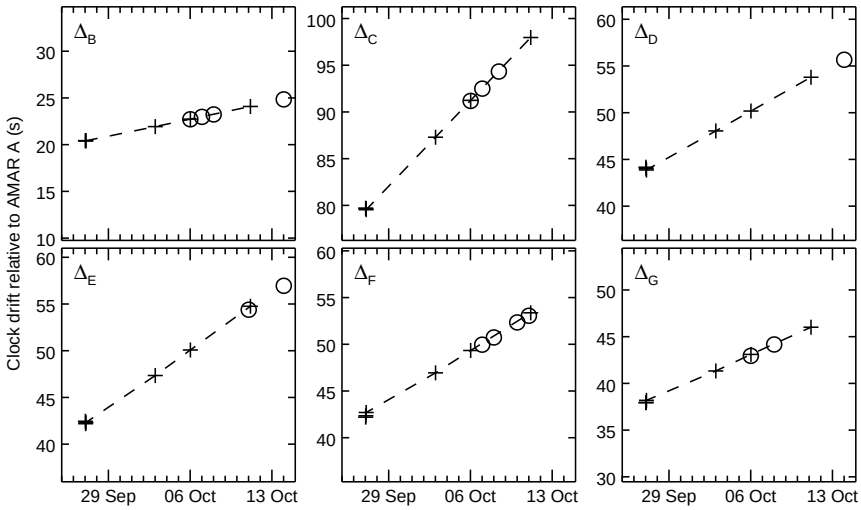

Figure 4.12: Relative recorder clock offset vs. time estimated from the TDOA inversion (+) and using ambient noise (∘).

Figure 4.13 shows an example of the derivative of the NCF obtained from a one-day averaged NCF on 7 October, 2013 with AMARs A and B, assuming a relative clock drift rate of 11 ms/hour for AMAR B. Although the function is not perfectly symmetric about the average of the peak lags, the relative recorder clock offset can still be estimated to sufficient accuracy for comparison with the whale-call inversion results. The two-way travel-time (TWTT) corresponds to an effective waveguide sound speed of approximately 1330 m/s based on the GPS-based AMAR separation distance of 486 m which is lower than the sound speed estimated in S5 (Table 4.3). This discrepancy may be due to inaccurate AMAR locations and/or the different frequency/modal content between the coherent ambient noise and the bowhead whale calls affecting the average mode group speed. The clock offsets from all suitable NCF derivatives are shown in Fig. 4.12 with circles.

Finally, the fit to the TDOA data achieved by the Bayesian inversion is illustrated in Fig. 4.14 for the first four calls in S1 with the observed TDOAs and the 5th and 95th percentiles for estimated TDOAs, calculated from a random sample of 5000 models from the PPD. The data index on the x-axis represents TDOA data from different AMAR pairs. The observed and estimated TDOAs were reduced by the difference of the MAP clock-offset estimates so the percentile differences are perceptible. The inversion sampled models that produced predicted TDOAs that are in good agreement with the measured data. The data fits to other calls and scenarios were qualitatively similar and are not shown for brevity; however, Table 4.3 lists the residual error

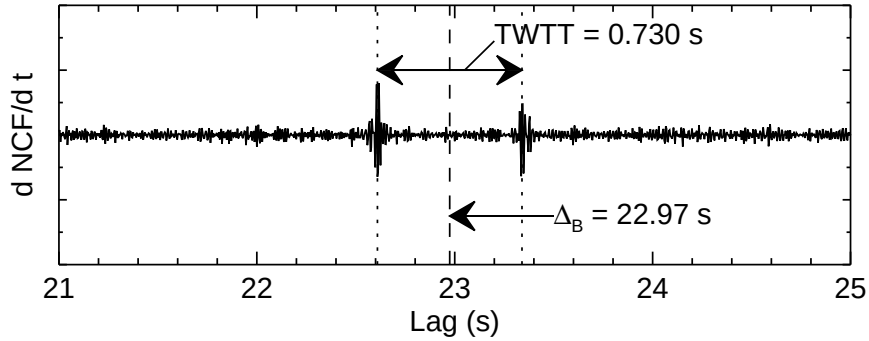

Figure 4.13: Time derivative of the one-day time-averaged NCF between AMARs A and B from 7 Oct., 2013. Dotted lines indicate peak times of the envelope of the derivative of the NCF and the dashed line indicates the relative recorder clock offset (i.e., average of the two peak times).

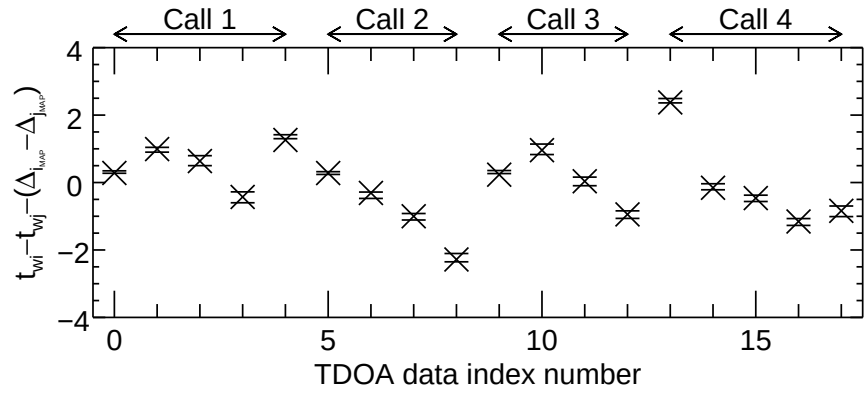

Figure 4.14: Measured (×) and predicted (−) TDOA data (s) for bowhead-whale calls 1–4 in S1, reduced by the difference in relative recorder clock offsets from the MAP model. Predicted data are shown for the 5th and 95th percentiles of TDOA data from a random sample of the PPD.

standard deviation statistics for all scenarios. The estimated error standard deviations varied from about $\sigma = 0.10$ to 0.14 s.

4.6 Summary and conclusion

This chapter presented Bayesian inversion of bowhead-whale call time-difference-of-arrival data from recordings on an asynchronous hydrophone cluster in the Chukchi Sea. Calls were first manually detected, annotated, and associated between recorders, and then TDOAs were calculated by cross-correlating filtered waveforms. Linearly-dependent data with lower peak cross-correlation values were not included in the

inversion. This data filtering was necessary for obtaining rigorous uncertainty estimates in the Bayesian inversion (which assumed independent errors) and also reduced the influence of modal dispersion on TDOA data that was not accounted for in the straight-path time-of-flight propagation model. The TDOA data were used to estimate the whale locations, effective waveguide sound speed, relative recorder clock offsets, receiver locations, data error statistics, and their uncertainties.

A simulation study based on the recorder geometry of the Chukchi Sea acoustic measurement program illustrated the degree to which model parameters could be estimated. Sound speed and receiver locations were poorly resolved within their prior bounds but clock offsets and whale locations were estimated with relatively small uncertainties. The source-receiver geometry had a large effect on whale location uncertainties and the PPD showed nonlinear effects including multi-modal structure and left-right ambiguities for whale locations in some cases.

The inversion of bowhead whale-call TDOA data from recordings in the Chukchi Sea showed similar effects to the simulation study. Whale location uncertainty was generally smaller for calls originating closer to the centre of the receiver cluster. Some calls were well localized in two dimensions whereas other calls were well resolved in bearing but poorly resolved in range to the cluster. Several bowhead whale locations estimated from TDOA data agreed well with estimates using modal-dispersion data, although the location uncertainties were typically larger for the TDOA data. A sequence of calls received over a one-hour period were localized and likely represent the track of a whale (or whale group) travelling at approximately 3 km/hr. Examples of possible whale responses were also presented but response delay uncertainties were typically large. Relative recorder clock offsets were estimated at several times spanning a two-week period and showed approximately linear drift rates. Estimated clock offsets agreed with estimates obtained by long-time cross-correlations of ambient noise.

Overall, the inversion approach applied in this chapter is capable of estimating marine-mammal locations with uncertainties as small as 70 m (standard deviation) from recordings of calls made on a large-aperture array of unsynchronized recorders. The method requires diversity of whale locations and minimal clock drift during the analysis window. The approach can be used to estimate marine mammal spatial density or to track individuals (or groups). The inversion is suitable to automatically detected and associated marine-mammal calls, allowing analysis of large data sets.

Chapter 5

Summary and Discussion

This thesis developed hydroacoustic inversion methods to estimate bowhead whale locations and estimate environmental properties, including fully nonlinear uncertainty estimates. Bowhead whales migrate through the Chukchi Sea, Alaska, where there has recently been substantial oil and gas exploration activity. There is concern that anthropogenic noise could injure marine mammals or disturb their behaviour. Localizing marine mammals and quantifying their sound-exposure levels is therefore important for understanding their interaction with anthropogenic noise. Accurate environmental models are required for predicting sound propagation but are often unknown to sufficient detail for modelling sound at the low frequencies that are often associated with anthropogenic noise sources. This thesis develops remote-sensing techniques to estimate environmental properties and whale locations over the scale of several kilometres. The methods are applicable to acoustic data recorded on asynchronous recorders which are relatively inexpensive and easy to deploy (compared to cabled systems or multichannel arrays), and are widely used to monitor large areas.

A nonlinear Bayesian framework is used for all inversions in this thesis. In a Bayesian approach, probability is considered to represent the degree of belief and the unknown parameters are considered random variables. The solution to the inverse problem consists of properties of the posterior probability density which combines the data and prior information. The PPD is sampled numerically using a Markov-chain Monte Carlo method (and in cases where the model parameterization is unknown, a reversible-jump MCMC method). Relatively uninformative bounded uniform prior probability densities are used so the information in the data primarily determines parameter uncertainties and resolved model structure.

The thesis considered three distinct but closely related data sets/inversion ap-

proaches. The first involved estimating environmental parameters from airgun modal-dispersion data in a trans-dimensional inversion. Airgun modal dispersion is quantified from single-channel autonomous recorder data using time-frequency analysis and inverted for the SSP and subbottom properties. A nonlinear resampling technique (warping) is used to improve the modal-dispersion resolution. The inversion is trans-D in terms of the number of water-column SSP nodes, subbottom layers, and first-order auto-regressive error parameters (modelling correlated errors). Estimated uncertainties for environmental properties include uncertainties associated with the uncertainty in model parameterization. A simulation study showed the inherent limitations of the data processing method can lead to autocorrelated errors of mode arrival times and can comprise a significant component of the total errors. Inversion of measured data yielded a SSP in excellent agreement with direct measurements (carried out with a CTD probe) and seafloor sound speeds in agreement with an independent headwave analysis.

The second data set/inversion in this thesis involved estimating bowhead whale locations and environmental parameters using modal-dispersion data. Bowhead whale-call dispersion data are quantified from asynchronous recorder data and inverted for the whale locations, environmental properties, source instantaneous frequency, and relative recorder clock offsets. A modified mode-warping technique is used to quantify modal-dispersion data from non-impulsive sources. The inversion is trans-D in terms of the SSP and subbottom layering in the same way as the airgun dispersion-based environmental characterization described above. A simulation study showed inaccurate environmental knowledge did not preclude localization as long as the environmental parameters were treated as unknown and estimated in the inversion (i.e., the data have sufficient information to constrain both the source locations and environmental parameters). Inversions of simulated and measured data showed that whale-location uncertainties decreased substantially in joint (multi-call) inversions. Estimated environmental-parameter uncertainties were larger than for airgun modal-dispersion data; however, the environmental knowledge gained by the whale-call inversions significantly reduced the uncertainties of predicted received levels as a function of range. In particular, the uncertainties in predicting the source range to a specified sound-level threshold were reduced significantly by applying environmental knowledge from the PPD rather than from the prior.

The third data set/inversion in this thesis also involved estimating bowhead whale locations but used time-difference-of-arrival data. Bowhead whale call TDOA data

were derived from asynchronous recorder data by cross-correlation and inverted for the whale locations, relative recorder clock offsets, effective waveguide sound speed, and recorder locations. A straight-path time-of-flight propagation model was used to predict TDOA data for bowhead-whale calls. The computational efficiency of this approach to data processing and propagation modelling allowed the corresponding inversion to be applied to many more whale calls than the modal dispersion-based localization. A simulation study showed nonlinear uncertainty estimates of whale locations were highly dependent on source-receiver geometry. In some cases, accurate whale locations were estimated; in others the whale's bearing, but not range, could be estimated accurately. Some localization uncertainties were multi-modal due to symmetries in the source-receiver geometry, indicating strong nonlinearity of the inverse problem. Inversions of measured data provided estimates of relative recorder clock drift rates that agreed with independent estimates from ambient noise cross-correlations. Location estimates of a repeatedly-calling whale (or whale group) suggest the track of a whale travelling at a speed of approximately 3 km/hr. An example of possible bowhead whale response to receiving another whale's call is shown.

All three inversion methods assume range-independent environments. The methods could be adapted for range-dependent environments by using a range-dependent forward propagation model in the inversions. This would increase the computational expense of the inversion but should provide accurate results if the range-dependence is known. It may be possible to include uncertainty in environmental range-dependence but this would significantly increase the computational expense and complexity of the algorithms.

Amplitude information is not used in this thesis since dispersion and TDOA data are independent of mode and bowhead whale call sound levels except in the sense that signals must not attenuate into the background before reaching the recorders. Environments with high sediment shear wave speeds may attenuate mode amplitudes, reducing the information in mode arrival time data. It may be possible to utilize amplitude information in a joint amplitude/arrival-time inversion but this would require treating additional parameters as unknowns (e.g., sediment attenuation or source depth). In deep-water environments where modes propagate in the deep sound channel with relatively low attenuation, the modal dispersion methods may work particularly well for localization and characterizing the SSP.

Rigorous uncertainty estimates are important for interpreting results of parameter estimation problems (e.g., inversions), and are critical when independent or "ground-

truth" information is unavailable. The Bayesian inversions developed and applied in this thesis provide rigorous parameter uncertainty estimates and account for uncertainties in model parameterization (when parameterization is unknown *a priori*). The airgun modal-dispersion inversion provides high-resolution environmental property estimates that are representative over a large area and can be used to accurately predict sound-exposure levels at marine-mammal locations. The bowhead-whale call dispersion inversion provides highly accurate whale location estimates and a passive-acoustic method for obtaining environmental information that could be used in a noise impact assessment prior to anthropogenic activity. The bowhead-whale call TDOA inversion provides a fast (but less precise) method for localizing relatively large numbers of whales using calls recorded on widely-distributed asynchronous recorders, allowing investigation into the effects of anthropogenic noise on marine-mammal behaviour.

In summary, the work in this thesis provides a significant contribution in terms of inversion approaches for passive whale localization and environmental characterization. A number of the inversion methods applied here (e.g., trans-D inversion, parallel tempering) have not been used previously in marine-mammal localization. The Bayesian formulation allows uncertain quantities (e.g., environmental properties, clock offsets, source IF, receiver locations) to be included in the localization inversion as unknown parameters constrained by available prior information. The whale localization uncertainties therefore account for the uncertainties of such parameters. Further, the Bayesian approach provides probabilistic estimates (combining data and prior information) for the environment, clock offsets, etc., some of which are of interest in their own right. The PPD over environmental properties is applied here in a forward-modelling application to produce probabilistic information on sound-exposure levels. The Bayesian approach quantifies the information content in an inverse problem, and the application here to different data sets (modal dispersion and TDOA) compares their accuracy for whale localization, which can be considered relative to the ease/efficiency of the data processing and inversion to evaluate the practical applicability to large data sets. Finally, it should be noted that the methods developed here are not limited to bowhead whale localization or environmental characterization in the Arctic, but could be applied generally in passive localization and/or environmental characterization applications.

Appendix A

Trans-dimensional inversion formulation

A.1 Trans-dimensional Bayesian inversion

This section develops a trans-dimensional (trans-D) Bayesian inversion for modal dispersion.[58,59] Let $\mathbf{d}$ be a random variable of N observed data and let $\mathbf{m}_k$ be a vector of M_k model parameters for a physical system of interest, where k ($\in \mathcal{K}$) indexes the form of the system representation. Green[32] showed that Bayes' rule can then be written

$$P(k, \mathbf{m}_k|\mathbf{d}) = \frac{P(k)P(\mathbf{m}_k|k)P(\mathbf{d}|k, \mathbf{m}_k)}{\sum_{k' \in \mathcal{K}} \int_{\mathcal{M}} P(k')P(\mathbf{m}'_{k'}|k')P(\mathbf{d}|k', \mathbf{m}'_{k'})d\mathbf{m}'_{k'}}. \tag{A.1}$$

Equation (A.1) represents a single hierarchical model of the physical system spanning several multi-dimensional subspaces. $P(k)$ is the prior distribution for k which indexes the number of subbottom interfaces, number of nodes defining the water-column SSP, and state of the first-order auto-regressive [AR(1)] error model (described in Secs. A.3, A.4, and A.5, respectively). $P(\mathbf{m}_k|k)$ is the prior probaility density function (PDF) for the M_k model parameters. $P(\mathbf{d}|k, \mathbf{m}_k)$ is the conditional data error PDF; however, for fixed (measured) data $\mathbf{d}$, this probability is interpreted as the likelihood of the model parameters, $L(k, \mathbf{m}_k)$.

The trans-D posterior probability density (PPD) $P(k, \mathbf{m}_k|\mathbf{d})$ in Eq. (A.1) can be approximated in a Markov-chain Monte Carlo (MCMC) simulation that can transi-

tion (jump) between system representations specified by k for models of dimension M_k. A reversible-jump MCMC (rjMCMC) algorithm[32] is used to sample the PPD while maintaining detailed balance for unbiased sampling.[100] Transitions from the current model $(k, \mathbf{m}_k)$ to a new model $(k', \mathbf{m}'_{k'})$ are proposed from a proposal density $Q(k', \mathbf{m}'_{k'}|k, \mathbf{m}_k)$ (i.e., the probability of proposing the new model given the current model) and accepted with probability given by the Metropolis-Hastings-Green criterion

$$\alpha = \min\left[1, \frac{P(k', \mathbf{m}'_{k'})}{P(k, \mathbf{m}_k)} \left(\frac{L(k', \mathbf{m}'_{k'})}{L(k, \mathbf{m}_k)}\right)^{1/T} \frac{Q(k, \mathbf{m}_k|k', \mathbf{m}'_{k'})}{Q(k', \mathbf{m}'_{k'}|k, \mathbf{m}_k)} |\mathbf{J}|\right], \tag{A.2}$$

where $|\mathbf{J}|$ is the determinant of the Jacobian for the diffeomorphism from $(k, \mathbf{m}_k)$ to $(k', \mathbf{m}'_{k'})$ and T is the sampling temperature which can be considered unity here but is varied in the method of parallel tempering (described below). The rjMCMC algorithm used here is the birth-death scheme,[31] which has been used in several trans-D geoacoustic inversion studies.[42,53,58] For the trans-D geoacoustic profile, I implement this scheme by adding or removing subbottom interfaces which define homogeneous layers with sound speed and density. For a birth step, a new subbottom interface is inserted at a random depth selected from a uniform prior. The physical properties of the layer above the new interface are chosen randomly from the prior PDF. For a death step, an existing interface is randomly selected and removed. The physical parameters of the new thicker layer are chosen from the layer below the removed interface.

This birth/death scheme differs from that used in most trans-D geoacoustic inversion work. Previous studies have used symmetric proposal probability densities centred around the current parameter values, so that high-likelihood models will be proposed if the current model has high likelihood and the proposal PDF width is relatively small.[53] However, this can cause the proposal and prior ratios in Eq. (A.2) to be small which decreases the acceptance probability. Dosso *et al.*[59] showed that birth acceptance rates could be much higher by proposing from the prior compared to proposing close to the current model (the formulation is also simpler). I performed inversions using both schemes and found the acceptance rate was approximately four times higher when proposing from the prior than when using Gaussian proposals, resulting in faster PPD convergence.

In the water column, I implement the birth-death scheme by adding or removing SSP nodes which define a piecewise $1/c_w^2$ linear profile. Birth steps involve inserting a node with a depth and sound speed selected randomly from bounded uniform prior

PDFs. For a death step, an existing node is randomly selected and removed. New parameter values are not needed for this step because the water SSP effectively heals by joining the SSP above and below the removed node. The acceptance probability for the birth and death moves for either the water column or subbottom is given by Eq. (A.2). These birth/death schemes ensure $|\mathbf{J}|$ is unity.[32]

Achieving efficient dimension jumps and complete sampling of potentially multimodal structure within fixed-dimensional subspaces is a challenge in trans-D inversion.[42,59,101] One strategy is to use parallel tempering[41–43,102,103] which applies a sequence of interacting Markov chains that sample the PPD at different temperatures T [Eq. (A.2)]. The acceptance probability α increases with T which allows more low-likelihood models to be accepted. Thus, higher-temperature chains sample the parameter space more freely, bridging potentially multimodal PPD structure or jumping dimension more readily. Lower temperature chains sample local PPD structure more efficiently. Chains with $T \neq 1$ do not provide unbiased sampling; however, the efficient exploration of the space provided by high temperature chains can be combined with unbiased $T = 1$ chains by allowing chains to probabilistically swap models according to the Metropolis-Hastings criterion: a swap of models between chains of temperatures T and T' is accepted with probability

$$p = \min\left[1, \left(\frac{L(k', \mathbf{m}'_{k'})}{L(k, \mathbf{m}_k)}\right)^{(1/T - 1/T')}\right]. \tag{A.3}$$

Although the computational expense of the inversion increases linearly with the number of parallel-tempering chains, the rate of PPD convergence may substantially outweigh this factor for suitably-chosen temperatures.[43,102] The chain temperatures are usually taken from a geometric sequence with swaps allowed between arbitrary chain pairs.[102] For this thesis, 10 rjMCMC chains were used with $T_i = 1.2^i, i = 0, \ldots, 9$.

There is no definitive test for convergence of Markov-chain sampling to the PPD[101] so it has been suggested that sampling should be conducted for some time after the PPD ceases to change significantly with new samples.[104] This can result in large sample populations which can take up large computer disk space and result in long post-processing times. Chain thinning[105] is used to reduce the correlation between samples and represent the PPD more efficiently, but it is difficult to know *a priori* how much to thin. The new method of fixed-length thinning[60] overcomes this by adaptively thinning samples based on a fixed number of desired PPD samples. New

samples are probabilistically added to the PPD sample population by overwriting randomly selected existing samples while ensuring the probability of any two samples existing in the population is identical. The acceptance probability for the ith model in the chain is

$$\alpha_i = \begin{cases} 1, & i \leq N_{\text{tot}} \\ \frac{\alpha_{i-1} N_{\text{tot}}}{\alpha_{i-1} + N_{\text{tot}}}, & i > N_{\text{tot}} \end{cases}$$

where N_{tot} is the total number of samples in the desired population.

A.2 Likelihood

The likelihood function is dependent on the residual error statistics. These errors result from measurement, data-processing, and theory errors, the statistics of which are often unknown. The errors may have an autocorrelated component that I model using an AR(1) process.[53,106] The total data residuals for model $\mathbf{m}_k$ are given by

$$r_i = d_i - d_i(\mathbf{m}_k) - d_i(a), \tag{A.4}$$

where

$$d_i(a) = a(d_{i-1} - d_{i-1}(\mathbf{m}_k)) \tag{A.5}$$

is the AR(1) process, $\mathbf{d}(\mathbf{m}_k)$ are the predicted data, and a is the AR(1) coefficient. The residual errors are assumed Gaussian distributed and a is restricted between -0.6 and 0.999. The validity of these error model assumptions are checked *a posteriori*. For N data with Gaussian-distributed errors the likelihood function is

$$L(k, \mathbf{m}_k) = \frac{1}{(2\pi)^{N/2} |\mathbf{C}_d|^{1/2}} \exp\left[-\frac{1}{2} (\mathbf{d} - \mathbf{d}(\mathbf{m}_k) - \mathbf{d}(\mathbf{a}))^T \mathbf{C}_d^{-1} (\mathbf{d} - \mathbf{d}(\mathbf{m}_k) - \mathbf{d}(\mathbf{a})) \right], \tag{A.6}$$

where $\mathbf{C}_d$ is a diagonal data covariance matrix [given that error covariances are represented by the AR(1) process]. Errors are assumed independent between modes and between pulses, but potential correlation over frequency for a given mode m and pulse p is characterized by the AR(1) coefficient a_{mp}. Further, the error standard deviation (σ_{mp}) is assumed constant over frequency but potentially changes between pulses and modes. Let $\mathbf{d}_{mp}$ represent a vector of modal arrival times at N_{mp} frequencies. The

likelihood function is the product

$$L(k, \mathbf{m}_k, \boldsymbol{\sigma}, \mathbf{a}) = \prod_{p=1}^{P_{\text{tot}}} \prod_{m=1}^{M_p} \frac{1}{(2\pi\sigma_{mp}^2)^{N_{mp}/2}} \exp\left[-\frac{|\mathbf{d}_{mp} - \mathbf{d}_{mp}(\mathbf{m}_k) - \mathbf{d}_{mp}(a_{mp})|^2}{2\sigma_{mp}^2} \right], \tag{A.7}$$

where P_{tot} is the total number of pulses considered and M_p is the number of modes considered for pulse p. Setting $\partial L/\partial\sigma_{mp} = 0$ leads to a maximum-likelihood estimate for σ_{mp}:

$$\hat{\sigma}_{mp}(\mathbf{m}_k) = \left[|\mathbf{d}_{mp} - \mathbf{d}_{mp}(\mathbf{m}_k) - \mathbf{d}_{mp}(a_{mp})|^2 / N_{mp} \right]^{1/2}. \tag{A.8}$$

Substituting Eq. (A.8) into Eq. (A.7) and neglecting multiplicative constants gives

$$L(k, \mathbf{m}_k, \mathbf{a}) = \exp\left[-\sum_{p=1}^{P_{\text{tot}}} \sum_{m=1}^{M_p} N_{mp} \log_e |\mathbf{d}_{mp} - \mathbf{d}_{mp}(\mathbf{m}_k) - \mathbf{d}_{mp}(a_{mp})| \right], \tag{A.9}$$

which provides an efficient treatment of unknown σ_{mp} without explicitly sampling additional parameters.[42]

A.3 Prior and proposal ratios—geoacoustics

Markov-chain moves for the geoacoustic parameters that do not change model dimension (i.e., number of subbottom layers) have unity prior and proposal ratios in Eq. (A.2) because I use a uniform prior $P(\mathbf{m}_k)$ and a symmetric (Gaussian) proposal PDF centred at the current parameter value. For moves that change dimension, the prior and proposal ratios are not unity. The prior PDF can be written

$$P(k, \mathbf{m}_k) = P(k)P(\mathbf{m}_k|k) = P(k)P(\mathbf{z}|k)P(\mathbf{c}_b, \boldsymbol{\rho}|k), \tag{A.10}$$

where $\mathbf{z}$ represents the set of subbottom interface depths, $\mathbf{c}_b$ and $\boldsymbol{\rho}$ represent layer sound speeds and densities, and k is taken here to represent the number of subbottom interfaces. The prior distribution for k is uniform from the assigned minimum to the maximum number of interfaces (0 and 10 for Chapter 2, respectively). The prior distribution for the depth partition (the set of interface depths) $\mathbf{z}$ is a Dirichlet distribution given by[59,60]

$$P(\mathbf{z}|k) = k! z_b^{-k}, \tag{A.11}$$

where z_b is a fixed maximum interface depth (50 m for this thesis), below which the data are insensitive and structure cannot be resolved, and the prior PDF for z_i is uniform over $[0,\ z_b]$. Intuitively, this distribution can be thought of as a uniform prior $(1/z_b)$ for each of the k interfaces with the factorial term accounting for the number of interface ordering permutations. The subbottom sound speed c_b and density ρ are bound by a joint prior PDF representing an empirical relationship based on a compilation of sediment samples to constrain models to physical speed and density combinations.[25,26] Density is constrained between bounds ρ_{low} and ρ_{high} (taken to be 1.3 and 2.5 g/cm^3, respectively) and sound speed (m/s) is constrained between empirical functions $c_{\text{low}}(\rho)$ and $c_{\text{high}}(\rho)$:

$$c_{\text{low}}(\rho) = (1.54 - 0.907\rho + 0.3659\rho^{1.88})1500.4 \tag{A.12}$$

$$c_{\text{high}}(\rho) = (1.60 - 0.907\rho + 0.3695\rho^{2.01})1501.4. \tag{A.13}$$

The joint prior PDF is therefore

$$P(\mathbf{c}_b, \boldsymbol{\rho}|k) = \begin{cases} A_{c\rho}^{-(k+1)}, & \rho_{\text{low}} \le \rho_i \le \rho_{\text{high}} \quad \forall\, i \\ 0, & \text{else,} \end{cases} \tag{A.14}$$

where $A_{c\rho}$ is the prior bound area,

$$A_{c\rho} = \int_{\rho_{\text{low}}}^{\rho_{\text{high}}} [c_{\text{high}}(\rho) - c_{\text{low}}(\rho)]d\rho. \tag{A.15}$$

Using equations (A.11) and (A.14), the prior ratios for birth and death moves are

$$\left[\frac{P(k', \mathbf{m}'_{k'})}{P(k, \mathbf{m}_k)}\right]_{\text{birth}} = \frac{k+1}{z_b A_{c\rho}}, \tag{A.16}$$

$$\left[\frac{P(k', \mathbf{m}'_{k'})}{P(k, \mathbf{m}_k)}\right]_{\text{death}} = \frac{z_b A_{c\rho}}{k}. \tag{A.17}$$

The proposal ratio for moves that jump dimension can be broken down into

$$\frac{Q(k, \mathbf{m}_k|k', \mathbf{m}'_{k'})}{Q(k', \mathbf{m}'_{k'}|k, \mathbf{m}_k)} = \frac{Q(k|k', \mathbf{m}'_{k'})}{Q(k'|k, \mathbf{m}_k)} \frac{Q(\mathbf{z}|k', \mathbf{m}'_{k'})}{Q(\mathbf{z}'|k, \mathbf{m}_k)} \frac{Q(\mathbf{c}_b, \boldsymbol{\rho}|k', \mathbf{m}'_{k'})}{Q(\mathbf{c}'_b, \boldsymbol{\rho}'|k, \mathbf{m}_k)}. \tag{A.18}$$

The proposal ratio for k cancels because $Q(k)$ is symmetric. Using the depth partition prior in Eq. (A.11) and drawing subbottom sound speed and density in birth steps

from the joint prior [Eq. (A.14)] results in proposal ratios

$$\left[\frac{Q(k,\mathbf{m}_k|k',\mathbf{m}'_{k'})}{Q(k',\mathbf{m}'_{k'}|k,\mathbf{m}_k)}\right]_{\text{birth}} = \frac{z_b A_{c\rho}}{k+1}, \tag{A.19}$$

$$\left[\frac{Q(k,\mathbf{m}_k|k',\mathbf{m}'_{k'})}{Q(k',\mathbf{m}'_{k'}|k,\mathbf{m}_k)}\right]_{\text{death}} = \frac{k}{z_b A_{c\rho}}. \tag{A.20}$$

The prior and proposal ratios cancel in the acceptance probability equation, leaving

$$\alpha = \min\left[1, \frac{L(k',\mathbf{m}'_{k'})}{L(k,\mathbf{m}_k)}\right]. \tag{A.21}$$

Equation (A.21) is therefore applicable in birth, death, and parameter perturbation steps for the geoacoustic parameters.

A.4 Prior and proposal ratios—sound-speed profile

The water-column SSP parameterization consists of sound speeds defined at the surface and seafloor, and sound speeds and depths defined at an unknown number of nodes within the water column (between 0 and 15 nodes are used in Chapter 2). A uniform prior is used for the number of nodes and for all speeds and depths, and proposals for parameter perturbations are based on a symmetric (Gaussian) PDF centred at the current parameter value. This ensures that most terms of the prior and proposal ratios in Eq. (A.2) cancel; however, in contrast to the geoacoustic layer-stack model, the prior distribution for the SSP node-depth partition does not generally cancel.

Markov-chain moves that do not change the dimension of the SSP have unity prior and proposal ratios, except for moves that change the water depth. The prior distribution for the node depth partition $P(\mathbf{z}|k)$ is of the same form as in Eq. (A.11) except that z_b is now the water depth and k is the number of water-column nodes. It is straightforward to show that the acceptance probability for birth, death, and perturbation moves for the SSP becomes

$$\alpha = \min\left[1, \left(\frac{z_b}{z'_b}\right)^k \frac{L(k',\mathbf{m}'_{k'})}{L(k,\mathbf{m}_k)}\right], \tag{A.22}$$

which reduces to the likelihood ratio for moves where z_b remains constant.

A.5 Trans-dimensional AR model

A trans-D algorithm is also applied to the residual error model[53] where index k takes one of two values: $k = 0$ indicates an error model without an auto-regressive component and $k = 1$ indicates an AR(1) process with coefficient $a \in [-0.6, 0.999]$. Let a_k represent the AR(1) parameter for a particular mode and pulse. Three moves are possible and are chosen with equal probability: birth of the AR(1) parameter, death of the AR(1) parameter, or a perturbation to a_1. If $k = 0$, only a birth move is possible and the prior probabilities $P(a_1')$ and $P(a_0)$ are $1/\Delta a$ and 1, respectively (here Δa is the width of the uniform prior PDF for a); therefore, the prior ratio is $P(a_1')/P(a_0) = 1/\Delta a$. The proposal probability is $Q(a_1'|a_0) = 1/\Delta a$ and the reverse step is $Q(a_0|a_1') = 1/2$ since the state a_1' could arise from either a birth or perturbation. The proposal ratio is $Q(a_0|a_1')/Q(a_1'|a_0) = \Delta a/2$. The birth acceptance probability is therefore

$$\alpha_{\text{birth}} = \min\left[1, \frac{1}{2}\frac{L(a_1')}{L(a_0)}\right]. \tag{A.23}$$

If $k = 1$, either death or perturbation moves are possible. For a death move, the prior probabilities $P(a_0')$ and $P(a_1)$ are 1 and $1/\Delta a$, respectively; therefore, the prior ratio $P(a_0')/P(a_1) = \Delta a$. The proposal probability is $Q(a_0'|a_1) = 1/2$ and the reverse-step probability is $Q(a_1|a_0') = 1/\Delta a$. The proposal ratio is $Q(a_1|a_0')/Q(a_0'|a_1) = 2/\Delta a$. The death acceptance probability is therefore

$$\alpha_{\text{death}} = \min\left[1, 2\frac{L(a_0')}{L(a_1)}\right]. \tag{A.24}$$

For a perturbation move, the prior ratio is unity and since symmetric (Gaussian) perturbation probability densities are used, the proposal ratio is also unity. The acceptance probability is simply the likelihood ratio

$$\alpha_{\text{perturb}} = \min\left[1, \frac{L(a_1')}{L(a_1)}\right]. \tag{A.25}$$

Bibliography

[1] L. T. Quakenbush, J. J Citta, J. C. George, R. J. Small, and M. P. Heide-Jørgensen. Fall and winter movements of bowhead whales (*Balaena mysticetus*) in the Chukchi Sea and within a potential petroleum development area. *Arctic*, 63(3):289–307, 2010.

[2] J. C. Comiso. A rapidly declining perennial sea ice cover in the Arctic. *Geophys. Res. Lett.*, 29(20):17–1–17–4, 2002.

[3] J. A. Hildebrand. Anthropogenic and natural sources of ambient noise in the ocean. *Mar. Ecol. Prog. Ser.*, 395:5–20, 2009.

[4] M. Guerra, A. M. Thode, S. B. Blackwell, and A. M. Macrander. Quantifying seismic survey reverberation off the Alaskan North Slope. *J. Acoust. Soc. Am.*, 130(5):3046–3058, 2011.

[5] C. Erbe, C. Reichmuth, K. Cunningham, K. Lucke, and R. Dooling. Communication masking in marine mammals: A review and research strategy. *Marine Poll. Bull.*, 103(1–2):15–38, 2015.

[6] W. J. Richardson, C. R. Greene Jr., C. I. Malme, and D. H. Thomson. *Marine mammals and noise*. Academic press, New York, 1995.

[7] W. J. Richardson, B. Würsig, and C. R. Greene Jr. Reactions of bowhead whales, *Balaena mysticetus*, to seismic exploration in the Canadian Beaufort Sea. *J. Acoust. Soc. Am.*, 79(4):1117–1128, 1986.

[8] S. B. Blackwell, C. S. Nations, T. L. McDonald, A. M. Thode, D. Mathias, K. H. Kim, C. R. Greene, and A. M. Macrander. Effects of airgun sounds on bowhead whale calling rates: evidence for two behavioral thresholds. *PloS One*, 10(6):1–29, 2015.

[9] R. A. Walker. Some intense, low-frequency, underwater sounds of wide geographic distribution, apparently of biological origin. *J. Acoust. Soc. Am.*, 35:1816–1824, 1963.

[10] W. A. Watkins and W. E. Schevill. Sound source location by arrival-times on a non-rigid three-dimensional hydrophone array. *Deep-Sea Res.*, 19:691–706, 1972.

[11] W. C. Cummings and D. V. Holliday. Passive acoustic location of bowhead whales in a population census off Point Barrow, Alaska. *J. Acoust. Soc. Am.*, 78:1163–1169, 1985.

[12] M. D. Collins, W. A. Kuperman, and H. Schmidt. Nonlinear inversion for ocean-bottom properties. *J. Acoust. Soc. Am.*, 93:2770–2783, 1992.

[13] S. E. Dosso, M. L. Yeremy, J. M. Ozard, and N. R. Chapman. Estimation of ocean-bottom properties by matched-field inversion of acoustic field data. *IEEE J. Ocean. Eng.*, 18:232–239, 1993.

[14] P. Gerstoft. Inversion of seismoacoustic data using genetic algorithms and a posteriori probability distributions. *J. Acoust. Soc. Am.*, 95:770–782, 1994.

[15] W. Menke. *Geophysical Data Analysis: Discrete Inverse Theory.* Academia Press, New York, 1984.

[16] R. C. Aster, B. Borchers, and C. H. Thurber. *Parameter Estimation and Inverse Problems*, pages 1–23. Elsevier, Amsterdam, second edition, 2013.

[17] C. M. Reiser, D. W. Funk, and D. Hannay. Marine mammal monitoring and mitigation during open water seismic exploration by Shell Offshore, Inc. in the Alaskan Chukchi Sea, July–October 2009: 90-day report. Technical Report P1112-1, LGL Alaska Research Associates Inc. and JASCO Research Ltd., 2010.

[18] J. Delarue, J. MacDonnell, B. Martin, X. Mouy, and D. Hannay. Northeastern Chukchi Sea joint acoustic monitoring program 2012–2013. Technical Report 00808, JASCO Applied Sciences, 2014.

[19] F. B. Jensen, W. A. Kuperman, M. B. Porter, and H. Schmidt. *Computational Ocean Acoustics, Series in Modern Acoustic and Signal Processing*, pages 271–333. AIP Press, New York, 1993.

[20] G. Le Touzé, B. Nicolas, J. I. Mars, and J. Lacoume. Matched representations and filters for guided waves. *IEEE Trans. Signal Process.*, 57:1783–1795, 2009.

[21] J. Bonnel, B. Nicolas, J. I. Mars, and S. C. Walker. Estimation of modal group velocities with a single receiver for geoacoustic inversion in shallow water. *J. Acoust. Soc. Am.*, 128:719–727, 2010.

[22] J. Bonnel, A. M. Thode, S. B. Blackwell, K. Kim, and A. M. Macrander. Range estimation of bowhead whale (*Balaena mysticetus*) calls in the arctic using a single hydrophone. *J. Acoust. Soc. Am.*, 136:145–155, 2014.

[23] A. Gelman, J. B. Carlin, H. S. Stern, and D. B. Rubin. *Bayesian Data Analysis*. Chapman, New York, 2004.

[24] T. J. Ulrych, M. D. Sacchi, and A. Woodbury. A Bayes tour of inversion: A tutorial. *Geophysics*, 66(1):55–69, 2001.

[25] Darrell R. Jackson and Michael D. Richardson. *High-Frequency Seafloor Acoustics*, pages 178–200. Springer, New York, 1st edition, 2007.

[26] J. E. Quijano, S. E. Dosso, J. Dettmer, L. M. Zurk, M. Siderius, and C. Harrison. Bayesian geoacoustic inversion using wind-driven ambient noise. *J. Acoust. Soc. Am.*, 131:2658–2667, 2012.

[27] W. H. Press, S. A. Teukolsky, W. T. Vetterling, and B. P. Flannery. *Numerical Recipies in FORTRAN: The Art of Scientific Computing*, pages 295–310. Cambridge University Press, Cambridge, second edition, 1992.

[28] N. Metropolis, A. Rosenbluth, M. Rosenbluth, and A. Teller A. E. Teller. Equations of state calculations by fast computing machines. *Journal of Chemical Physics*, 21:1087–1092, 1953.

[29] W. K. Hastings. Monte Carlo sampling methods using markov chains and their applications. *Biometrika*, 57:97–109, 1970.

[30] D. G. T. Denison, C. C. Holmes, B. K. Mallick, and A. F. M. Smith. *Bayesian Methods for Nonlinear Classification and Regression*, pages 1–277. Wiley, New York, 2002.

[31] C. Geyer and J. Moller. Simulation procedures and likelihood inference for spatial point processes. *Scand. J. Stat.*, 21(4):359–373, 1994.

[32] P. J. Green. Reversible jump Markov chain Monte Carlo computation and Bayesian model determination. *Biometrika*, 82:711–732, 1995.

[33] A. Malinverno. Parsimonious Bayesian Markov chain Monte Carlo inversion in a nonlinear geophysical problem. *Geophys. J. Int.*, 151:675–688, 2002.

[34] M. Sambridge, K. Gallagher, A. Jackson, and P. Rickwood. Trans-dimensional inverse problems, model comparison and the evidence. *Geophys. J. Int.*, 167:528–542, 2006.

[35] G. A. Warner, S. E. Dosso, J. Dettmer, and D. E. Hannay. Bayesian environmental inversion of airgun modal dispersion using a single hydrophone in the Chukchi Sea. *J. Acoust. Soc. Am.*, 137:3009–3023, 2015.

[36] W. M. Telford, L. P. Geldart, R. E. Sheriff, and D. A. Keys. *Applied Geophysics*, pages 218–441. Cambridge University Press, Cambridge, 1976.

[37] G. A. Warner, S. E. Dosso, D. E. Hannay, and J. Dettmer. Bowhead whale localization using asynchronous hydrophones in the Chukchi Sea. *J. Acoust. Soc. Am.*, 140:20–34, 2016.

[38] S. Dosso and M. Wilmut. Uncertainty estimation in simultaneous Bayesian tracking and environmental inversion. *J. Acoust. Soc. Am.*, 124(1):82–97, 2008.

[39] G. A. Warner, S. E. Dosso, and D. E. Hannay. Time-difference-of-arrival localization of bowhead whales using asynchronous hydrophones. *J. Acoust. Soc. Am.*, Submitted.

[40] C. J. Geyer. Markov chain Monte Carlo maximum likelihood. In *Computing Science and Statistics: Proceedings of the 23rd Symposium on the Interface*, pages 156–163. Interface Foundation, Fairfax Station, VA, 1991.

[41] A. Jasra, D. A. Stephens, and C. Holmes. Population-based reversible jump Markov chain Monte Carlo. *Biometrika*, 94:787–807, 2007.

[42] J. Dettmer and S. E. Dosso. Trans-dimensional matched-field geoacoustic inversion with hierarchical error models and interacting Markov chains. *J. Acoust. Soc. Am.*, 132:2239–2250, 2012.

[43] S. E. Dosso, C. W. Holland, and M. Sambridge. Parallel tempering for strongly nonlinear geoacoustic inversion. *J. Acoust. Soc. Am.*, 132:3030–3040, 2012.

[44] J. Bonnel and N. R. Chapman. Geoacoustic inversion in a dispersive waveguide using warping operators. *J. Acoust. Soc. Am.*, 130, 2011. EL101–EL107.

[45] J. Zeng, N. R. Chapman, and J. Bonnel. Inversion of seabed attenuation using time-warping of close range data. *J. Acoust. Soc. Am.*, 134, 2013. EL394–EL399.

[46] J. Bonnel, C. Gervaise, B. Nicolas, and J. I. Mars. Single-receiver geoacoustic inversion using modal reversal. *J. Acoust. Soc. Am.*, 131:119–128, 2012.

[47] J. Bonnel, S. E. Dosso, and N. R. Chapman. Bayesian geoacoustic inversion of single hydrophone light bulb data using warping dispersion analysis. *J. Acoust. Soc. Am.*, 134:120–130, 2013.

[48] G. Potty, J. Miller, P. Wilson, J. Lynch, and A. Newhall. Geoacoustic inversion using combustive sound source signals. *J. Acoust. Soc. Am.*, 124, 2008. EL146–EL150.

[49] G. Potty, J. Miller, J. Lynch, and K. Smith. Tomographic inversion for sediment parameters in shallow water. *J. Acoust. Soc. Am.*, 108:973–986, 2000.

[50] G. Potty, J. Miller, and J. Lynch. Inversion for sediment geoacoustic properties at the New England Bight. *J. Acoust. Soc. Am.*, 114:1874–1887, 2003.

[51] G. Potty, J. Miller, P. Dahl, and C. Lazauski. Geoacoustic inversion results from the ASIAEX East China Sea Experiment. *IEEE J. Ocean. Eng.*, 29:1000–1010, 2004.

[52] G. Schwartz. Estimating the dimension of a model. *Ann. Statist.*, 6:461–464, 1978.

[53] G. Steininger, J. Dettmer, S. E. Dosso, and C. W. Holland. Trans-dimensional joint inversion of seabed scattering and reflection data. *J. Acoust. Soc. Am.*, 133:1347–1357, 2013.

[54] H. M. Feder, A. S. Naidu, S. C. Jewett, J. M. Hameedi, W. R. Johnson, and T. E. Whitledge. The northeastern Chukchi Sea: benthos-environmental interactions. *Mar. Ecol. Prog. Ser.*, 111:171–190, 1994.

[55] A. L. Blanchard, C. L. Parris, A. L. Knowlton, and N. R. Wade. Benthic ecology of the northeastern Chukchi Sea. Part i. Environmental characteristics and macrofaunal community structure, 2008–2010. *Cont. Shelf Res.*, 67:52–66, 2013.

[56] E. K. Westwood, C. T. Tindle, and N. R. Chapman. A normal mode model for acousto-elastic ocean environments. *J. Acoust. Soc. Am.*, 100:3631–3645, 1996.

[57] G. MacGillivray. *Acoustic modelling study of seismic airgun noise in Queen Charlotte Basin*. PhD thesis, School of Earth and Ocean Sciences, University of Victoria, Victoria, BC, 2006.

[58] J. Dettmer, S. E. Dosso, and C. W. Holland. Trans-dimensional geoacoustic inversion. *J. Acoust. Soc. Am.*, 128:3393–3405, 2010.

[59] S. E. Dosso, J. Dettmer, G. Steininger, and C. Holland. Efficient trans-dimensional Bayesian inversion for geoacoustic profile estimation. *Inverse Problems*, 30:1–29, 2014.

[60] G. Steininger. *Determination of Seabed Acoustic Scattering Properties by Trans-Dimensional Bayesian Inversion*. PhD thesis, School of Earth and Ocean Sciences, University of Victoria, Victoria, BC, 2013.

[61] R. A. Woodgate, K. Aagaard, and T. J. Weingartner. A year in the physical oceanography of the Chukchi Sea: Moored measurements from autumn 1990-1991. *Deep-Sea Res. II*, 52:3116–3149, 2005.

[62] W. J. Richardson, B. Würsig, and C. R. Greene. Reactions of bowhead whales, *Balaena mysticetus*, to seismic exploration in the Canadian Beaufort Sea. *J. Acoust. Soc. Am.*, 79:1117–1128, 1986.

[63] S. B. Blackwell, C. S. Nations, T. L. McDonald, C. R. Greene, A. M. Thode, M. Guerra, and A. M. Macrander. Effects of airgun sounds on bowhead whale calling rates in the Alaskan Beaufort Sea. *Marine Mam. Sci.*, 29:E342–E365, 2013.

[64] F. C. Robertson, W. R. Koski, T. A. Thomas, W. J. Richardson, B. Würsig, and A. W. Trites. Seismic operations have variable effects on dive-cycle behavior of bowhead whales in the Beaufort Sea. *Endanger. Species Res.*, 21(2):143–160, 2013.

[65] D. E. Hannay, J. Delarue, X. Mouy, B. S. Martin, D. Leary, J. N. Oswald, and J. Vallarta. Marine mammal acoustic detections in the northeastern Chukchi Sea, September 2007–July 2011. *Cont. Shelf Res.*, 67:127–146, 2013.

[66] S. E. Moore and R. R. Reeves. Distribution and movement. In J. J. Burns, J. J. Montague, and C. J. Cowles, editors, *The Bowhead Whale*, volume 2, pages 313–388. Society for Marine Mammalogy, 1993.

[67] C. T. Mitchell, editor. *Arctic seismic synthesis and mitigating measures workshop proceedings*. Minerals Management Service, 1997.

[68] C. W. Clark and J. H. Johnson. The sounds of the bowhead whale, *Balaena mysticetus*, during the spring migrations of 1970 and 1980. *Can. J. Zool.*, 62:1436–1441, 1984.

[69] C. R. Greene, M. Wm. McLennan, R. G. Norman, T. L. McDonald, R. S. Jakubczak, and W. J. Richardson. Directional frequency and recording (DIFAR) sensors in seafloor recorders to locate calling bowhead whales during their fall migration. *J. Acoust. Soc. Am.*, 116:799–813, 2004.

[70] A. M. Thode, K. H. Kim, S. B. Blackwell, C. R. Greene, C. S. Nations, T. L. McDonald, and A. M. Macrander. Automated detection and localization of bowhead whale sounds in the presence of seismic airgun surveys. *J. Acoust. Soc. Am.*, 131:3726–3747, 2012.

[71] S. H. Abadi, A. M. Thode, S. B. Blackwell, and D. R. Dowling. Ranging bowhead whale calls in a shallow-water dispersive waveguide. *J. Acoust. Soc. Am.*, 136:130–144, 2014.

[72] C. W. Clark and W. T. Ellison. Calibration and comparison of the acoustic location methods used during the spring migration of the bowhead whale, *Balaena mysticetus*, off Pt. Barrow, Alaska, 1984–1993. *J. Acoust. Soc. Am.*, 107:3509–3517, 2000.

[73] A. M. Thode, P. Gerstoft, W. C. Burgess, K. G. Sabra, M. Guerra, M. D. Stokes, M. Noad, and D. H. Cato. A portable matched-field processing system using passive acoustic time synchronization. *IEEE J. Ocean. Eng.*, 31(3):696–710, 2006.

[74] Y.-T. Lin, A. E. Newhall, and J. F. Lynch. Low-frequency broadband sound source localization using an adaptive normal mode back-propagation approach in a shallow-water ocean. *J. Acoust. Soc. Am.*, 131:1798–1813, 2012.

[75] A. E. Newhall, Y.-T. Lin, J. F. Lynch, M. F. Baumgartner, and G. G. Gawarkiewicz. Long distance passive localization of vocalizing sei whales using an acoustic normal mode approach. *J. Acoust. Soc. Am.*, 131(2):1814–1825, 2012.

[76] S. M. Wiggins, M. A. McDonald, L. M. Munger, S. E. Moore, and J. A. Hildebrand. Waveguide propagation allows range estimates for North Pacific right whales in the Bering Sea. *Can. Acoust.*, 32(2):146–154, 2004.

[77] L. Cohen. *Time-Frequency Analysis*, pages 27–43. Prentice Hall PTR, Englewood Cliffs, New Jersey, 1995.

[78] M. D. Collins and W. A. Kuperman. Focalization: Environmental focusing and source localization. *J. Acoust. Soc. Am.*, 90(3):1410–1422, 1991.

[79] C. F. Mecklenbräuker and P. Gerstoft. Objective functions for ocean acoustic inversion derived by likelihood methods. *J. Comput. Acoust.*, 8:259–270, 2000.

[80] T. J. Weingartner. Vessel collected CTD, NE Chukchi Sea 2008–2013 (Ed5), 2013. Alaska Ocean Observing System, Ocean Workspace.

[81] T. Weingartner, E. Dobbins, S. Danielson, P. Winsor, R. Potter, and H. Statscewich. Hydrographic variability over the northeast Chukchi Sea shelf in summer-fall 2008–2010. *Cont. Shelf Res.*, 67:5–22, 2013.

[82] W. A. Watkins and W. E. Schevill. Listening to hawaiian spinner porpoises, *Stenella cf. Longirostris*, with a three-dimensional hydrophone array. *J. Mammal*, 55:319–328, 1974.

[83] A. S. Frankel, C. W. Clark, L. M. Herman, and C. M. Gabriele. Spatial distribution, habitat utilization, and social interactions of humpback whales, *Megaptera novaeangliae*, off Hawai'i, determined using acoustic and visual techniques. *Can. J. Zool.*, 73:1134–1146, 1995.

[84] K. M. Stafford, C. G. Fox, and D. S. Clark. Long-range acoustic detection and localization of blue whale calls in the northeast Pacific Ocean. *J. Acoust. Soc. Am.*, 104:3616–3625, 1998.

[85] V. M. Janik, S. M. Van Parijs, and P. M. Thompson. A two-dimensional acoustic localization system for marine mammals. *Marine Mam. Sci.*, 16:437–447, 2000.

[86] R. P. Morrissey, J. Ward, N. DiMarzio, S. Jarvis, and D. J. Moretti. Passive acoustic detection and localization of sperm whales (*Physeter macrocephalus*) in the tongue of the ocean. *Appl. Acoust.*, 67:1091–1105, 2006.

[87] P. B. Muanke and C. Niezrecki. Manatee position estimation by passive acoustic localization. *J. Acoust. Soc. Am.*, 121:2049–2059, 2007.

[88] X. Li, Z. D. Deng, L. T. Rauchenstein, and T. J. Carlson. Contributed review: source-localization algorithms and applications using time of arrival and time difference of arrival measurements. *Rev. Sci. Instrum.*, 87:1–13, 2016.

[89] J. L. Spiesberger. Probability distributions for locations of calling animals, receivers, sound speeds, winds, and data from travel time differences. *J. Acoust. Soc. Am.*, 118:1790–1800, 2005.

[90] A. Širović, J. A. Hildebrand, and S. M. Wiggins. Blue and fin whale call source levels and propagation range in the Southern Ocean. *J. Acoust. Soc. Am.*, 122:1208–1215, 2007.

[91] K. G. Sabra, P. Roux, A. M. Thode, G. L. D'Spain, W. S. Hodgkiss, and W. A. Kuperman. Using ocean ambient noise for array self-localization and self-synchronization. *IEEE J. Ocean. Eng.*, 30(2):338–347, 2005.

[92] B. Møhl, M. Whalberg, and A. Heerfordt. A large-aperature array of nonlinked receivers for acoustic positioning of biological sound sources. *J. Acoust. Soc. Am.*, 109:434–437, 2001.

[93] Y. Simard and N. Roy. Detection and localization of blue and fin whales from large-aperature autonomous hydrophone arrays: a case study from the St. Lawrence Estuary. *Can. Acoust.*, 36:104–110, 2008.

[94] B. Miller and S. Dawson. A large-aperature low-cost hydrophone array for tracking whales from small boats. *J. Acoust. Soc. Am.*, 126:2248–2256, 2009.

[95] B. Miller, S. Dawson, and R. Vennell. Underwater behavior of sperm whales off Kaikoura, New Zealand, as revealed by a three-dimensional hydrophone array. *J. Acoust. Soc. Am.*, 134:2690–2700, 2013.

[96] C. W. Clark. Call tracks of bowhead whales based on call characteristics as an independent means of determining tracking parameters. Report of the sub-committee on protected species and aboriginal subsistence whaling, Appendix 2. *Rep. int. Whal. Commn*, 39:111–113, 1989.

[97] B. Würsig and C. Clark. Behavior. In J. J. Burns, J. J. Montague, and C. J. Cowles, editors, *The Bowhead Whale*, volume 2, pages 157–199. Society for Marine Mammalogy, 1993.

[98] W. J. Teague, M. J. Carron, and P. J. Hogan. A comparison between the Generalized Digital Environmental Model and Levitus climatologies. *Geophys. Res.*, 95:7167–7183, 1990.

[99] M. R. Carnes. Description and evaluation of GDEM-V 3.0. Technical Report 733009-9165, Naval Research Lab Stennis Space Center MS Oceanography Div, 2009.

[100] D. J. C. MacKay. *Information Theory, Inference, and Learning Algorithms*, pages 343–386. Cambridge University Press, Cambridge, 2003.

[101] C. J. Geyer. *Introduction to Markov chain Monte Carlo*, pages 3–47. Springer, New York, 2011.

[102] M. Sambridge. A parallel tempering algorithm for probabilistic sampling and multimodal optimization. *Geophys. J. Int.*, 196:357–374, 2013.

[103] D. J. Earl and M. W. Deem. Parallel tempering: Theory, applications, and new perspectives. *Phys. Chem. Chem. Phys.*, 7:3910–3916, 2005.

[104] A. Jasra, D. A. Stephens, and C. C. Holmes. On population-based simulation for static infrerence. *Stat. Comp.*, 17:263–279, 2007.

[105] A. F. M. Smith. Bayesian computational methods. *Phil. Trans. R. Soc. Lond.*, 337:369–386, 1991.

[106] J. Dettmer, S. Molnar, G. A. M. W. Steininger, S. E. Dosso, and J. F. Cassidy. Trans-dimensional inversion of microtremor array dispersion data with hierarchical autoregressive error models. *Geophys. J. Int.*, 188:719–734, 2011.